



# SYNAPSE-TO-NETWORK PLASTICITY IN THE HIPPOCAMPUS

Presented by:  
EFRÉN ÁLVAREZ SALVADO

For the degree of Doctor in Neuroscience  
from the Universidad Miguel Hernández

Director:  
Dr. SANTIAGO CANALS GAMONEDA

San Juan de Alicante, 2015



A QUIEN CORRESPONDA:

El Profesor **Juan Lerma Gómez**, Director del Instituto de Neurociencias de Alicante, Centro Mixto de la Universidad Miguel Hernández (UMH) y de la Agencia Estatal Consejo Superior de Investigaciones Científicas (CSIC)

INFORMA:

Que la Tesis Doctoral "*Synapse-to-network plasticity in the hippocampus*" ha sido realizada por D. Efrén Álvarez Salvado, Máster en NEUROCIENCIAS, bajo la dirección del Dr. Santiago Canals Gamoneda, y da su conformidad para que sea presentada a la Comisión de Doctorado de la Universidad Miguel Hernández.

Y para que así conste a los efectos oportunos, firma el presente informe en San Juan de Alicante, a 9 de enero de 2015

Fdo.: Juan Lerma





A QUIEN CORRESPONDA:

El Dr. SANTIAGO CANALS GAMONEDA, Científico Titular del Consejo Superior de Investigaciones Científicas (CSIC) en el Instituto de Neurociencias de Alicante, Centro Mixto de CSIC-Universidad Miguel Hernández,

CERTIFICA,

Que Don EFRÉN ÁLVAREZ SALVADO, Máster en Neurociencias, ha realizado bajo su dirección el trabajo experimental que recoge su Tesis Doctoral "SYNAPSE-TO-NETWORK PLASTICITY IN THE HIPPOCAMPUS". Que ha revisado los contenidos científicos y los aspectos formales del trabajo y da su conformidad para su presentación y defensa pública.

Y para que así conste a los efectos oportunos, firma el presente Certificado en San Juan de Alicante, a 9 de enero de 2015.



Fdo.: Santiago Canals Gamoneda



## AKNOWLEDGEMENTS

*“Just because you read it in a magazine or see it on the TV screen don't make it factual”*  
Michael Jackson

*Esta tesis no podría haber sido posible sin la presencia, el apoyo y la ayuda de distintas personas, que colaboraron en mayor o menor medida, directa o indirectamente, en su realización. A todos los implicados, de un modo u otro, les quiero agradecer de todo corazón su papel.*

*En primer y en segundo lugar, a Santiago. Al margen de ser la mano que firma esta tesis (y todo lo que ello ha conllevado durante estos años), nunca podré agradecerle suficiente toda su confianza, su generosidad, su apoyo constante, su inestimable ayuda, su infinita paciencia y sus enseñanzas. Todo ello se ha hecho notar desde el primer día y cada día durante cinco años, y no me cabe duda de que este tiempo no habría sido ni remotamente igual de grato si no hubiera contado con un mentor y compañero tan genial como Santiago. Espero haber sabido estar a la altura y también que, de alguna manera, se me haya pegado algo bueno. De corazón, gracias.*

*Gracias a Luis por ponerme en el camino que me trajo hasta aquí, prueba irrefutable de que las casualidades no existen. Gracias por su tiempo, sus consejos y su apoyo en todo, y por ser siempre una persona tan asequible y tan única. Gracias por estar siempre ahí, a una escalera de distancia.*

*Muchas gracias a todos mis compañeros y compañeras del laboratorio, incluso a quienes ya se fueron y quienes acaban de llegar. Es importante que un laboratorio sea algo más que una habitación en la que trabajar, y yo puedo decir que en ese aspecto tuve la mayor de las suertes. Gracias a todos y todas por vuestra presencia, vuestra compañía, vuestra ayuda y vuestro tiempo. Un agradecimiento especial para Begoña, mi querida capataz, por toda su inestimable ayuda y su gran trabajo, que sin duda alguna hizo posible todo lo que se ve hoy reflejado en esta tesis.*

*Gracias también a todas las personas con las que tuve la suerte de coincidir durante este tiempo, dentro y fuera de los muros del laboratorio; a todas ellas mi más sincero agradecimiento por todos los buenos momentos pasados y el tiempo compartido. En especial, infinitas gracias a Cris por su apoyo y por ser tan genial.*

*Gracias a Kamila por estar a mi lado todo este tiempo, y por aguantar el tirón final sin dejarme perder el ánimo y siendo siempre un ejemplo y una inspiración para mí. Una tesis parecería vacía sin esos varios años de vida que hay detrás, y en mi caso esos años parecerían sin duda vacíos sin Kamila. Gracias por todo.*

*Es mucho más importante de lo que creemos el saber a veces que en un lugar lejano hay alguien convencido de que lo que haces es bueno, necesario, y que además lo haces muy bien. Por ello doy las gracias de todo corazón a mi familia y a mis amigos, por tratarme siempre como al más eminente de los científicos, por todo su apoyo y su cariño, sin el cual hacer una tesis habría sido infinitamente más difícil. En especial gracias a mis padres, por creer en mí y por quererme como soy, con mi ciencia y mis rarezas, y por apoyarme desde siempre en cada cosa que hago.*

*Muchas gracias por todo.*



# INDEX

<b>ABSTRACT.....</b>	<b>1</b>
<b>I. INTRODUCTION.....</b>	<b>5</b>
<b>1.1. Why are hippocampus and synaptic plasticity important for memory?.....</b>	<b>5</b>
Hippocampal formation and memory.....	5
Synaptic plasticity and memory.....	5
How does synaptic plasticity in the hippocampus create a memory?.....	6
<b>1.2. An overview of the anatomy of the hippocampal system.....</b>	<b>9</b>
Cellular organization of the hippocampus.....	10
Extrinsic connections of the hippocampal formation.....	12
Differences across species.....	13
<b>1.3. Synaptic plasticity in hippocampal circuits.....</b>	<b>13</b>
Main properties of synaptic plasticity.....	14
Long-Term Depression.....	14
Influence of synaptic plasticity on hippocampal local networks.....	15
Influence of hippocampal local networks on synaptic plasticity.....	16
<b>II. OBJECTIVES.....</b>	<b>17</b>
<b>III. MATERIALS AND METHODS.....</b>	<b>19</b>
<b>3.1. Experiments on anesthetized rats.....</b>	<b>19</b>
Animals used.....	19
Surgery and preparation.....	19
LTP induction.....	21
Pharmacological experiments.....	21
fMRI-pharmacological experiments.....	22
MRI-compatible carbon fiber electrodes.....	23
<b>3.2. Experiments on awake rats.....</b>	<b>23</b>
Animals used.....	23
Housing.....	23
Experimental room.....	23
Habituation.....	24
Surgery for electrodes implantation.....	24
Electrophysiological and video recordings.....	25
Behavioral Novelty task.....	25
Immuno-histochemical analysis.....	26
<b>3.3. Data analysis.....</b>	<b>27</b>
Selection of the LFP.....	27
Separation of the LFP signals with Independent Component Analysis (ICA).....	28
Identification of the LFP generators.....	29

Reconstruction of virtual-LFP signals from the generators.....	30
Analysis of spontaneous signals.....	30
Analysis of sub-threshold evoked-LFP.....	32
Analysis of fMRI images.....	33
Statistical analysis.....	33
Behavioral video-tracking.....	33
<b>IV. RESULTS.....</b>	<b>35</b>
<b>4.1. Identification of the main generators of the hippocampus.....</b>	<b>35</b>
<b>4.2. Induction of Long-Term Potentiation (LTP).....</b>	<b>38</b>
<b>4.3. LTP induction changes the spontaneous activity of the hippocampal local circuits</b> <b>.....</b>	<b>39</b>
<b>4.4. Independent components of sub-threshold evoked potentials.....</b>	<b>44</b>
<b>4.5. Pharmacological and electrophysiological characterization of the generators... </b>	<b>47</b>
<b>4.6. Changes in the sub-threshold evoked potentials with LTP.....</b>	<b>51</b>
<b>4.7. Local supression of the GABAergic activity affects ongoing activity and</b> <b>information propagation.....</b>	<b>54</b>
<b>4.8. Learning modulates the generators' spontaneous activity.....</b>	<b>55</b>
<b>V. DISCUSSION.....</b>	<b>63</b>
<b>5.1. LFP-Generators are a reliable representation of hippocampal Local Field</b> <b>Potentials.....</b>	<b>63</b>
<b>5.2. Hilar generator reflects local feed-forward inhibition.....</b>	<b>63</b>
<b>5.3. LTP in the dentate gyrus decreases local inhibition and changes the</b> <b>excitation-inhibition balance.....</b>	<b>65</b>
<b>5.4. Decreases in inhibition in the dentate gyrus are sufficient to induce a functional</b> <b>reorganization in the brain.....</b>	<b>67</b>
<b>5.5. Context novelty is sufficient to change the excitation-inhibition balance in the</b> <b>dentate gyrus and to induce a subsequent functional reorganization.....</b>	<b>68</b>
<b>5.6. Concluding remarks.....</b>	<b>71</b>
<b>VI. CONCLUSIONS.....</b>	<b>73</b>
<b>VII. ABBREVIATIONS.....</b>	<b>75</b>
<b>VIII. BIBLIOGRAPHY.....</b>	<b>77</b>
<b>IX. ANNEX.....</b>	<b>85</b>

## LIST OF FIGURES

Figure 1.1. Schematic representation of the episodic memory system.....	7
Figure 1.2. Schematic illustration of intrinsic connectivity of the hippocampal system.....	10
Figure 1.3. Drawing of the different sub-areas and layers of the hippocampal formation.....	11
Figure 3.1. Illustration of the experimental preparation.....	20
Figure 3.2. Hystological post mortem location of the electrodes for the anesthetized experiments.....	20
Figure 3.3. Illustration of the preparation for the pharmacological experiments.....	22
Figure 3.4. Illustration of the Novelty task.....	26
Figure 3.5. Hystological post mortem location of the electrodes in the behavioral experiments .....	27
Figure 3.6. Frequency bands' power of the selected LFP from anesthetized experiments.....	28
Figure 3.7. Example of separation of LFP into its components with ICA.....	29
Figure 3.8. Simplified illustration of cross-correlation analysis and representation of the results.....	31
Figure 3.9. Method for analysis of the sub-threshold evoked-LFP and its components.....	32
Figure 4.1. Example of separation of LFP into its components with ICA.....	36
Figure 4.2. Average power of the hippocampal LFP-generators during the injection of TTX in the perforant path.....	38
Figure 4.3. Effects of LTP induction on the perforant path evoked-LFPs.....	39
Figure 4.4. Changes in the power of the generators with LTP.....	40
Figure 4.5. Changes in the band-power of the generators with LTP.....	41
Figure 4.6. Simplified illustration of cross-correlation analysis and representation of the results.....	42
Figure 4.7. Functional coupling between generators measured by cross-correlation before and after potentiation of the perforant path.....	43
Figure 4.8. Characterization and separation of the sub-threshold evoked-LFP into independent components.....	45
Figure 4.9. Modulation of the Hilar generator by spontaneous Gamma and Theta oscillations .....	47
Figure 4.10. Effect of Gabacine on sub-threshold evoked-LFP.....	48
Figure 4.11. Effect of Bicuculine on sub-threshold evoked-LFP.....	49
Figure 4.12. Schematic illustration of paired-pulses stimulation protocol.....	49
Figure 4.13. Effect of pairing on sub-threshold e-LFP.....	50
Figure 4.14. Pharmacological reversal of the effect of pairing on sub-threshold evoked-LFP.....	51
Figure 4.15. Changes in the sub-threshold evoked-LFP with LTP.....	52
Figure 4.16. Blockade of the effects of LTP on evoked-LFP with AP5.....	53
Figure 4.17. Effects of Gabacine on BOLD signal maps across the brain.....	55
Figure 4.18. Illustration of the Novelty task and trajectory of the animals.....	57
Figure 4.19. Average power of the generators during a novelty.....	58
Figure 4.20. Average frequency bands-power of the generators during a novelty.....	58
Figure 4.21. Time course of the power of the generators during a novelty.....	59
Figure 4.22. Functional coupling between generators measured by cross-correlation during a novelty.....	60
Figure 4.23. Effects a novelty on the time course of the sub-threshold evoked-LFP.....	61
Figure 5.1. Schematic representation of our theory.....	70
Figure 5.2. Summary of the main results found in LTP experiments.....	72



## ABSTRACT

The hippocampal formation has been known for decades for its central role in the formation of new episodic memories. Although synaptic plasticity is a well accepted and dominant mechanism underlying the process of learning, and current theories include a communication between hippocampus and cortical structures during such process, the truth is that not much is known regarding the gap between the synapse and the network; i.e. how local plasticity at the level of the neurons can affect a whole network nearby and at distant regions of the brain as well. It has been previously demonstrated that indeed this occurs with Long-Term Potentiation (LTP) of the perforant path, but the *how* still remains to be clarified. The aim of this work was to study in depth the specific phenomena that turn synaptic plasticity into a network emergent property, and which could be its role in learning and memory.

We studied the hippocampus of rats *in vivo* using electrophysiological techniques and pharmacological manipulations, as well as functional magnetic resonance imaging (fMRI). We recorded the extracellular Local-Field Potentials (LFP), and since these signals are a summation of several different neuronal sources or “generators”, we analyzed them using independent component analysis as a method of source separation; we then studied separately the spontaneous and the evoked activity of the different hippocampal LFP-generators during the induction of LTP in the perforant path.

Synaptic potentiation produced a decrease of the feed-forward inhibition on granule cells in the dentate gyrus and an increase in their excitatory input, and thus a net change in the local excitation-inhibition balance. Moreover, the functional coupling between the local inhibitory and excitatory network decreased, and in turn there was an enhanced coordination of the entorhinal input with the activity at CA1 area. This evidences a rearrangement of the hippocampal network starting from the dentate gyrus, and therefore suggests that feed-forward inhibition in this area is acting as a gating mechanism for information propagation.

Moreover, we could demonstrate that the reach of these functional changes is larger than the hippocampal network and it affects also distant regions of the brain; we observed with fMRI that a pharmacological blockade of GABAergic activity in the dentate gyrus provoked an increased activation of new cortical and subcortical areas.

We reproduced the electrophysiological preparation to perform similar experiments in awake behaving rats, substituting LTP for a physiological behavioral task, in which animals were confronted with a novelty in a familiar environment. The results revealed equivalent changes to those found with anesthetized animals in the hippocampal network, further supporting our theory that this functional reorganization may indeed subserve learning and memory, regarded as a routing mechanism to preferentially process novel and relevant environmental information.

## RESUMEN

La formación hipocampal es conocida desde hace décadas por su papel central en la formación de nuevas memorias episódicas. Del mismo modo, aunque la plasticidad sináptica está muy aceptada y se considera el mecanismo que subyace al proceso de aprendizaje, y aunque las teorías actuales que explican este proceso implican comunicación entre el hipocampo y estructuras corticales, la verdad es que no se sabe mucho respecto a la transición entre la sinapsis y la red; es decir, cómo la plasticidad sináptica al nivel celular puede afectar a la red neuronal tanto localmente como en áreas distantes del cerebro. Se ha demostrado previamente que esto ocurre efectivamente con la Potenciación a Largo Plazo (“LTP”, de sus siglas en inglés) del tracto perforante, pero el *cómo* ello ocurre se desconoce todavía. El objetivo de este trabajo es estudiar en profundidad los fenómenos específicos que convierten la plasticidad sináptica en una propiedad emergente de las redes neuronales, y cuál puede ser su rol en el aprendizaje y la memoria.

Hemos estudiado el hipocampo de ratas anestesiadas empleando técnicas electrofisiológicas y manipulaciones farmacológicas, así como imagen por resonancia magnética funcional (“fMRI”, de sus siglas en inglés). Registramos los Potenciales de Campo Locales (“LFP”, de sus siglas en inglés) extracelulares, y dado que estas señales son una sumación de distintas fuentes neuronales o “generadores”, les aplicamos un análisis de componentes independientes como método de separación de fuentes; después analizamos individualmente la actividad espontánea y evocada de los distintos generadores del LFP hipocampal durante la inducción de LTP en el tracto perforante.

La potenciación sináptica produjo una disminución de la inhibición prealimentada o *feed-forward* sobre las células granulares del giro dentado y un aumento de la excitación sobre ellas, con un consiguiente cambio neto en el balance excitación-inhibición local. Además, el acoplamiento funcional entre la red local excitatoria e inhibitoria disminuyó, y en cambio aumentó la coordinación de la aferencia entorrinal con la actividad en el área CA1. Esto evidencia un reajuste de la red hipocampal que comienza desde el giro dentado, y sugiere por tanto que la inhibición *feed-forward* en esta área actúa como “compuerta” para la propagación de información.

Adicionalmente, demostramos que el alcance de estos cambios funcionales trasciende la red hipocampal y afecta también regiones distantes del cerebro; mediante fMRI, observamos que bloqueando farmacológicamente la actividad GABAérgica en el giro dentado se producía la activación de nuevas áreas corticales y subcorticales.

Reprodujimos la preparación electrofisiológica para realizar experimentos similares con ratas despiertas, sustituyendo la LTP por una tarea conductual más fisiológica, durante la cual los animales encontraron una novedad en un entorno familiar. Los resultados de estos experimentos revelaron cambios en la red hipocampal equivalentes a los encontrados en animales anestesiados, lo cual apoya nuestra teoría de que esta reorganización funcional participa en efecto en el aprendizaje y la memoria, entendiéndola como un mecanismo de enrutamiento para procesar preferentemente información novedosa y relevante del entorno.





# I. INTRODUCTION

## ***1.1. Why are hippocampus and synaptic plasticity important for memory?***

Memory is such a great feature of our brain, and represents an important part of our lives. As the dramatic case of Henry Molaison (also known as “patient H.M.”) demonstrated (Scoville & Milner, 1957), without our memory we cannot be ourselves. Not only it is important in the personal aspect, but it has been hypothesized, from a computational perspective, that this feature of our brain might be the basis and the whole point in actually having a neocortex as big as we do (Hawkins & Blakeslee, 2004). So it would be probably right to state that in neuroscience, knowing how memory works is quite an interesting topic.

### ***Hippocampal formation and memory***

As we mentioned, one of the most famous and important evidences we have about memory is the case of Henry Molaison (Scoville & Milner, 1957). When he was young he had both hippocampi and parahippocampal cortices (relatively small structures located in the temporal part of the brain) surgically removed for curing the severe epilepsy he was suffering. Unfortunately he acquired in turn anterograde amnesia: the permanent loss of the capacity to create new recollections. He was not capable of remembering a person who left his presence for more than a few minutes, although he kept intact his memories from the years before the surgery. This case set the first evidence that the hippocampal system is necessary to create episodic memories (i.e. memories of events). In the following decades, several studies with animals replicated and explored further the contribution of the hippocampus to memory encoding, fundamentally through elimination or inactivation of this structure. They provided clear evidence of its key role in the memory process, but also served to establish the important idea that such role is temporary (although its temporal extent is controversial) (reviewed by Squire, 1992).

### ***Synaptic plasticity and memory***

One fundamental mechanism involved in memory is synaptic plasticity, the change in the efficacy of the connections between neurons. The notion that such modifications could underlie learning and memory was suggested already long time ago by Eugenio Tanzi (1893) and Santiago Ramón y Cajal (1894), and formally postulated decades later by Donald Hebb (1949). A critical discovery was that of the synaptic long-term potentiation (LTP) of hippocampal neurons (Bliss & Lømo 1973). It showed that neurons in the dentate gyrus (a sub-region of the hippocampus) can undergo plastic changes in their inputs when they are stimulated electrically at high frequency. This finding can be considered a demonstration of Hebb's postulate, i.e. a long-lasting and activity-dependent synaptic strengthening in the sense of “neurons that fire together wire together” (Hebb, 1949). LTP, and more generally synaptic plasticity, became –and have been since then– the dominant model that accounts for an experience-dependent modification of brain circuits, believed to underlie memory formation.

The first evidence linking learning with synaptic plasticity was provided already from conditioning studies in the mollusc *Aplysia* (Castelluci et al., 1970; Kupfermann et al., 1970), and during the following decades, several other authors proved -using rabbits, rats or mice- that when learning occurred it was accompanied by synaptic potentiation in whichever structure of the brain was involved. This was done in studies in the hippocampus (Weisz et al., 1984; Barnes & McNaughton, 1985; Moser et al., 1993; Whitlock et al., 2006; Gruart et al., 2006), but also in other areas of the brain (Rogan et al., 1997; Tang et al., 2001; Monfils & Teskey, 2004; Roman et al., 2004; Sevelinges et al., 2004; Sacchetti et al., 2004; Rumpel et al., 2005). Overall they evidence an unequivocal involvement of synaptic plasticity in learning, although they might have not demonstrated a causal relationship. Complementary studies addressed this point and showed that a pharmacological blockade of NMDA receptor-dependent synaptic plasticity in the hippocampus could actually impair hippocampal-dependent spatial memory (Morris et al., 1986; Kentros et al., 1998), and also that artificial saturation of LTP prevented any further learning (Moser et al., 1998). Taken together, this evidence demonstrates that synaptic plasticity occurs in physiological conditions associated with learning, and moreover that it is actually necessary for learning to happen (at least for the hippocampal dependent memories). This has been formulated as the “synaptic plasticity and memory hypothesis” (reviewed by Martin et al., 2000; Takeuchi et al., 2013), and it leads to the next question.

### ***How does synaptic plasticity in the hippocampus create a memory?***

Being already established the notion of synaptic plasticity as a mechanism underlying the formation of memories, and knowing that the hippocampus is essential in order to create new episodic memories, we now need to know how this process happens.

First, it might be necessary to define the concepts of *anatomical connectivity* and *functional connectivity*, that may help us set an appropriate focus of research to address this issue. “Anatomical connectivity” (or simply referred to as “connectivity” in the present work) refers to the structure, the wiring of the brain; it is to a large extent unchangeable, especially at the macroscopic scale (i.e. dendritic and axonal arborizations and projections). The “functional connectivity” is defined by temporal relations between the activations or neuronal processes in different brain areas, and is measured by statistical methods like correlation, coherence or phase locking (Lang et al., 2012). In the literature of brain connectivity it is also usual the term *effective connectivity*, which describes the actual influence that a network exerts upon another. For practical reasons, in the present work we will imply these last two concepts together as “functional connectivity”.

A widely accepted theory supports that the connections of the hippocampus with nearby related cortices, and in turn their connections with more distributed areas, provide the former with an input representation of the environment in the form of a complex set of information; this is achieved mostly through the entorhinal cortex, that has connections with multisensory cortical areas. The resulting spatio-temporally distributed, complex pattern of activity representing external events is processed by the hippocampus to create a simplified new pattern of output activity that goes all the way back to the corresponding areas of the brain (see Figure 1.1 for an illustration of this). The connections within the hippocampal formation would undergo plastic modifications, and the subsequent changes in the short and long-range (functional) connectivity would, in turn, set and stabilize the engagement between the involved cortical areas (Teyler & Rudy, 2007). The activation of that specific set of synapses, and the subsequent reactivation of the retrieved sites, could take place repeatedly over time, making the specific memory stable and independent from the hippocampus. Let's now review the evidence supporting the different parts of this theory.

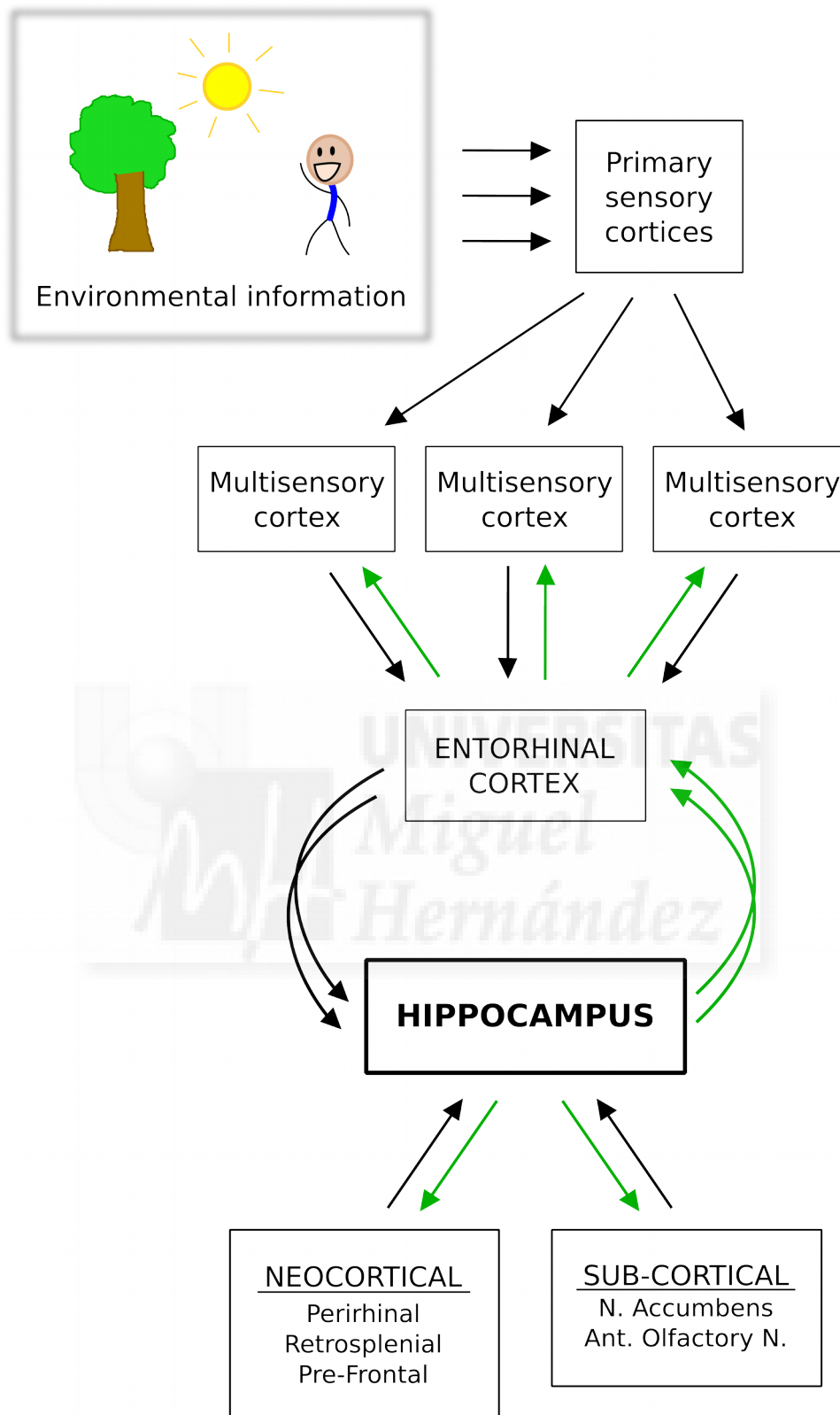


**Figure 1.1. Schematic representation of the episodic memory system.** The arrows illustrate information travelling through anatomical connections between different structures of the brain (represented in the boxes). Black arrows represent information going towards the hippocampus, and green arrows information originating from the hippocampus. The multisensory information of the environment reaches primary sensory cortices of different modalities, and is then processed until it is eventually received at associative cortices. The entorhinal

cortex is known to receive input from several different cortices of this kind (see below), and it transfers that information in turn to the hippocampus, which also receives direct inputs from several sub-cortical and neocortical areas (in the lower boxes appear only some examples of these two groups of structures). After incoming information traverses the different sub-regions of the hippocampus, it is transferred back to different associative cortices (in part through entorhinal cortex) and sub-cortical areas.

The idea of the hippocampus playing only a temporary role in memory formation appeared with the study of cases of temporally graded retrograde amnesia in humans, in which the lesion of the hippocampal formation eliminated the ability to create new recollections, but spared the older ones (Ribot, 1882; Scoville & Milner, 1957; Rempel-Clower et al., 1996). Therefore it can be concluded that memories must at some point -once the role of the hippocampus is fulfilled- be stored elsewhere in the brain, so they become hippocampus-independent. This notion was proposed by several authors (Teyler & Discenna, 1986; Squire, 1992; Alvarez & Squire, 1994; Nadel & Moscovitch, 1997), and every account agrees that an interaction between hippocampus and neocortex is necessary in order to consolidate new memories. This process is called “systems consolidation” (Marr, 1970; Alvarez & Squire, 1994; Wang & Morris, 2010) and entails an interaction (a communication) with distant areas of the brain.

From this perspective, a key finding that also set the path for the present work was made by Canals and colleagues (2009). Using functional magnetic resonance imaging (fMRI), they found that localized synaptic plasticity at the hippocampus (induced by electrical stimulation) provoked a change in the functional connectivity between this structure and distant areas of the brain, activating with identical stimulation structures that were not active previously. In a recent work published by the author of the present thesis and our group (see annex), we also found evidence of an increased communication and qualitative change in the bilateral connectivity of the hippocampal system due to unilateral synaptic potentiation in the perforant path (Álvarez-Salvado et al., 2013; Annex 1). Both these works serve to demonstrate that synaptic plasticity at a local level triggers a functional reorganization that has a measurable polysynaptic effect on circuits across the whole brain, and it might represent a mechanism to support long-range hippocampal interactions and therefore memory consolidation.

There are several studies supporting the view that functional connectivity between hippocampus and distant brain areas underlies memory formation. Ranganath and collaborators (2005) studied with fMRI the activation of the brain in human subjects while they performed a working memory task, being presented with drawings and having to tell apart later the known ones from the new ones. The authors found that a higher transient functional connectivity between hippocampus and a series of cortical areas predicted successful remembering of a picture; among those areas were retrosplenial, prefrontal, perirhinal or cingulate cortices. These results are in line with previous findings that showed with fMRI an increased activation of (partly) the same cortical areas upon successful memory formation in an almost identical task (Brewer et al., 1998). Moreover, Takashima and colleagues (2006) showed that this hippocampal-cortical coupling decreases over time for successful memory retrieval, supporting the idea previously mentioned that such coupling is temporary and subserves memory encoding. Other recent studies supported this network for encoding new memories and deeper explored functional connectivity related to memory (Wang et al., 2010; Manelis et al., 2013; Schott et al., 2013). A different study with awake, behaving rats went further into the mechanisms of hippocampal-cortical interaction, and demonstrated a phase relation between prefrontal cortex neurons and hippocampal Theta oscillations (Siapas et al., 2005), suggesting that it could serve to guide plasticity at the network level. Remarkably, they can be found several cortical areas in common from the cortical networks related to the hippocampus in all these works, that moreover are among the cortical areas described by Canals et al. (2009).

Using metabolic and morphological methods, several other studies demonstrated as well that there is a

coincident activation of hippocampus and other cortical regions during memory encoding, and they evidenced a different involvement at different times during long-term memory consolidation and retrieval (Bontempi et al., 1999; Maviel et al., 2004; Restivo et al., 2009; Lesburguères et al., 2011), with a decreased participation of the hippocampus over time. Moreover, among the cortical areas involved in memory encoding, and activated along with the hippocampus in the early stages of this process, were again prefrontal, retrosplenial and cingulate cortices.

The evidence reviewed demonstrates the temporary role of hippocampal system in memory consolidation, and proves that such transfer of the processing of information is achieved through transitory hippocampal-cortical functional coupling. But although systems consolidation is supported by numerous evidence, it is admitted too that we do not know in detail what mechanisms underlie the communication between hippocampal and cortical and subcortical areas (Takeuchi et al., 2013). More specifically, we do not know how synaptic plasticity at the cellular level can exert an effect on the network, changing its dynamics in the form of network plasticity, and in turn changing communication with distant areas of the brain where the information about specific episodes might eventually remain “stored”. Therefore, it is the long-range connections and the global integration at the system level that we must aim for understanding in order to investigate complex brain functions (Park & Friston, 2013). In the present work we wanted to approach the qualitative leap that is between the individual synaptic processing and the final of storage of information in the brain in the form of a new memory; this inevitably leads us to set the focus of our research on the network level, which becomes the intermediate level of study between the synapses and cognitive processes.

## **1.2. An overview of the anatomy of the hippocampal system**

In order to study hippocampal network in depth and interpret the results of the present work, we must understand the anatomy of this structure. In the following paragraphs we will review and summarize the morphology and intrinsic connections of this area of the brain, as well as the main afferent and efferent pathways that connect with other cortical and sub-cortical areas.

In the present work we speak sometimes of “hippocampal formation”; with this term we refer to the ensemble formed by entorhinal cortex, dentate gyrus, hippocampus proper (also *cornu ammoni* or abbreviated “CA” area), subiculum, presubiculum and parasubiculum, as defined by Amaral and Lavenex (2007). However, at the same time, the term “hippocampus” most usually refers to the sub-group of dentate gyrus, CA (with its sub-areas CA1, CA2 and CA3) and subiculum, for they form a differentiated macroscopic structure. And even sometimes, the CA sub-region is referred to as “hippocampus proper”. In the present work we will use this terminology in that way.

All mentioned areas are a set of cortices located in the medial temporal lobe in humans (in the temporal region for other animals), and in all mammals they form a more or less rolled up structure (Figures 1.2 and 1.3). In the hippocampal formation, the organization of the connections entails a basically unidirectional flow of information, although it is not exactly this way, as will be explained below. A main route of information through the hippocampus, most extensively studied, is as follows: entorhinal cortex projects from layers 2-3 to the dentate gyrus through an axon bundle called the “perforant path”. These axons contact the dendrites of the granule cells (the principal cells of the dentate gyrus). The granule cells emit axons called “mossy fibers” that contact with CA3 pyramidal cells, that in turn project to the ones in CA1 area through the “Schaffer collateral”. Finally, CA1 pyramidal cells send connections to subiculum. Neither dentate gyrus, CA1 or subiculum send connections back to the preceding neurons, therefore in this pathway the information travels mostly in one direction across the different parts of the hippocampal formation. Moreover, both CA1 and subiculum project to the entorhinal cortex, forming a loop circuit.

However, as mentioned before, there are other connections that complete this scheme and turn it into a more complex network. CA3 pyramidal neurons send connections to the mossy cells of the hilus and even to the molecular layer (Li et al., 1994) and they exert recurrent excitation on themselves (Amaral & Lavenex, 2007). Additionally, entorhinal cortex also sends projections to CA3, CA1 and subiculum, providing these areas with input information from the environment. Finally and very importantly, every excitatory connection of this circuit contacts not only principal neurons, but also local interneurons at their target sub-areas; in some cases (like for dentate gyrus-CA3 connections) these collaterals to interneurons even represent the majority of the output, and in general they provide the circuit with very precise and complex regulatory mechanisms, which will be discussed in the present work.

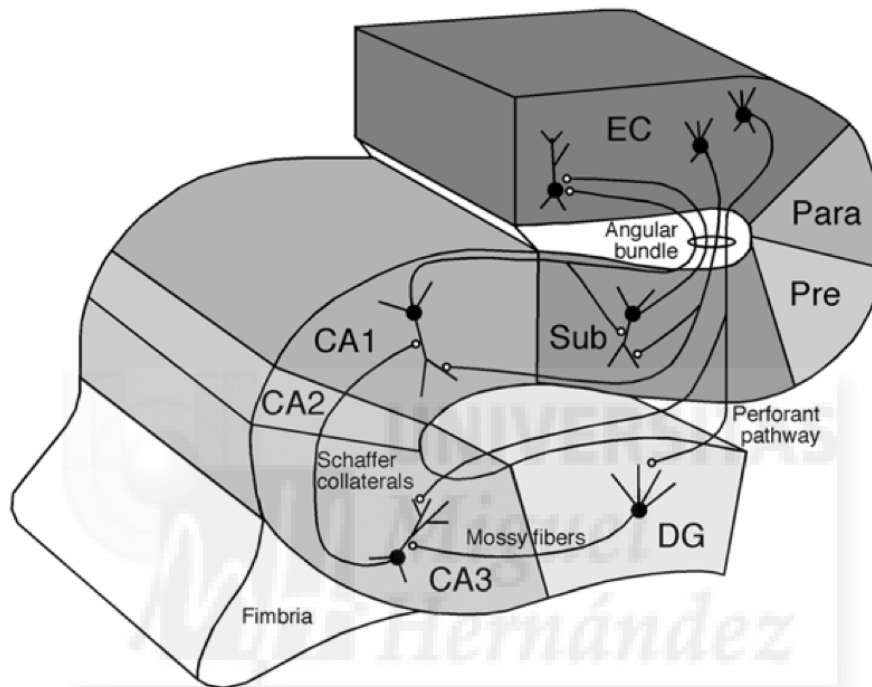


**Figure 1.2. Schematic illustration of intrinsic connectivity of the hippocampal system.** The different sub-areas of the system are represented as segments in different tones of gray along the folded lamina. The black big dots represent the neurons' somas of principal cells; black lines are axons connecting the different sub-regions, with blank small circles in the end representing synapses. This illustration provides a summary of the main intrinsic connections of the hippocampal formation. EC=Entorhinal Cortex; Para=parasubiculum; Pre=Presubiculum; Sub=Subiculum; DG= Dentate gyrus. (Adapted from Amaral & Lavenex, 2007).

### ***Cellular organization of the hippocampus***

In general, for dentate gyrus, CA and subiculum, we can recognize a common cytoarchitecture. They have one layer of principal cells, always tightly packed and easily recognizable. The dendrites of those neurons are strictly distributed in one or two directions, forming and occupying adjacent layers. The different intrinsic and extrinsic connections and axonal pathways are distributed rigorously in separated domains of the dendritic layers. There are sparse populations of interneurons in every layer, with many different distributions of dendritic and axonal trees (Freund & Buzsaki, 1996). In the next paragraphs we review in detail the specific characteristics of each of the sub-areas of the hippocampus.

The **dentate gyrus** is formed by three layers. From the outermost to the innermost, we find first the

molecular layer, consisting fundamentally of the dendrites of the granule cells, the principal neurons of this structure. There are also at least two types of interneurons present in this layer (Soriano & Froscher, 1989). The main input to this layer is the perforant path, which terminals end either in the middle third of the layer (if they come from the medial entorhinal area) or in the distal third (if they come from the lateral entorhinal area). The next layer is the granule cell layer, containing the somas of those neurons very tightly packed. The internal portion of this layer is one of the two places that are known to produce new neurons in the adult mammalian brain (Altman & Das, 1965). The last layer is the hilus, also known as “polimorphic layer”, that has a more irregular structure and contains a heterogeneous population of neurons (Amaral, 1978). This layer is crossed by all the axons of the granule cells (called “mossy fibers”) in their way towards CA3. Also, this layer contains two important elements. First, a population of large, excitatory neurons called mossy cells, that receive input from collaterals of the mossy fibers and from CA3 pyramidal neurons, and that send in turn their axons to the proximal third of the dendrites of the granule cells, at both ipsilateral and contralateral hemispheres, defining the associative/commissural pathway of the dentate gyrus (reviewed by Scharfman & Myers, 2013). And second, in the hilus there is an abundant and diverse population of interneurons, which is partly unknown concerning its morphology and neurochemical nature (Amaral, 1978; Amaral & Lavenex, 2007). Among them there are the basket cells and the axo-axonic cells (also called chandelier cells). These two subtypes of interneurons are located close to the granule cell layer and their axon terminals form plexuses surrounding granule cells' somas and dendritic proximal segments (basket cells) and axons initial segments (axo-axonic cells). Due to this very specific connectivity they exert a strong control over information output and have the capacity to coordinate large networks of granule cells (reviewed by Houser, 2007). There are other interneurons located in the hilus (which comprise in turn several sub-groups) that project to the dendrites of granule cells; together with interneurons from the molecular layer that contact dendrites as well, this group of cells may have an important role regulating how granule cells respond to their inputs. This heterogeneous population of interneurons in the hilus is of special interest in the context of the present work.

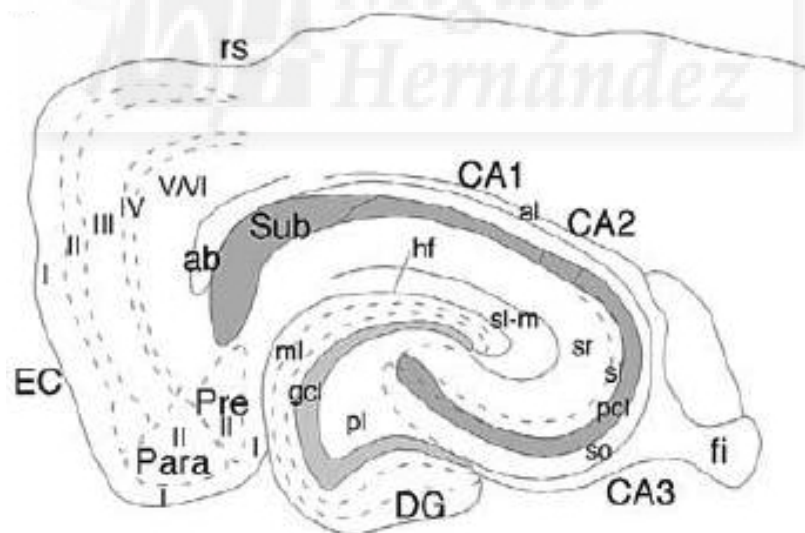


**Figure 1.3. Drawing of the different sub-areas and layers of the hippocampal formation.** Transversal cut of the hippocampus at its most temporal level, marking with straight and dashed lines the divisions and sub-divisions between and inside layers, respectively. In gray are marked the areas occupied by principal neurons' somas. EC=Entorhinal Cortex; Para=parasubiculum; Pre=Presubiculum; Sub=Subiculum; DG=Dentate gyrus; ml=molecular layer; gcl=granule cell layer; pl=polimorphic layer (or hilus); so=stratum oriens; pcl=pyramidal cell layer; sl=stratum lucidum; sr=stratum radiatum; sl m=stratum lacunosum-moleculare; hf=hippocampal fissure; al=alveus; fi=fimbria; ab=angular bundle; roman numbers=cortical layers. (Adapted from Amaral & Lavenex, 2007).

**CA3 and CA1** regions share their main anatomical characteristics. They have also one layer of pyramidal cells that are densely packed forming the pyramidal-cell layer. The dendrites of these neurons form two branches in opposite directions, superior and inferior. The superior dendritic trees form a layer called stratum oriens, and the proximal part of the inferior trees form the stratum radiatum. In CA3 area, the most proximal portion of the stratum radiatum is differentiated and called stratum lucidum, and it is there where the axon terminals of the mossy fibers make contact. The distal end of the inferior dendritic tree is called stratum lacunosum-moleculare, and it receives specifically a direct input from the entorhinal cortex (called the temporo-ammonic pathway). The axons of CA3 pyramidal cells make contact with CA1 pyramidal cells at the proximal part of the stratum radiatum, and CA1 send its axons to an equivalent part of the subiculum (see below).

**Subiculum** is the last sub-area of the hippocampal loop circuit that we mentioned before. It has an analogous cytoarchitecture to that of CA3 and CA1 areas, although it lacks a second dendritic layer like the stratum oriens. The pyramidal cell layer is bigger and less dense, and the dendritic layer (called molecular layer) receives connections from CA1 (in its proximal part) and from entorhinal cortex (in its distal part). It is however the major source of output of the hippocampus; it projects to all parts of entorhinal cortex and to other neocortical and sub-cortical areas (see below).

### ***Extrinsic connections of the hippocampal formation***

The hippocampus receives (and sends) connections from and to cortical and subcortical regions of the brain.

One of the main **sub-cortical projections** comes from the septum, specifically from the medial septal nucleus and the diagonal band of Broca, and it contacts neurons in the dentate gyrus, CA3, CA1 and subiculum. In the dentate gyrus it innervates, with GABAergic projections, GABAergic neurons in the hilus (mainly), and granule and mossy cells with cholinergic fibers; CA3, CA1 and subiculum have reciprocal connections with the septum. Hypothalamic nuclei send projections as well to dentate gyrus, CA2 and subiculum, and receive in turn projections only from subiculum. Innervation from the brain stem also reaches the hippocampus; they have been described noradrenergic (from locus coeruleus), dopaminergic (from ventral tegmental area) and serotonergic (from raphe nuclei) projections that reach dentate gyrus, CA3, CA1 and subiculum. Moreover, the medial thalamus sends efferents to CA1 and establishes reciprocal connections with the subiculum. Finally, the amygdaloid complex projects to CA3, CA1 and subiculum, though only CA1 projects back.

Concerning the **cortical connections**, the dentate gyrus and CA3 receive no other cortical input than the one from the entorhinal cortex, and they don't project but to the hippocampus proper. Conversely, CA1 and especially the subiculum have connections with several cortical areas. CA1 receives its major cortical input from entorhinal cortex, although it is also contacted by perirhinal and postrhinal cortices. In turn, it sends efferents to entorhinal, perirhinal, retrosplenial and medial frontal cortices. The subiculum has a more extensive connectivity with cortex, therefore being the main output structure of the hippocampus. It receives a strong innervation from the entorhinal cortex, and in turn its major projection goes back to this cortex as well, but also to a series of other cortical areas: perirhinal, presubiculum and parasubiculum, orbito-frontal, prelimbic and infralimbic, anterior olfactory nucleus, retrosplenial and (weakly) anterior cingulate cortices.

**Entorhinal cortex** is considered itself a part of the hippocampal formation. It plays a key role in the function of this complex because it provides both the main input and the output from and to several different areas of the brain; it is located in the circuit so that it acts as the interface between the neocortex and the hippocampus. In the rat brain, they have been described connections from piriform,

temporal, frontal, insular, cingular, parietal and occipital cortices (Burwell & Amaral, 1998a, 1998b). The entorhinal cortex projects in turn to infralimbic, prelimbic, orbito-frontal, insular, perirhinal and postrhinal cortices, all polymodal or associative areas of the neocortex. The portion of the entorhinal cortex that limits with the perirhinal cortex projects to other sensory regions (the ones from which it receives afferents)(Sarter & Markowitsch, 1985); however there is a certain controversy regarding this point, because it is not yet clear whether the transition area should be considered part of the entorhinal or the perirhinal cortex (Amaral & Lavenex, 2007). In conclusion, it seems clear that the rat hippocampus receives a diverse polymodal input and does distribute information to high-level integrative areas of the brain.

### ***Differences across species***

The present study is done with rats, as the vast majority of the scientific literature concerning the hippocampus. However, it is important to note that the primate hippocampal formation (there are studies in monkeys and humans) is qualitatively different than that of rodents. This could mean that results and conclusions drawn from studies in rodents might not be directly extrapolated to monkeys or humans.

In general, the main structures and sub-regions are present, and the hippocampus is clearly recognizable by the eye in rats, monkeys and humans. Nonetheless, the structural complexity of the different sub-areas increases progressively from the dentate gyrus to the entorhinal cortex (following the order of the connections explained before), gaining relative size, number of cells and (remarkably) several sub-divisions with different laminar organization and greater complexity in the entorhinal cortex. Therefore, dentate gyrus would be the most conserved structure and the entorhinal cortex the most expanded among these species.

Regarding the hippocampus, the granule cell layer of the dentate gyrus is still densely packed in humans and monkeys, but the relative size of the hilus layer is smaller than in rats, and it is greatly occupied by CA3 pyramidal cells. Also, in monkeys part of the mossy cells have dendrites in the molecular layer and project to CA3. Remarkably, commissural connections of both dentate gyrus and CA3 are virtually absent in monkeys (Amaral et al., 1984).

On the other hand, there is an important similarity across species: in both rats and monkeys the entorhinal cortex is highly connected with multisensory associational cortices, either directly or indirectly through perirhinal and parahippocampal areas (the majority) (Insausti et al., 1987; Sarter & Markowitsch, 1985). Thus we can say that entorhinal cortex represents the major input of cortical information to the hippocampus in both rats and monkeys. This scheme of communication is fundamental to support the theories about systems consolidation of memory (see before). Unfortunately, it appears that there is not many data concerning the connections of the human hippocampal formation (Amaral & Lavenex, 2007).

### ***1.3. Synaptic plasticity in hippocampal circuits***

As we mentioned before, synaptic plasticity is thought of as the mechanism underlying memory formation, and it has been demonstrated its implication in functional reorganization across the brain that might be responsible for the consolidation of memories (Canals et al., 2009; Álvarez-Salvado et al., 2013). Therefore, to approach the present work it is necessary that we review some basic and key concepts regarding synaptic plasticity. It has been extensively studied in the hippocampal formation, and it is known to occur in excitatory synapses at every level of this structure (actually it is believed to occur in virtually every excitatory synapse in the brain). We will concentrate on some important

properties of synaptic plasticity (often speaking of LTP) and how they might affect local circuits and different neuronal populations.

First of all, it is important to say that there has been a huge amount of research about the exact cellular processes taking place during synaptic plasticity, from its induction to its expression and maintenance (Bliss et al., 2007); especially active has been the debate about the pre-synaptic or post-synaptic site of expression of LTP. However, in the present work we didn't address these issues, and we will only provide a general overview of synaptic plasticity at the cellular level, and then emphasize those aspects that might be of interest for understanding and discussing our study.

### ***Main properties of synaptic plasticity***

Summarizing, synaptic plasticity might occur at synapses that are repeatedly active, causing a change in the efficacy of these connections so that they respond more or less than normally. Its development may involve changes in the sensitivity to neurotransmitters and modulation of their release by the pre-synaptic terminal, as well as protein synthesis (reviewed by Bliss et al., 2007). Importantly, synaptic plasticity has several different functional properties that depend on different molecular mechanisms and that allow its role modulating circuits' properties.

First, LTP is input-specific (Andersen et al., 1977; Lynch et al., 1977). This means that it happens selectively at -and only at- the terminal synapses of a specific subset of potentiated axons. This is important because allows that specific channels of information, in the form of a unique group of axons, are potentiated. If we think that any information (for example, a conversation) is represented in the brain as a unique spatio-temporal pattern of activations, conducted through an equally unique set of neurons and axons, the input-specificity of synaptic plasticity equals to a different processing for every piece of information, or more generally speaking, for every single event or episode in our lives.

Another important property of LTP that has been studied at hippocampal circuits is associativity, a feature that allows that the activity in two different neighboring pathways influences activity on each other in a durable manner (McNaughton et al., 1978; Levy & Steward, 1979). This was demonstrated combining simultaneous weak stimulation -incapable of potentiation by itself- in two convergent pathways (Barrionuevo & Brown, 1983), or pairing weak stimulation with prior depolarization of the target cells (Kelso et al., 1986); in all cases the manipulations facilitated the emergence of LTP. This property is important because it provides a synaptic mechanism for binding simultaneously occurring events. It supports information integration, allowing that prior or simultaneous activity in the local network changes the effect of activity-dependent plasticity at a given moment.

The above mentioned properties of LTP may be partly explained from a molecular point of view by the properties of the NMDA receptors. These ionotropic receptors for glutamate are voltage dependent (Ferguson and Wojtowicz, 1980), because of the blockade of the channel by  $Mg^{2+}$  in normal conditions. Thus they require the joint activation of the pre-synaptic and the post-synaptic terminal in order to open. Also, their high permeability to  $Ca^{2+}$  (MacDermott et al., 1986; Jahr and Stevens, 1987, 1993) ensures that they trigger the protein-kinase reactions necessary for expression of LTP (Lynch et al., 1983). However, this is not the only molecular mechanism for LTP -though it may be the most frequent-, since it has been described in different connections that LTP can occur without the mediation of NMDA receptors (Harris & Cotman, 1986), like for example in dentate gyrus-CA3 projections.

### ***Long-Term Depression***

So far we have emphasized synaptic plasticity from the point of view of potentiation, i.e. the

strengthening of synaptic efficacy. However, it is known that synapses can also decrease their efficacy (Lynch et al., 1977; Levy & Steward, 1979). The experimental phenomenon measured in this regard is called “long-term depression” (LTD). It also exists another mechanism known as “depotentialiation”, that corresponds more precisely to the decay or erasure of LTP. LTD is known to be dependent on either NMDA receptors or metabotropic glutamate receptors (mGluR) (Oliet et al., 1997). It can be expressed either only post-synaptically (NMDA receptor dependent) or both pre- and post-synaptically (mGluR-dependent).

Although the role of LTD in learning and memory is not fully understood, it is normally conceptualized as the counterpart of LTP. If it was only possible to potentiate synapses, at some point they would be saturated and no further learning would be possible (Moser et al., 1998). Moreover, it has been proved that these mechanisms increase the flexibility and storage capacity of the system (Dayan & Willshaw., 1991). Importantly, stabilizing the level of excitation helps to prevent abnormal neuronal activity that could lead to altered states (Traub et al., 2005; del Pino et al., 2013).

### ***Influence of synaptic plasticity on hippocampal local networks***

Since synaptic plasticity inherently changes the microscopic structure of synapses, it necessarily affects the dynamics of the local network because it modifies the local circuit's properties.

One of such cases is that of EPSP-to-Spike (E-S) potentiation (Bliss & Lømo, 1973). Although usually in the hippocampus synaptic potentiation provokes an increase in the EPSP (input) and a proportional increase in the population spike (PS) (output) of the affected neurons, sometimes this relation may be non-linear, so the increase of the PS is bigger than what could be predicted by the increase of the EPSP. There is evidence supporting that it could be due to changes in inhibitory synapses on the principal cells (Lu et al., 2000), changes in the excitatory synapses on the interneurons (Laezza et al., 1999), or changes in the intrinsic excitability of principal cells, and different molecular mechanisms could be operating behind this (Bliss et al., 2007). Therefore, E-S potentiation can be a mechanism to regulate communication with subsequent targets thanks to an increase in the probability of transmitting action potentials “downstream”.

In line with this, it is important to know that synaptic plasticity may affect different neuronal populations in different ways. It is known that a high frequency stimulation can induce potentiation in synapses on excitatory neurons (Bliss & Lømo, 1973), but it was proved that the same protocols may induce different changes in synapses contacting inhibitory interneurons. It may depend on factors like a different subunit composition in the glutamate receptors (McBain et al., 1999; Lawrence & McBain, 2003), the type of input activity (or stimulation protocol), the exact location of the cell, its subtype among interneurons or its membrane potential (reviewed by Bliss et al., 2007). On the other hand, it has been demonstrated that both LTP and LTD can occur in GABAergic synapses on pyramidal cells (Shew et al., 2000; Lu et al., 2000; Chevaleyre & Castillo, 2003); more importantly, it was observed that it happened at the same time as LTP in the same connected cells, which proves that plasticity affects differently different neuronal populations.

Another way in which plasticity may affect the local network is through heterosynaptic depression. It was first described by Lynch and colleagues (1977), and it has been most studied in the perforant path (Levy & Steward, 1979). It consists in a depression (or depotentialiation) of nearby non-activated synapses by the activity of a given pathway. For example, there are two portions of the axon bundle of the perforant path (medial and lateral), and induction of LTP in one causes LTD in the other (Abraham & Goddard, 1983). This mechanism might work to give preferential pass to certain information and hamper the rest, thus helping to channel relevant information, or to down-regulate inactive synapses, decreasing noise interference and saving metabolic energy.

### ***Influence of hippocampal local networks on synaptic plasticity***

Besides the effects of plasticity on the network, the network can affect plasticity; i.e. the local circuitry may be set up so that plasticity exerts very specific changes in information processing. This happens particularly in feed-forward inhibitory connections. It is known that activation of an afferent pathway (for example perforant pathway or Schaffer collateral) entails the activation of feed-forward interneurons and the subsequent release of GABA neurotransmitter. This will first activate the GABA<sub>A</sub> type receptors present on target excitatory neurons, thus hyperpolarizing them and intensifying the blockade of Mg<sup>2+</sup> on NMDA receptors (Herron et al., 1985; Dingledine et al., 1986), decreasing the probability that they activate. Such state makes more difficult the occurrence of synaptic potentiation, and thus it could constitute a mechanism for limiting plasticity upon single-pulse activations (that could possibly result from simply unimportant information). After activating GABA<sub>A</sub> receptors, the GABA also activates GABA<sub>B</sub> autoreceptors present on the presynaptic terminal, what will lead in turn to a decrease in the release of GABA neurotransmitter. This implies that after activation of feed-forward interneurons, there will be a time window of decreased inhibition on the excitatory neurons, with a maximal effect from 100 to 200 ms after the activation (Davies et al., 1990). This mechanism could serve to facilitate plasticity upon repetitive activation. In this regard, it is interesting to note that the possible frequencies of this GABA<sub>B</sub>-mediated effect would be between 5 and 10 Hz, the frequency of the Theta-band oscillations, because actually it has been shown that there is a different modulation of synaptic plasticity during the different phases of the hippocampal Theta cycle (Pavrides et al., 1988; Holscher et al., 1997; Orr et al., 2001; Hyman et al., 2003). This oscillation is known to be especially strong during locomotion and exploration, and so this mechanism could be underlying a facilitation of plasticity during such relevant behavioral states (Bliss et al., 2007).



## II. OBJECTIVES

Knowing that LTP in the hippocampus is critically involved in memory acquisition and that it actually induces a long-range functional reorganization in the brain (Canals et al., 2009), we concluded that there must be changes taking place in the hippocampal network that cause and support these observations; furthermore, we wondered whether the same phenomena are involved in learning. Therefore, with the present work we aimed for understanding how synaptic plasticity leads to network plasticity in the hippocampus; i.e. how plasticity at the synaptic and cellular level can provoke quantitative changes in other nearby connections with different neurons, and in nearby connections not directly involved in the microcircuit originally modified. To achieve this, we pursued two subsequent objectives:

1- To investigate in depth the mechanisms taking place in the hippocampus during synaptic potentiation of the perforant path, that allow a functional reorganization of the whole brain network.

2- To study whether the same or similar phenomena could be found in an awake animal experiencing physiological learning instead of electrically induced Long-Term Potentiation (LTP).

Our experimental model was the rat, both in anesthetized and awake preparations. In order to achieve the first objective, we had the following goals:

-To develop an experimental preparation in which to simultaneously record and stimulate the hippocampus, as well as inject drugs locally, in the anesthetized rat. Such preparation would allow us to study and manipulate the hippocampal network in well controlled conditions, which is necessary to reach conclusions about its basic function.

-To identify the different Local Field Potential (LFP)-generators in hippocampal recordings of spontaneous activity. The LFP-generators (obtained with independent component analysis) allow us to study separately different elements of the local networks without altering their activity, and therefore constitute a basic tool to carry out a proper characterization of their role in hippocampal function.

-To study the behavior of the hippocampal LFP-generators during potentiation of the perforant path and during pharmacological manipulations. LTP of the perforant path represents an experimental model for learning, approaching our main goal of studying the mechanisms behind memory formation. The pharmacological procedures permit, on the other hand, a deeper testing and understanding of the putative neuronal populations involved in such process and what their roles might be.

For the second objective, we had the following goals:

-To develop chronic implants for simultaneously recording and stimulation of the hippocampus in an awake animal, while allowing to perform behavioral tasks with during the recording. This type of preparation becomes fundamental in order to test the effects of the behavior of an animal in physiological conditions without directly manipulating the neuronal circuits.

-To design and carry out a behavioral task that mirrored as much as possible the qualitative properties of the electrical tetanization: instantaneous and unique stimulation with accurate behavioral

correlates. Such features facilitate the reliability of the analysis of the results and their interpretation, being easier to identify relevant behavioral correlates of the electrophysiological activity.

-To study the behavior of the hippocampal LFP-generators during the behavioral task, trying to establish whether the results are comparable or not to any observations made in the anesthetized animals. In this way, the data from anesthetized animals (that have in turn an abundant background support in the scientific literature) serve as support and validation for results obtained in the awake animals.



## III. MATERIALS AND METHODS

### 3.1. Experiments on anesthetized rats

In these experiments we implant acute recording and stimulating electrodes in the hippocampus and perforant path, respectively, and recorded the spontaneous and evoked activity in different conditions (i.e. before and after synaptic potentiation of the entorhinal input, or during the local administration of different drugs).

#### *Animals used*

We used male Sprague-Dawley rats, with a weight of 250-300 g. All animal procedures were approved by the corresponding ethical committee (IN-CSIC) and were performed in accordance with Spanish law (32/2007) and European regulations (EU directive 86/609, EU decree 2001-486).

#### *Surgery and preparation*

The rats were anesthetized with 1.2–1.5 g/kg of urethane (Sigma-Aldrich, Missouri, USA) injected intraperitoneally. Supplemental doses (10-20% of initial dose) were applied on appearance of the withdrawal reflex in response to foot pinching. When the absence of reflexes was confirmed, animals were placed in a stereotaxic frame (Narishige, Tokyo, Japan). After injecting subcutaneously a dose of 8 mg/kg of local anesthetic (Bupivacaine, Braun Medical S.A., Barcelona, Spain) the scalp and periosteum were separated and the skull opened over the recording and stimulation sites with a manual drill. The dura was carefully punctured at the craniotomies with a needle, making the smallest hole possible to facilitate the penetration of the electrodes.

For orthodromical stimulation of the dentate gyrus, a tungsten bipolar electrode (10-15 k $\Omega$ , 325  $\mu$ m diameter, World Precision Instruments, Florida, USA) was positioned in the medial perforant path (coordinates with respect to lambda: A-P 0 mm, M-L 4.1 mm, 2.3–2.7 mm ventral to the dural surface, with an angle of 15° at the sagittal plane directing the tip to rostral). All the coordinates used in this work were taken from Paxinos and Watson (2007). A multielectrode silicon probe (32 recording sites, 100  $\mu$ m inter-site distance, 413  $\mu$ m<sup>2</sup> electrode area, Neuronexus Technologies, Michigan, USA) was placed at the dorsal hippocampus to record the LFP (coordinates with respect to bregma: A-P -3.5 mm, M-L 2.6 mm, 3.2-3.5 mm ventral to the dural surface). An Ag/AgCl wire (World Precision Instruments, Florida, USA) electrode was placed in contact with the skin on the sides of the surgery area, and used as ground. We adjusted the final position of both electrodes using as a reference the typical evoked potentials at the dentate gyrus (Andersen et al., 1966), so that a maximal population spike (PS) in the dentate gyrus was recorded. The position was further confirmed by means of *post-mortem* histology techniques thanks to prior immersion in a DiI-Ethanol solution of the recording electrode. Figure 3.1 shows a scheme of this experimental preparation.

The brain electrophysiological signals were filtered (high-pass 0.1 Hz), amplified and digitalized (20

kHz acquisition rate) (Multi Channel Systems, Reutlingen, Germany), and stored for posterior analysis with Matlab (The Mathworks Inc., Massachusetts, USA), Spike2 (Cambridge Electronic Design Ltd., Cambridge, UK) and custom made software. During the whole duration of the experiment the temperature of the animal was monitored and kept at 37°C, the vital signs were monitored (heart rate, breath rate, oxygen saturation) and oxygen was provided.

After the experiments, the animals were transcardially perfused with saline solution and paraformaldehyde 4% (BDH Prolabo, VWR International, Leuven, Belgium), and the brain collected for histological analysis. The brain was cut in 100 µm thick slices and stained with DAPI (4',6-diamidino-2-phenylindole), and later images were captured under a fluorescence magnifying glass. In the resulting pictures the position of the electrodes could be easily seen (Figure 3.2).

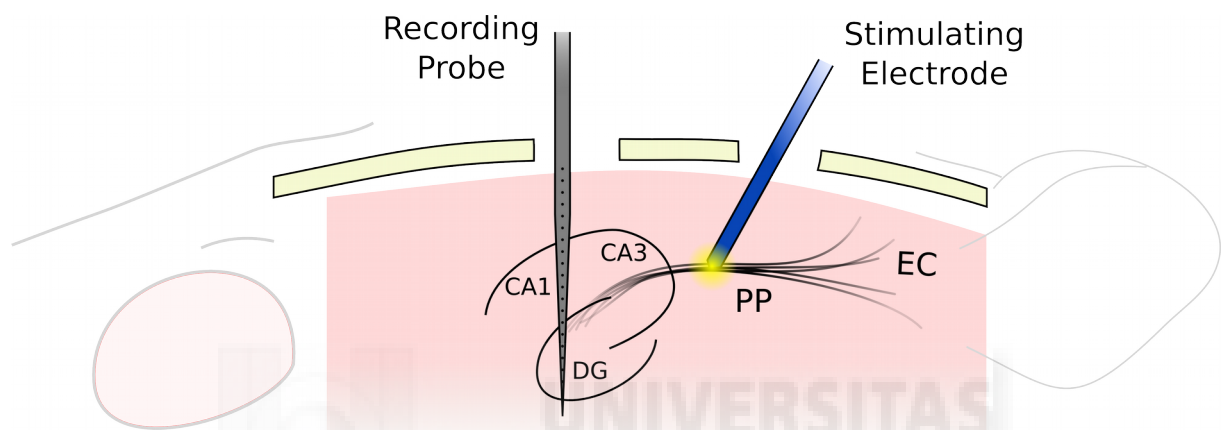


**Figure 3.1. Illustration of the experimental preparation.** This drawing represents schematically a part of the head of the animal (background light traces) and the experimental preparatio. The pink area represents the brain and the light-yellow bands the cranium bone, opened at the sites of penetration of the electrodes (Recording electrode probe: gray; stimulating bipolar electrode: blue). At the tip of the stimulation electrode traverses the perforant path (bundle of black lines) in its way from entorhinal cortex (“EC”) to the dentate gyrus (“DG”); the volume affected by the current from the stimulation electrode is marked as a light yellow circle. Under the recording probe is drawn a scheme of a coronal cut of the dorsal hippocampus, with the different sub-areas indicated; note that the electrode crosses both CA1 and dentate gyrus areas.

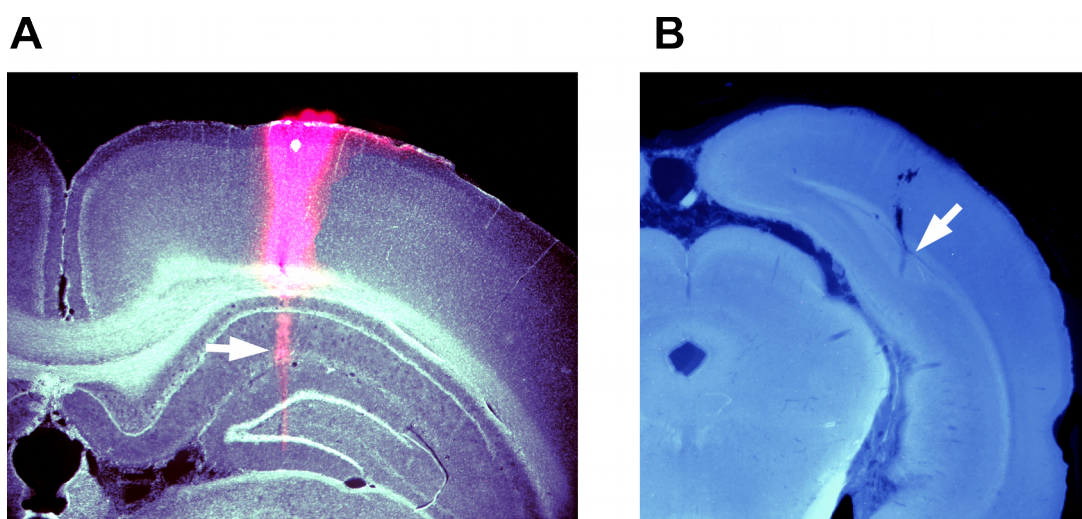


**Figure 3.2. Hystological *post mortem* location of the electrodes for the anesthetized experiments.** Representative examples of the position of the recording (A) and stimulating (B) electrodes, done in coronal cuts

of the rat brain at the level of the dorsal hippocampus and perforant path, respectively. The position of the recording electrode was observed in the pink fluorescence (white arrow in A) (due to the DiI staining). The stimulation electrode leaves an observable scar in the tissue (white arrow in B).

### ***LTP induction***

LTP was regularly induced using a high-frequency stimulation protocol of the perforant path (Davis et al., 2000). This tetanic stimulation consisted of six trains of pulses (400 Hz, lasting 20 ms), delivered at a 10 s interval, and repeated six times at an interval of 2 minutes. In a series of experiments, an alternative LTP-inducing protocol (theta-burst stimulation), was used in which five trains of pulses (100 Hz, lasting 30 ms) were delivered at a 150 ms interval and repeated three times at an interval of 1 minute. To evaluate the synaptic potentiation, we measured the population spike, ("PS", as the amplitude from the precedent positive crest to the negative peak in the hilar evoked LFP) and the excitatory post-synaptic potential ("EPSP", as the maximal negative slope of the falling potential in the molecular layer evoked LFP) at different stimulation intensities (the so called input-output curve). We collected Input-Output curves before, immediately after and up to 3 hours after the tetanizing protocol. These curves consisted of a series of stimuli delivered at low frequency (0.05-0.1 Hz) and at increasing current intensities, ranging from mild subthreshold stimulation to suprathreshold saturating intensities. The analysis of the evoked potentials collected in this way allowed us to quantify different parameters of the local response to electrical stimulation.

### ***Pharmacological experiments***

In some experiments, in addition to the stimulating and recording electrodes, a borosilicate glass pipette (World Precision Instruments, Florida, USA) was implanted to deliver different pharmacological agents (dissolved in artificial cerebrospinal fluid). The pipettes were further equipped with Ag/AgCl electrodes to guide their precise implantation. The pipette was implanted in the hilus tightly close to the multielectrode probe, guided to the hilar layer of the dentate gyrus by the recorded evoked potentials. To allow a close proximity to the recording probe, the pipette tip was bent in an angle of approximately 90°. In another group of experiments, the pipette with drug was placed in the perforant path, rostral and close to the stimulation electrode. In all cases, the drug was released through the pipette with an air puff delivered with a picospritzer (custom-built), except for the Gabacine, that was administered by microiontophoresis. Control experiments with artificial cerebrospinal fluid demonstrated absence of non-desired electrophysiological changes due to volume injection in the above conditions. Additional test of injection specificity were performed in which an additional tungsten bipolar stimulation electrode (10-15 k $\Omega$ , 325  $\mu$ m diameter, World Precision Instruments, Florida, USA) was placed in the CA3 area (with respect to bregma: A-P -1.2 mm, M-L 2.6, 3 mm ventral to the dural surface, with a 30° angle at the sagittal plane directing the tip to caudal) to stimulate orthodromically CA1 pyramidal neurons. This stimulus was used to obtain evoked potentials at the CA1 area and check the absence of drug spill-over (and the resulting effect on LFP) into other hippocampal territories. An illustration of this preparation is shown in Figure 3.3.

The drugs used for these experiments were Gabacine 1 mM (SR95531 hydrobromide, GABA<sub>A</sub> type receptor-specific antagonist; Tocris Bioscience, Bristol, UK), Bicuculine 100  $\mu$ M (Bicuculine metiodide, GABA<sub>A</sub> type receptor-specific antagonist; Sigma-Aldrich, Missouri, USA), CGP 1 mM (CGP 52432, GABA<sub>B</sub> type receptor-specific antagonist; Tocris Bioscience, Bristol, UK), AP5 30 mM (D(-)-2-Amino-5-phosphonopentanoic acid, NMDA receptor antagonist; Sigma-Aldrich, Missouri, USA), TTX 100  $\mu$ M (tetrodotoxin, voltage-gated sodium channels blocker; Sigma-Aldrich, Missouri, USA)

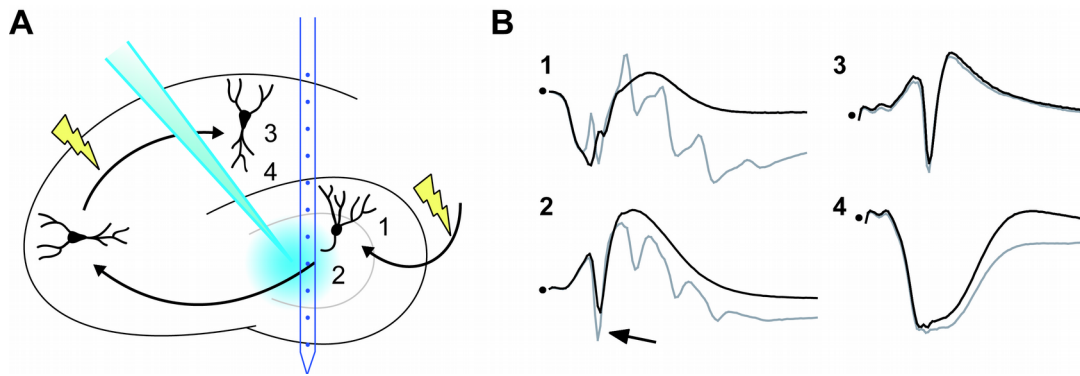


**Figure 3.3. Illustration of the preparation for the pharmacological experiments.** (A) Scheme of the preparation on a drawing of a hippocampal coronal cut with arrows and neurons representing the main axonal pathways. The vertical blue array with dots marks the recording electrode; obliquely located, in cyan is represented the pipette, with the tip placed in the hilus and a diffuse cyan-colored area illustrating the theoretical area of effect of the injection; marked with yellow lightnings are the sites of stimulation; signaled with numbers are the locations where the different evoked-LFP were recorded (1-molecular layer, 2-hilus, 3-CA1 pyramidal layer, 4-CA1 stratum radiatum). (B) Representative example traces of supra-threshold evoked-LFP recorded at such sites during administration of Gabazine, before (black traces) and during the drug effect (gray traces). Marked with a black arrow under number 2 is the bigger size of the PS evoked in the hilus, which was followed by subsequent multiple PS. Note the absence of changes in the slope of the EPSP at both molecular layer and stratum radiatum, as well as in the population spike evoked in CA1.

### **fMRI-pharmacological experiments**

The anesthesia and surgery procedures were performed as described above, and were implanted with MRI-compatible recording and stimulation electrodes. The recording electrode consisted of a borosilicate glass pipette; it had a Ag/AgCl wire inside, it was filled with Gabazine 1 mM solution, and it had the tip bent approximately 90°, so it could go inside the brain leaving the main body of the pipette outside parallel to the head of the rat, thus allowing the minimum space between the animal brain and the radio-frequency coil used for imaging. This configuration maximizes signal-to-noise ratio in the functional images. The tip of the pipette was positioned in the hilus using the coordinates previously described. The custom made stimulation electrode consisted of glass insulated carbon fibers (see below), bent as previously described for the pipettes for the pharmacological experiments. This electrode was positioned in the Perforant Path using the coordinates previously described. After positioning the electrodes, they were fixed to the skull with dental cement (Palacos, Heraeus Medical GmbH, Wehrheim, Germany), after applying a small drop of biological tissue-compatible glue (3M Animal Care products, Minnesota, USA) to the surface of the bone to improve the bond with the cement.

For the MRI data collection, animals were transferred to the magnet room, placed in a custom-made animal holder with movable bite and ear bars and positioned fixed on the magnet chair. This allowed precise positioning of the animal with respect to the coil and the magnet and avoided movement artifacts. Animal body temperature was monitored and kept at physiological temperature (37°C) using a water blanket. Experiments were carried out in a horizontal 7 Tesla scanner with a 30 cm diameter bore (Biospec 70/30v, Bruker Medical, Ettlingen, Germany). The system had a 675 mT/m actively shielded gradient coil (Bruker, BGA 12-S) of 11.4 cm inner diameter. A 1H rat brain receive-only phase array coil with integrated combiner and preamplifier, and no tune/no match, was employed in combination with the actively detuned transmit-only resonator (Bruker BioSpin MRI GmbH, Germany). Functional MRI (fMRI) was performed in 15 coronal slices using a Gradient Echo Echo-Planar Imaging (GE-EPI) sequence applying the following parameters: Field of View (FOV), 25 x 25 mm; slice thickness, 1 mm; matrix, 96 x 96; segments, 1; Flip Angle (FA), 60°; Echo Time (TE),

15 ms; Repetition Time (TR), 2000 ms. Data were acquired during electrical stimulation of the Perforant Path both before and after Gabazine administration. The stimulation consisted in 10 stimulation trains of 4 s duration at 5 and 10 Hz, delivered every 30 s. As anatomical reference for the functional maps, high resolution T2-weighted anatomical images were collected using a rapid acquisition relaxation enhanced sequence (RARE): : FOV, 25 x 25 mm; 15 slices; slice thickness, 1 mm; matrix, 192 x 192; TE, 56 ms; TR, 2 s; RARE factor, 8.

### ***MRI-compatible carbon fiber electrodes***

Glass-coated carbon fiber monopolar electrodes were developed for the present study based on previous reports (Shyu et al., 2004). Individual 7 mm long, 7  $\mu$ m diameter carbon fibers (Goodfellow Cambridge Limited, England) were used. These consisted of a bundle of fibers inserted into a theta-shaped glass capillary (World Precision Instruments, Florida, USA) previously pulled to form 7 mm long pipettes with  $\sim$ 200  $\mu$ m tip diameter and adjusted to produce an electrical impedance of 40-65 k $\Omega$ . A regular wire with a pin connector was attached to the pipette, connected to the carbon fibers using silver conductive epoxy resin (RS Components, UK), and isolated with clear epoxy resin. Afterwards, the tip was bent in a flame to form a 90° angle to minimize implant size, and thereby allow close proximity between the MRI array coil and the head of the animal.

### ***3.2. Experiments on awake rats***

In these experiments we implanted rats with recording and stimulation electrodes, and trained and tested them in a series of behavioral tasks, done consecutively over the days, while we recorded the electrophysiological activity of the hippocampus.

#### ***Animals used***

We used male Long-Evans rats, with a weigh of approximately 250 grams at the day of implantation. All animal procedures were approved by the corresponding ethical committee (IN-CSIC) and were performed in accordance with Spanish law (32/2007) and European regulations (EU directive 86/609, EU decree 2001-486).

#### ***Housing***

The rats were housed in the animal facilities, with water and food *ad libitum*, and in a 12 hours light cycle; the experiments were carried out during the light phase (07:00-19:00).

#### ***Experimental room***

The room where all the experiments took place was specially devoted to this purpose. The apparatuses were placed for the tasks inside a rectangular enclosure of four panels 2 m high, covered with black fabric to the floor and placed at least 50 cm apart from the apparatuses. The room was dimly lightened up with too small spotlights placed on the floor out of the enclosure and directed to the ceiling, producing an indirect symmetric illumination. On the panels corresponding to the laterals and the back of the enclosure, different visual cues were attached. The cues were 65 cm wide and 50 cm high, and consisted of patterns of paralel black and white stripes 5 cm wide, one horizontal and the other vertical, and a black background with white spots of 7 cm of diameter.

### ***Habituation***

In order to habituate the animals to the experimenter and the required manipulations (mainly electrode connection/disconnection), they were first handled for 5 consecutive days, two times per day (in the morning and in the afternoon) during 1 to 5 minutes. Starting from gentle caresses on the back of the animal the first day, we introduced different and more “daring” manipulations as we detected a decrease in the animals' signs of stress. After the habituation process, the animals showed no signs of stress or resistance while being grabbed and immobilized, or walking on the arms of the experimenter. Importantly, they were habituated to the presence and movements of the experimenter too, by leaving them in the experimental room during the brief daily maintenance (no more than 10 minutes), which exposed them to a moderate level of noise; this could prevent possible disturbances because of accidental noises during the tasks.

### ***Surgery for electrodes implantation***

The animals were anesthetized with isoflurane (Braun Medical S.A., Barcelona, Spain) (mixture of oxygen and isoflurane in concentrations from 1 to 5%). An initial dose of 5% and was administered in a transparent methacrylate induction chamber for no longer than 5 minutes, until the animal showed no withdrawal reflexes and had regular vital signs. Then it was transferred to a heating blanket, and the dose was reduced to 1,5-2,5% and maintained at this level during the rest of the surgery, adjusting it when the vital signs fluctuated. The hair on the head of the animal was cut and shaved, the area cleaned with a solution of povidone-iodine 10%, and a dose of 8 mg/kg of local anesthetic was injected subcutaneously (Bupivacaine, Braun Medical S.A., Barcelona, Spain). Additionally, we administered subcutaneously an analgesic on the back of the rat (Buprenorphine, dose 2-5 µg/kg, RB Pharmaceutical Ltd., Berkshire, UK), so that the effect was maximal by the time the rat would wake up after the operation. The surgical procedure, the stereotaxic coordinates and the method for positioning the electrodes were the same as described before for the experiments on anesthetized rats.

The recording electrode was a multisite silicon probe (Neuronexus Technologies, Michigan, USA) specially designed with a miniature connector. This electrode was connected in turn to a jumper consisting of two corresponding connectors joined by 5 cm of flexible cable (Neuronexus Technologies, Michigan, USA), that later during the experiments would allow the daily connection to be made on the jumper and not on the electrode itself. This ensured that no pressure was done on the implant or the head of the animals, decreasing greatly the possible distress of the animals. The wires of the jumper were kept out of the cement during the preparation and tightly rolled up in the Faraday cage (see below). The stimulating electrode was bipolar and custom-built, made by twisting together two teflon-coated 0.1 mm diameter platinum-iridium wires (World Precision Instruments, Florida, USA). 6 watchmaker screws were fastened to the frontal, parietal and occipital bones for anchorage of the implant (two of them with a short copper wire soldered, to work as ground and reference sites). A small drop of biological tissue-compatible glue (3M Animal Care products, Minnesota, USA) was applied to the surface of the bone to improve the bond with the cement. Next, several layers of dental cement were applied consecutively until the screws and the electrodes were completely embedded (Palacos, Heraeus Medical GmbH, Wehrheim, Germany). Additionally, one piece of thin copper mesh was attached to the cement surrounding it. This was done after the first or second layer of cement, and once applied the last layer of cement, the mesh was soldered close and shaped forming a cylinder that covered the implant, building a Faraday cage. The reference wire of the recording electrode was soldered to the bone-reference wire, and the ground wires both from the bone and the recording electrode were soldered to the Faraday cage. The connectors of the stimulating and recording electrodes were attached inside the cage close to the border, to allow easy connection. A layer of dental

cement was applied covering the copper mesh, giving it consistence and filling the gaps to prevent damage from the rat paws.

After the surgery, the rats were left for at least 10 days until they recovered completely. During the first 72 hours, they were injected subcutaneously with analgesic twice per day (Buprenorphine, dose 2-5  $\mu\text{g}/\text{kg}$ , RB Pharmaceutical Ltd., Berkshire, UK). During 1 week, they had as well antibiotic dissolved in the water (Enrofloxacin, dose 10  $\text{mg}/\text{kg}$ , Syva, León, Spain). The behavioral tasks were not started until the animals showed no signs of discomfort with the manipulation of the implants.

### ***Electrophysiological and video recordings***

Before every behavioral session, the implanted electrodes were plugged to the recording and electrical stimulation equipment, leaving the cables hanging loose above the apparatus from an extendible light stand. The equipment had a swivel so the cables wouldn't twist and get stuck with the animals' movements. During every task, the LFP was continuously recorded at a 5000 Hz sampling rate. We also stimulated the perforant path at 0.1 Hz with low current intensities (30-100  $\mu\text{A}$ ) to evoke sub-threshold potentials.

We video-recorded all behavioural tasks using a web-camera (Logitech HD Webcam C310, Logitech International S.A., Lausanne, Switzerland) at a 14,57 frames per second rate. The camera was located over or next to the apparatus thanks to an extendible light stand. The videos were collected using a personal computer and user-level video recording software, and were stored for later analysis.

### ***Behavioral Novelty task***

The animals were first habituated to an open field, being allowed to freely explore it during 10 minutes every day for 8-10 days. The open field consisted in a black methacrylate box with an area of 50 x 50 cm, and 40 cm high, opened at the top. There was three different visual cues attached to three of the inner walls of the open field (see Figure 3.4 for a picture of the open field). We used a separate box for each rat; the floor was covered with rat home bedding, and the same bedding was kept for the whole duration of the experiment, so the animals could get used to their corresponding boxes and recognize them as familiar environments.

After the habituation period, we carried out a Novelty session. The rats were exposed to a novelty by introducing them in a “novelty chamber” located inside the familiar open field; such chamber was a transparent methacrylate box with a square base 35 cm wide, and 40 cm high, opened at the top, with sand paper on the floor to provide a noticeable tactile stimulus (see Figure 3.4 for a picture of the novelty chamber).

The test was done the day after the last session of the open field habituation. The novelty chamber was placed inside and in the middle of the familiar open field, and the rats were left inside for 10 minutes. After this time, the novelty chamber was removed and the animals were left another 10 minutes in the open field (Control session).

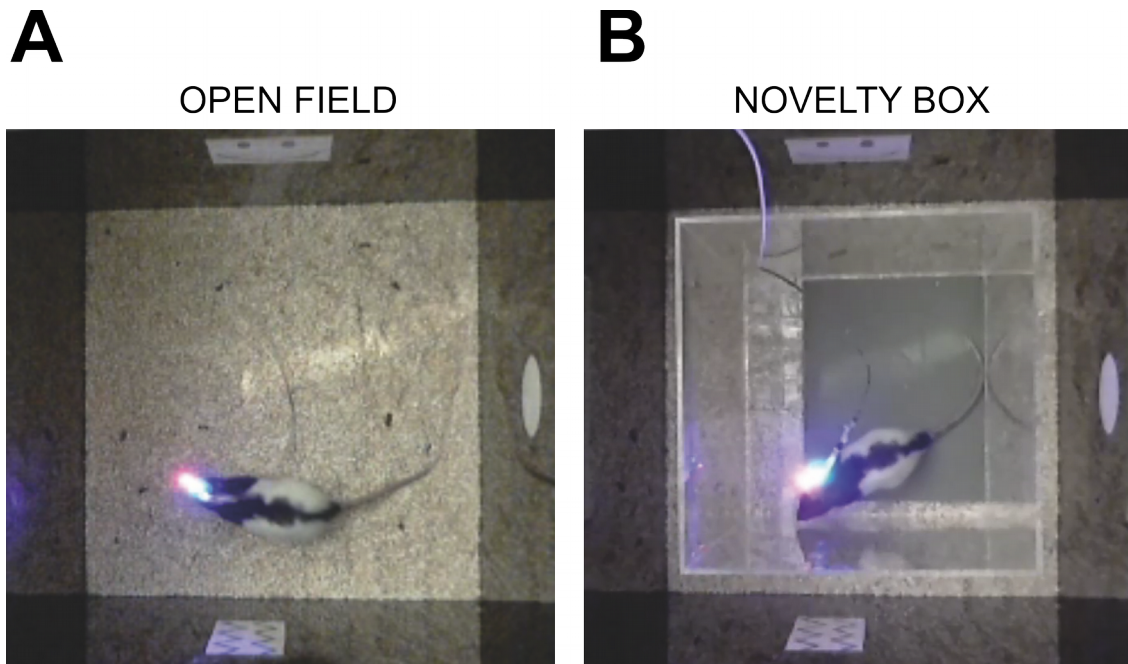


**Figure 3.4. Illustration of the Novelty task.** (A) Picture showing an animal during a Novelty task, in the familiar open field (A) and in the novel box (B). Note the LED lights installed in the recording pre-amplifiers, that facilitate the video tracking of the animals.

#### ***Immuno-histochemical analysis***

After the behavioral experiments ended, the animals were transcardially perfused with saline solution and paraformaldehyde 4% (BDH Prolabo, VWR International, Leuven, Belgium), and the brain collected for hystological analysis. The brain was cut in 100  $\mu\text{m}$  thick slices and treated with an antibody anti-GFAP (glial fibrillary acidic protein, that is present in astrocytes). Then, images were captured under a fluorescence magnifying glass. In the resulting pictures the position of the electrodes could be seen by the mark that the electrode left in the tissue; due to the prolonged presence of the probes in the brain, these “scars” had a distinctive distribution of astrocytes that unequivocally indicated the precise location of the electrode (Figure 3.5).

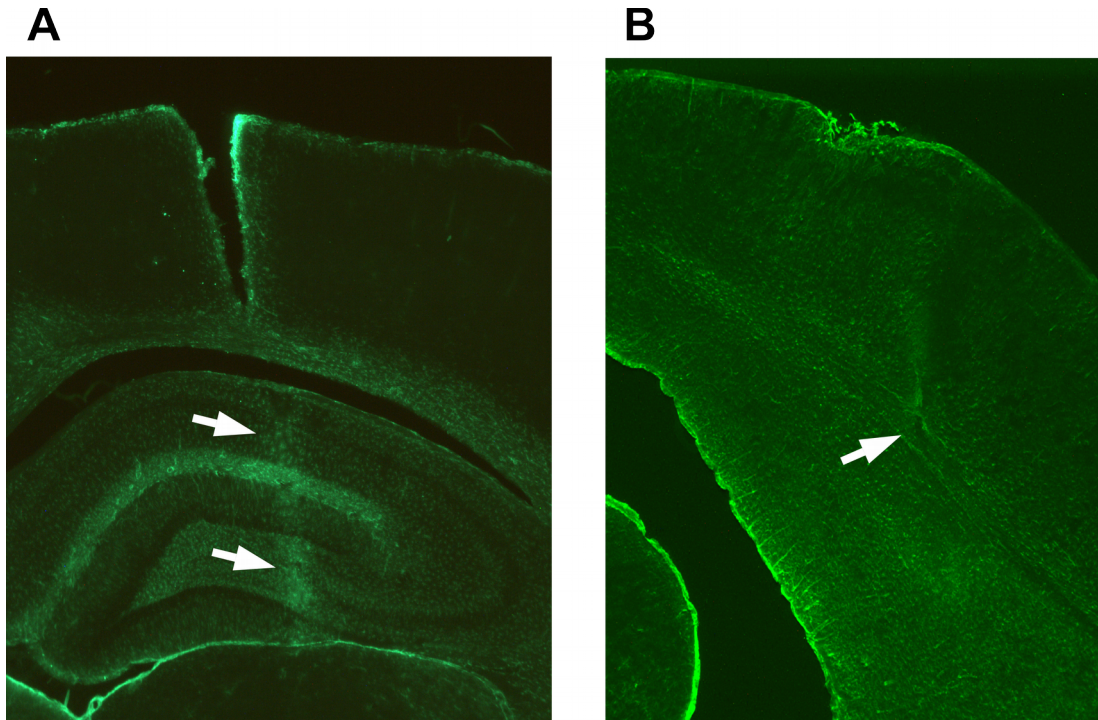


**Figure 3.5. Hystological *post mortem* location of the electrodes in the behavioral experiments.** Representative examples of the position of the recording (A) and stimulating (B) electrodes from coronal cuts of the rat brain at the level of the dorsal hippocampus and perforant path, respectively. The sections were stained with an antibody against GFAP that shows astrocytes with green fluorescence in the images. The position of the electrodes was revealed by the increased presence of astrocytes along the scar left by the electrodes (indicated with white arrows) after the whole time that the experiments lasted.

### **3.3. Data analysis**

All the analysis done in this work was performed using our own algorithms (and others provided by collaborators), developed with the software Matlab (The Mathworks Inc., Massachusetts, USA), and described in this chapter.

#### ***Selection of the LFP***

In order to have reliable and comparable LFP signals, we selected them to take only those where the activity of the cortex was minimal and the Theta-band oscillation (4-12 Hz) in CA1 was robust and constant. To achieve that and to ensure the similarity of our recordings, we extensively observed the signals and calculated a series of ratios between the power of specific frequency bands in characteristic selected channels (i.e. channels at cortex, CA1 and dentate gyrus). We made sure that all of them were comparable (Figure 3.6). In addition, we discarded any LFP which delta/gamma power ratio was bigger than 100 at the cortex, or any LFP which delta/theta power ratio was bigger than 5 at CA1.

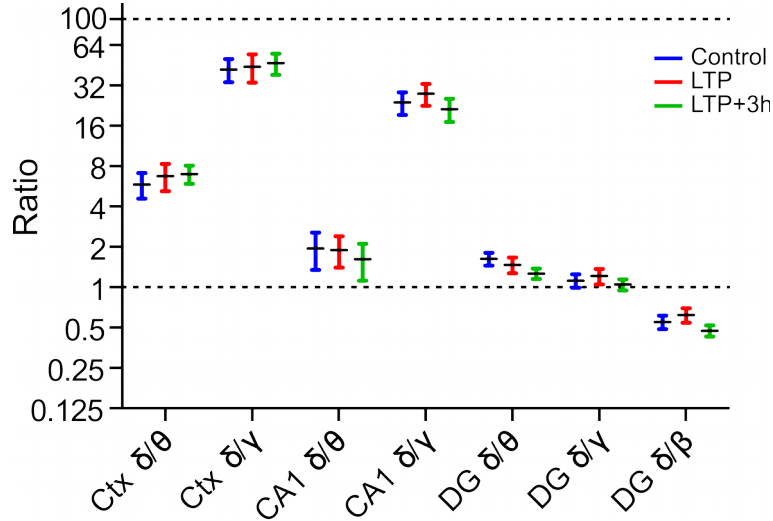


**Figure 3.6. Frequency bands' power of the selected LFP from anesthetized experiments.** The figure represents the different ratios calculated between the power of frequency bands for each of the selected areas (i.e. cortex [Ctx], detate gyrus [DG], CA1), during the three experimental conditions (Control [blue], after induction of LTP [red] and three hours later [green]). Note that each ratio is comparable for the three conditions.  $\delta$ =delta (0.5-4 Hz);  $\theta$ =theta (4-12 Hz);  $\beta$ =beta (12-30 Hz);  $\gamma$ =gamma (30-100 Hz).

### Separation of the LFP signals with Independent Component Analysis (ICA)

The LFP observed at any extracellular recording site is produced by linear sum of the electrical activity produced by several different sources or “LFP generators”. These generators describe trans-membrane currents from different local networks and cell types. In order to study separately the activity of such groups of cells, we dissected the LFP signal in the original parts that compose it (a process known as “source separation”) using Independent Component Analysis (ICA). There are several algorithms to perform ICA. For the present work, we used one of the most popular, the *runica* algorithm, that implements the infomax principle -originally proposed by Bell and Sejnowski (1995)- that is part of the EEGLAB MATLAB toolbox (Delorme & Makeig, 2004). The method was developed and tested previously using brain signals and numerical models (Makarov et al., 2010; Makarova et al., 2011).

The ICA assumes a statistical data model in which the observed variables (LFP) are a linear mixture of a priori unknown, mutually independent components that have non-Gaussian distributions. In this model the LFP signals are considered as a sum of products of spatial voltage loadings  $V_n(z)$  and temporal activations  $s_n(t)$  of  $N$  LFP generators:

$$u(z, t) = \sum V_k(z) \cdot s_k(t), \quad \Delta V_k(z) = I_k(z) / \sigma$$

where  $V = [V_1, V_2, \dots, V_N]$  is a  $(K \cdot N)$  matrix composed of the spatial voltage loadings,  $\{s_n(t)\}_{n=1}^N$  are their temporal activations of  $N$  LFP generators,  $\{I_n(z)\}_{n=1}^N$  are their spatial current density loadings, and  $\sigma$  is the conductivity of the extracellular space. Since the ICA algorithm might be biased by the presence in our LFP signals of extrinsic generators (generators originated in nearby areas which activity propagates into the area of study), a preliminary data preprocessing was performed to calculate and subtract their activity. In this way, the capacity of ICA to detect intrinsic generators was significantly improved (Martin-Vázquez et al., 2013).

To optimally calculate the LFP generators, we proceeded in two consecutive steps, just as explained in the work of Makarov et al. (2010). First, the most stable and strong generators were identified in long time windows (tens of seconds), since they should be present in most of the epochs of the recording; second, we applied ICA over consecutive 1 s periods of the same recording in order to identify other generators which appearance could last shorter (e.g. due to being noisy, transitory, unstable or weak) and therefore could have more variable spatial loadings over time. Then, to select the most stable ones among all the spatial loadings obtained, the similarity between them was quantified by the  $H_2$  distance in the Hilbert functional space, and they were clustered following statistical significance criteria. Finally, the isolated clusters were used for obtaining mean templates of spatial loadings for the resulting generators and for estimating their variance.

### Identification of the LFP generators

The resulting generators are single entities composed by two parts: the voltage loadings  $V_n(z)$  and the temporal activations  $s_n(t)$  (see an example in Figure 3.7). The voltage loadings represent spatial distribution and are individual for each generator; for linear recording track, the voltage loading is a curve of coefficients defining the strength and the polarity of the generator at each recording site (32 sites in the present work) (Figure 3.7-C). The temporal activation or time course shows the oscillations of the synaptic and synaptically activated transmembrane currents at the cells of the generator (Figure 3.7-B).

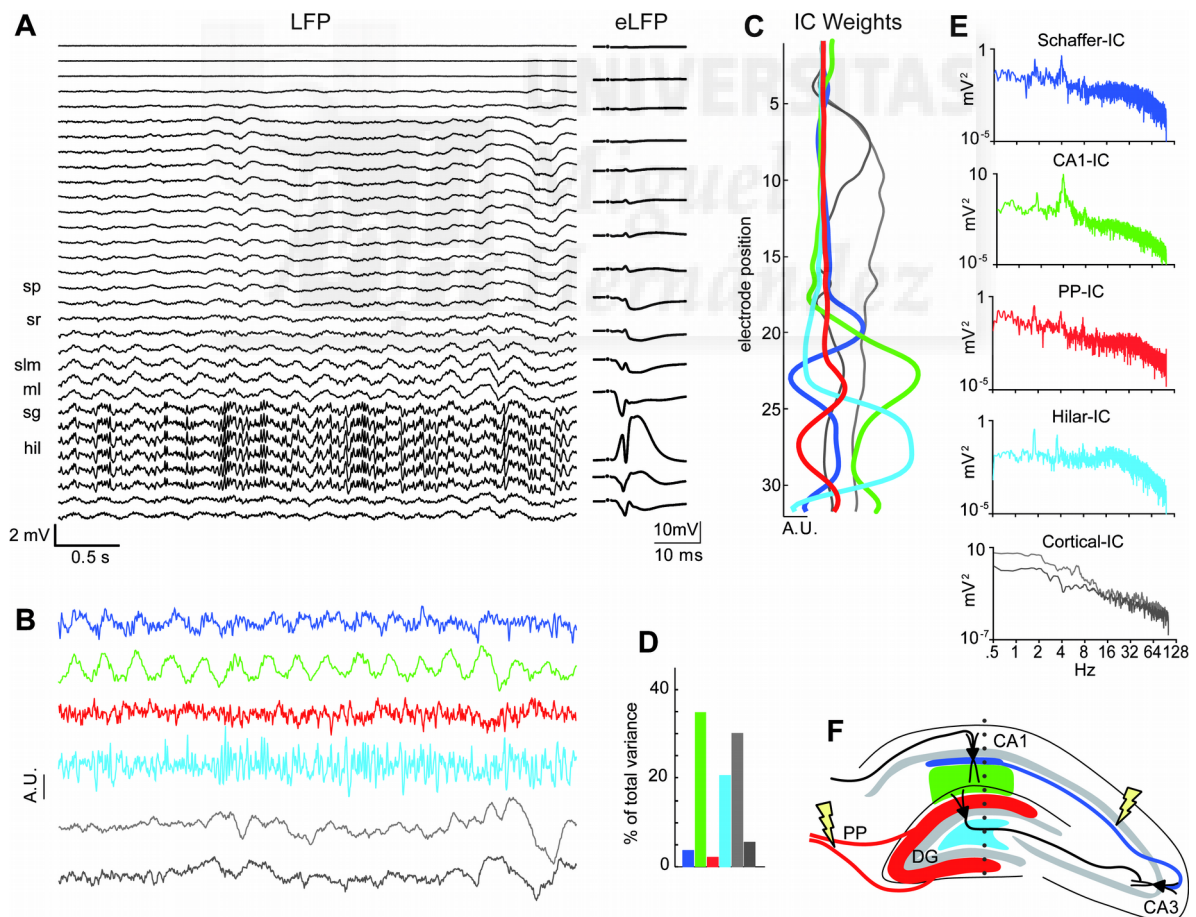


**Figure 3.7. Example of separation of LFP into its components with ICA.** (A) Representative recording from 32-channels probe showing spontaneous LFPs acquired in the dorsal hippocampus and overlying neocortex (left

panel) and corresponding evoked potentials (evoked-LFP) upon stimulation of the medial perforant path in selected contacts (right panel). The letters on the left of the left panel mark the anatomical territories of the hippocampus: sp, *stratum pyramidale*; sr, *stratum radiatum*; slm, *stratum lacunosum-moleculare*; ml, *molecular layer*; sg, *stratum granular*; hil, *hilus*.(B) Time course (in arbitrary units, A.U.) of the six LFP-generators extracted from and aligned to the same LFP recording. The color-code for the different generators is maintained for all figures in this work as follows (see text for details): Schaffer-blue, CA1-green, PP-red, Hilar-cyan. (C) Spatial distribution of voltage weights of the same six LFP-generators along the 32-channels axis (showed aligned to the LFP recording channels). They represent the contribution from each generator in the different recording sites. (D) Relative contributions of each generator to the total variance of the LFP (accounting for a typical total of 80 % of variance explained). (E) Power spectra of the different generators showing the complex and characteristic oscillatory behavior of each component. (F) Drawing representing a coronal section of the hippocampus and its main pathways; in colors are the topographic localizations of the generators and the related axonal pathways. Marked with yellow lightning bolts are the sites of stimulation in the different experiments (see *Methods*).

The spatial and temporal information of the generators was used to identify cellular or synaptic populations of the hippocampus that produce them. This was done first by relating the spatial distribution of the generators to the well known anatomy of the hippocampus, characterized by its stratified cytoarchitecture where subcellular domains are organized in very differentiated layers. Therefore the generators can be assigned to specific afferent pathways or local neuronal populations (see scheme in Figure 3.7-F). Moreover, this comparison could be refined by using evoked potentials of the main axonal pathways (i.e. perforant path and Schaffer collateral) (Korovaichuk et al., 2010), what allowed us to specifically identify generators associated with these pathways. In addition, we carried out pharmacological experiments (see above) in order to investigate what type of neurotransmitter the generators use (see *Results*). We used as a reference the work done by the group of Óscar Herreras and Valeri Makarov in characterizing not only the anatomical correspondence of the generators, but also their neurotransmitter contributions (Makarov et al., 2010; Korovaichuk et al., 2010; Makarova et al., 2011; Benito et al., 2013).

### ***Reconstruction of virtual-LFP signals from the generators***

The LFP-generators consist of temporal activation and voltage loadings. However, due to the method employed to calculate them, the generators are given in arbitrary units. In order to analyze them, we have to reconstruct what we call the “virtual-LFP” of the generators. This is done by simply multiplying the coefficients of the voltage loadings by the values in the temporal activation. We will then obtain a set of signals (one per recording site, 32 in the present work) that correspond to the relative contribution of a given generator to the total LFP. This virtual-LFP shows the correct polarity of the potentials, and allows us to quantitatively analyze the signal of each generator (e.g. to know their relative variance, or their power).

### ***Analysis of spontaneous signals***

To study the functional interdependency of two signals, we calculated the cross-correlation between them using a moving time-window; i.e. taking consecutive fragments of 500 ms of the signal and calculating the cross-correlation. We performed an additional statistical test, based on analyzing the same signals randomly rearranged, to discard any spurious correlations. We observed that the functional coupling between any pair of generators varies dynamically (and significantly) from positive to negative correlations with different delays (delay or anticipated synchronization). Therefore we classified the resulting population data for each generator pair in four possible groups, corresponding to the four possible combinations of positive/negative correlation coefficients with positive/negative delays. As a result, for each generator pair that we compared, we obtained four

separated groups of results, and each of those groups represented a specific mode of connectivity between those two generators. In Figure 3.8 there is a schematic example of this process.

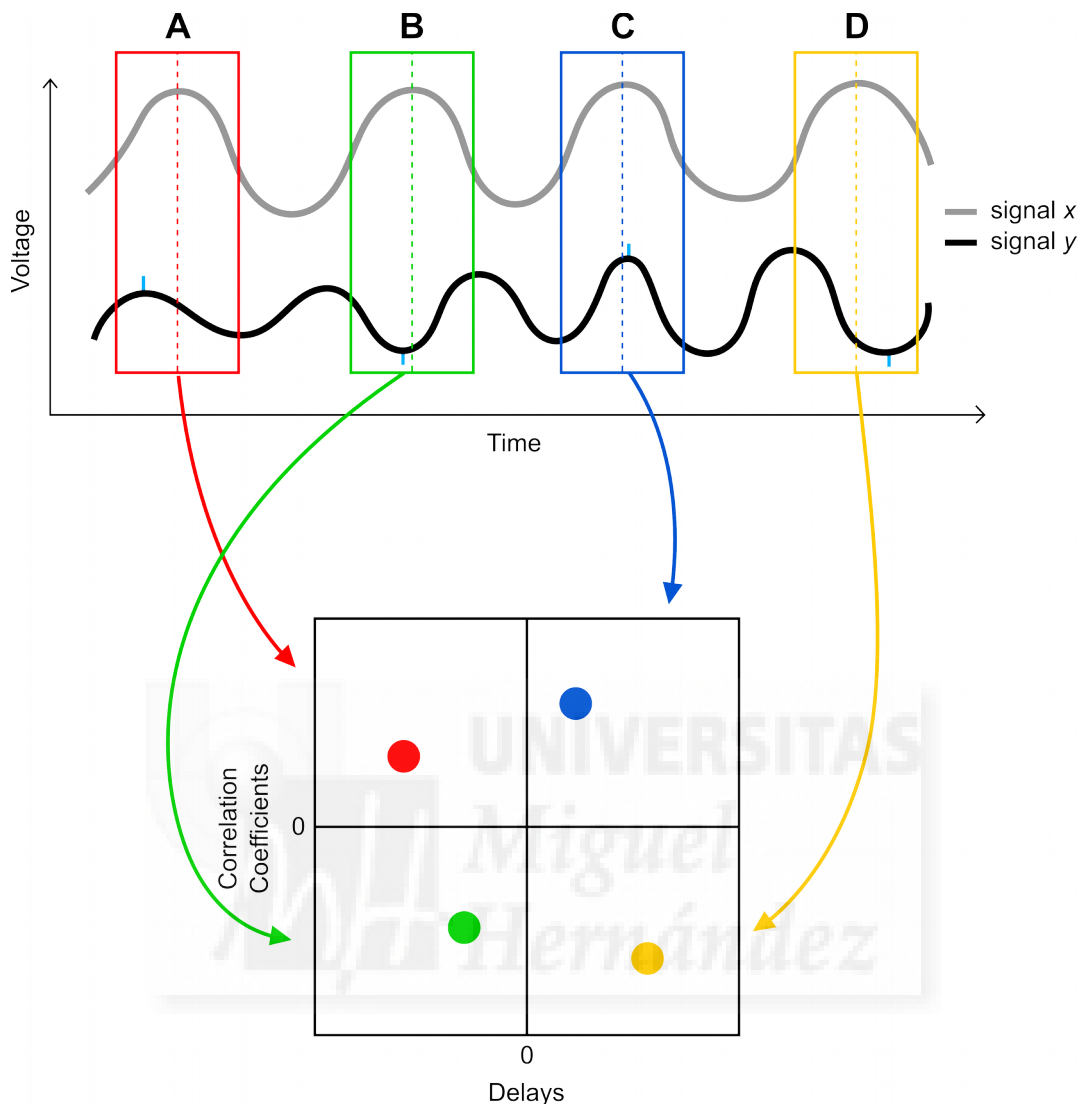


**Figure 3.8. Simplified illustration of cross-correlation analysis and representation of the results.** In the upper panel there are two schematic oscillating signals (traces in gray and black, x and y respectively). The four rectangles in colors represent possible analysis time-windows for calculating the cross-correlation between those two signals. With the real data we used actual consecutive time-windows; in this example they are placed to illustrate different possible results. Note that in each window (A-D) the relation between x and y is different and the corresponding results map into a different quadrant of the figure (example in the lower panel). Some maximal and minimal amplitudes of signal ‘y’ are marked by cyan ticks. Together the different combinations of positive or negative correlation coefficients and delays actually reflect different forms of engagement, as illustrated in this figure, and as reflected in the segregation of the results among the four quadrants of our graphics.

Furthermore, the amount of time-windows that correspond to each of the four groups of results in each quadrant, reflect the relative dominance in time of the engaging mode represented by a quadrant. In our graphics, the amount of time-windows corresponding to each quadrant is expressed as a proportion of the total windows analyzed, and this is translated to the graphic in the size of the symbol. Therefore, if two signals are clearly correlated in a specific manner most of the time, one of the four quadrants will display a bigger proportion of the total time-windows. At the same time, changes in the proportion

of results among the quadrants would reflect changes in the time occupied by specific engaging modes, and thus a functional reorganization.

The power of the signals was calculated as the square of the signal. The power for specific frequency bands was calculated integrating the area under the periodogram of the signal in the range of that frequency, using the trapezoidal rule. The frequency bands considered were Delta (0.5-4 Hz), Theta (4-12 Hz), Beta (12-30 Hz) and Gamma (30-100 Hz).

### ***Analysis of sub-threshold evoked-LFP***

The maximal amplitude (often referred to in this work as simply “amplitude”) of the sub-threshold evoked LFP at the hilus layer of the dentate gyrus (hereafter “e-LFP”) was calculated as the difference between the maximal amplitude of the potential and the potential less than 1 ms after the stimulation (considered this as baseline). The latency of the maximum of the potential (often referred to in this work as simply “latency”) was calculated as the time difference between the stimulation and the maximal amplitude of the potential (Figure 3.9).

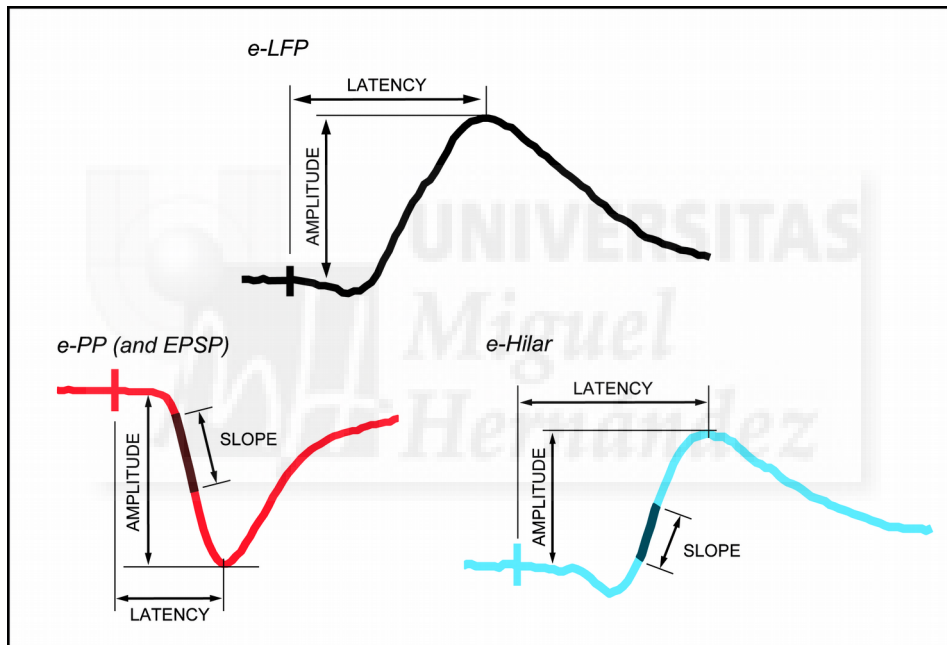


**Figure 3.9. Method for analysis of the sub-threshold evoked-LFP and its components.** Illustration showing how each parameter from the sub-threshold evoked-LFP is obtained. With thin black straight lines are marked the reference points and the arrows between them with an associated label represent the interval for the corresponding calculation. The analyses explained on the red trace are valid for the raw EPSP (not shown) because both have an equivalent shape.

The slope of the sub-threshold negative EPSP recorded at the molecular layer of the dentate gyrus was calculated identifying first the point of the potential where the falling slope was maximal. Then the slope of the segment of 0.8 ms surrounding that point was calculated, and that measure was considered as the final slope of the potential (Figure 3.9).

The amplitude, the latency and the slope of the LFP-generators of the evoked potentials were calculated in the same way as just described (see *Results* for details on the main LFP-generators identified and on the separation of the sub-threshold evoked-potentials into LFP-generators)(Figure

3.9).

All these parameters were measured when sub-threshold evoked-LFP were studied, although they are not plotted in the graphics when they were displaying the same changes than a similar parameter (for example, slope and amplitude of e-Hilar used to be modulated exactly in the same way by experimental manipulations, and therefore only one of them was represented in the graphics).

### ***Analysis of fMRI images***

Functional MRI data were analysed offline using our own software developed in Matlab, which included Statistical Parametric Mapping package (SPM8, [www.fil.ion.ucl.ac.uk/spm](http://www.fil.ion.ucl.ac.uk/spm)), Analysis of Functional NeuroImages (AFNI, <http://afni.nimh.nih.gov/afni>) and FSL Software (FMRIB <http://fsl.fmrib.ox.ac.uk/fsl/>). For electric-stimulation fMRI, after linear detrending, temporal (0.015–0.2 Hz) and spatial filtering (3 x 3 Gaussian kernel of 1.5 sigma) of voxel time series, a general linear model or cross-correlation analysis was applied with a simple boxcar model shifted forward in time, typically by 2 s, or a boxcar convolved with a gamma probability density function (Matlab). Functional maps were generated from voxels that had a significant component for the model and they were clustered together in space ( $p < 0.01$ ). Similar results were obtained with the different analytical methods. For functional connectivity between brain areas, images are brain extracted, co-registered and intensity normalized. Afterwards, temporal data were corrected by applying detrending, global regression and time filtering (0.002–0.1 Hz). BOLD time courses of hippocampal voxels, extracted using a rat atlas registered to the functional images (Schwarz et al., 2006), were used to compute the bilateral cross-correlation coefficients.

### ***Statistical analysis***

For all the data sets analyzed we performed a normality test (Shapiro-Wilk test). We then applied statistical tests according to whether the distribution of the samples was Gaussian or non-Gaussian.

When comparing one or two samples (one in the cases they were compared to a hypothetical value) we used: t-test (obtaining the  $t$  statistic) for unpaired Gaussian samples; a paired t-test ( $t$  statistic) for paired Gaussian samples; a Mann Whitney test ( $U$  statistic) for unpaired non-Gaussian samples; and a Wilcoxon signed-rank test ( $W$  statistic) for paired non-Gaussian samples.

For comparing three or more samples we used: one-way ANOVA test ( $F$  statistic) for unpaired Gaussian samples; a repeated measurements ANOVA test ( $F$  statistic) for paired Gaussian samples; a Kruskal-Wallis test ( $K$  statistic) for unpaired non-Gaussian samples; and a Friedman test ( $Q$  statistic) for paired non-Gaussian samples. For comparing two variables and their interaction we used a repeated measurements two-way ANOVA test ( $F$  statistic) for paired Gaussian samples.

All the statistical analysis were performed using the software Prism 5 (GraphPad Software, Inc., California, USA) and Matlab (The Mathworks Inc., Massachusetts, USA).

### ***Behavioral video-tracking***

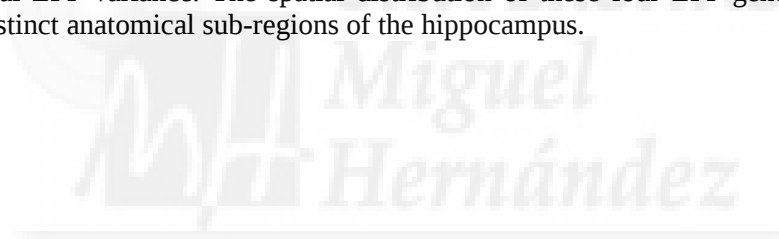
The videos recorded during the novelty task were analyzed using the video-tracking software Tracker (Open Source Physics Project, <http://www.cabrillo.edu/~dbrown/tracker/>). The coordinates and velocity of the movements of the animals were calculated by the software.



## IV. RESULTS

### ***4.1. Identification of the main generators of the hippocampus***

Using independent component analysis ICA (Makarov et al., 2010), the LFPs recorded in the dorsal hippocampus and the overlying parietal association cortex could be separated into several stereotypic LFP-generators, based on their spatial distribution, time courses and their relative contribution to the total variance of the LFP, in good agreement with previous reports (Korovaichuk et al., 2010; Benito et al., 2013). These generators were extracted from selected periods of LFP with spectral characteristics corresponding to a Theta-dominant state (see *Methods* section for details). They were found in every recording analyzed for each animal, both in anesthetized and awake subjects, which evidences their reliability. From the set of stereotypic LFP-generators that we found, two originate from the overlying parietal association cortex and will not be explored in the present work. Four additional generators contained in the dorsal hippocampus have been selected for further study that overall represent  $79.3 \pm 1.5$  % of the total LFP variance. The spatial distribution of these four LFP-generators corresponds precisely with distinct anatomical sub-regions of the hippocampus.



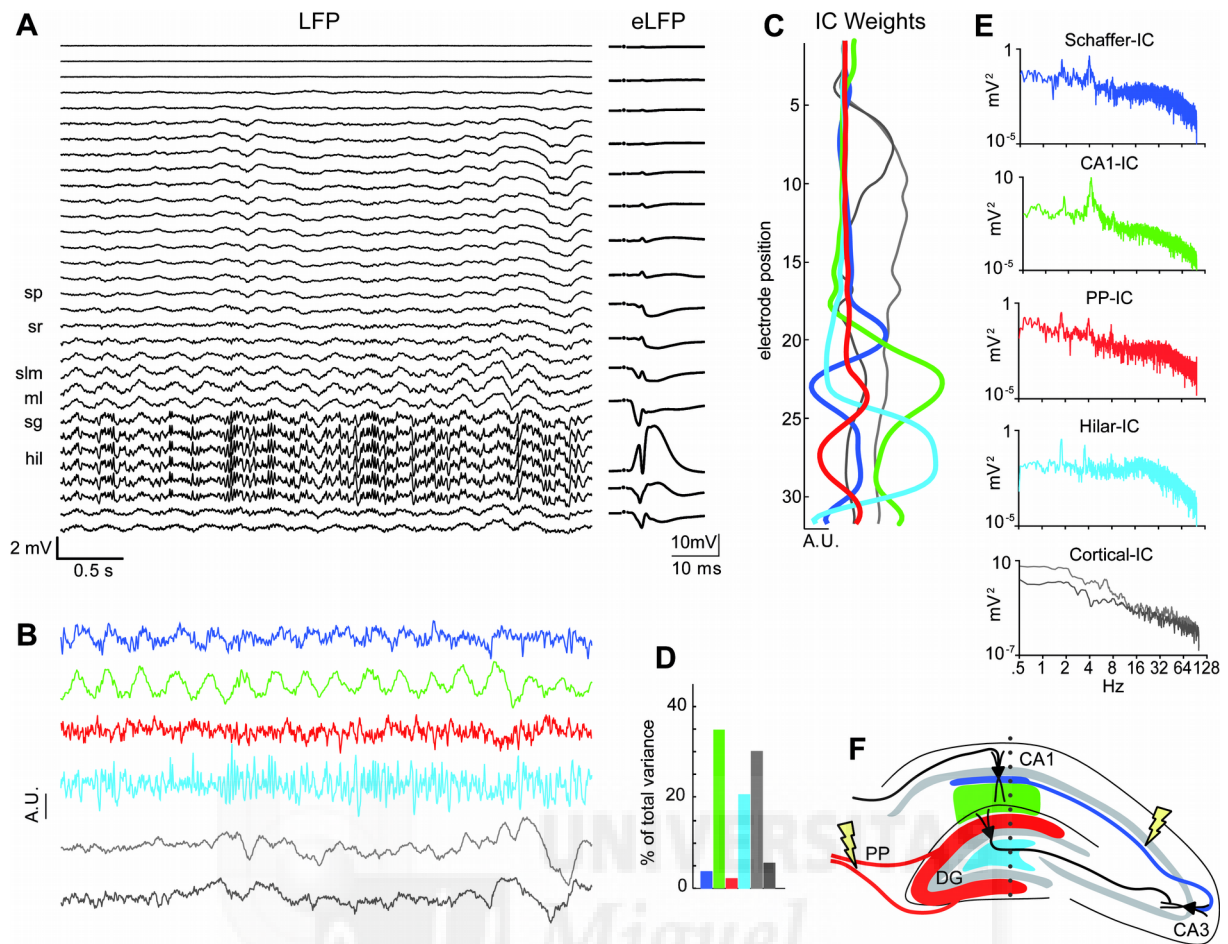


**Figure 4.1. Example of separation of LFP into its components with ICA.** (A) Representative recording from 32-channels probe showing spontaneous LFPs acquired in the dorsal hippocampus and overlying neocortex (left panel) and corresponding evoked potentials (evoked-LFP) upon stimulation of the medial perforant path in selected contacts (right panel). The letters on the left of the left panel mark the anatomical territories of the hippocampus: sp, *stratum pyramidale*; sr, *stratum radiatum*; slm, *stratum lacunosum-moleculare*; ml, *molecular layer*; sg, *stratum granular*; hil, *hilus*. (B) Time course (in arbitrary units, A.U.) of the six LFP-generators extracted from and aligned to the same LFP recording. The color-code for the different generators is maintained for all figures in this work as follows (see text for details): Schaffer-blue, CA1-green, PP-red, Hilar-cyan. (C) Spatial distribution of voltage weights of the same six LFP-generators along the 32-channels axis (shown aligned to the LFP recording channels). They represent the contribution from each generator in the different recording sites. (D) Relative contributions of each generator to the total variance of the LFP (accounting for a typical total of 80 % of variance explained). (E) Power spectra of the different generators showing the complex and characteristic oscillatory behavior of each component. (F) Drawing representing a coronal section of the hippocampus and its main pathways; in colors are the topographic localizations of the generators and the related axonal pathways. Marked with yellow lightning bolts are the sites of stimulation in the different experiments (see *Methods*).

The first LFP-generator that we identified corresponds to the input from the perforant path to the granule cells in the dentate gyrus, so we called it **perforant path generator (PP)** (Figure 4.1, in red). The spatial distribution of this generator typically presents two peaks matching the two molecular layers of the dentate gyrus. The field potential evoked by electrically activating the fibers of the perforant pathway with its typical negative-going EPSP at the level of the molecular layer (dorsally and ventrally to the hilus) in the raw LFP (hereafter referred to as simply “EPSP”), could only be recovered in the PP generator after analysis with ICA, thus evidencing the entorhinal origin of the

fibers generating this excitatory input to the dentate gyrus (see below *Independent components of sub-threshold evoked potentials* for results in this topic). Further evidence for the entorhinal origin of this generator was obtained by injecting tetrodotoxin (100  $\mu$ M; TTX) in the perforant path, which translated into an immediate and robust decrease in the power of the PP generator (63-75 % reduction, Figure 4.2). PP generator is also characterized by a minor contribution to the total variance ( $1.65 \pm 0.15$  %,  $n=26$ ) in the anesthetized rat, as was already described (Korovaichuk et al., 2010).

The second LFP-generator is the so-called **Hilar generator** (Figure 4.1, in cyan), and has a spatial distribution overlapping with the dentate gyrus area, with its maximum at the center of the hilus. It has a remarkable contribution to the total variance of the LFP ( $26.8 \pm 1.4$  %,  $n=26$ ). The fact that this generator displays a characteristic activity in response to electric stimulation of the perforant pathway, suggests that it is at least partially driven by entorhinal cortex activity. However, such activation does not correspond to the negative EPSP at the molecular layer and suggests a contribution of different nature. Such a contribution will be investigated in detail in the present work (see below). In addition, pharmacological experiments performed by Herreras and col (benito et al 2013) and also presented in this work (see below) suggest a GABAergic origin for this LFP-generator. Additional support to the entorhinal cortex origin of this generator is also provided by the TTX experiment described before. The application of TTX to the perforant pathway provides fast and strong (56-90 %) reduction of the hilar generator power (Figure 4.2).

The third LFP-generator corresponds to the Schaffer collateral input to CA1 pyramidal neurons (**Schaffer generator**)(Figure 4.1, in blue). It presents a peak of activity right under the pyramidal layer of CA1, in the proximal portion of the stratum radiatum, where the axons of the Schaffer collateral coming from CA3 are known to contact the dendrites of CA1 neurons (Ishizuka et al., 1990). It contains high frequency sharp-wave and ripple activity and was also identified by means of electrical stimulation to the Schaffer collateral, resulting in the complete and selective recovery of the evoked EPSP in its time course (Korovaichuk et al., 2010). Just like the PP, the Schaffer generator has a minor contribution to the LFP ( $5.6 \pm 1$  %,  $n=26$ ), but contrary to the previously described generators its power is not affected by the pharmacological blockade of the perforant path (Figure 4.2).

The fourth LFP-generator is the **CA1 generator** (Figure 4.1, in green), with a spatial distribution covering most of the hippocampus and dentate gyrus, with a big peak at the CA1 dendritic layer stratum radiatum/stratum lacunosum-moleculare. It is the major generator of the hippocampus, contributing  $45.1 \pm 1.4$  % of the total LFP variance. Importantly, it is characterized by a strong oscillatory activity in the Theta band of frequency (3-4 Hz in anesthetized animals, 7-8 Hz in awake animals)(see representative example trace in Figure 4.1). The origin of this generator is not as well characterized as the previous ones, being contributed by GABAergic currents most likely of local origin (Benito et al., 2013) but also by an input from the entorhinal cortex as demonstrated by the 49% power reduction registered after TTX injection in the perforant path (Figure 4.2).

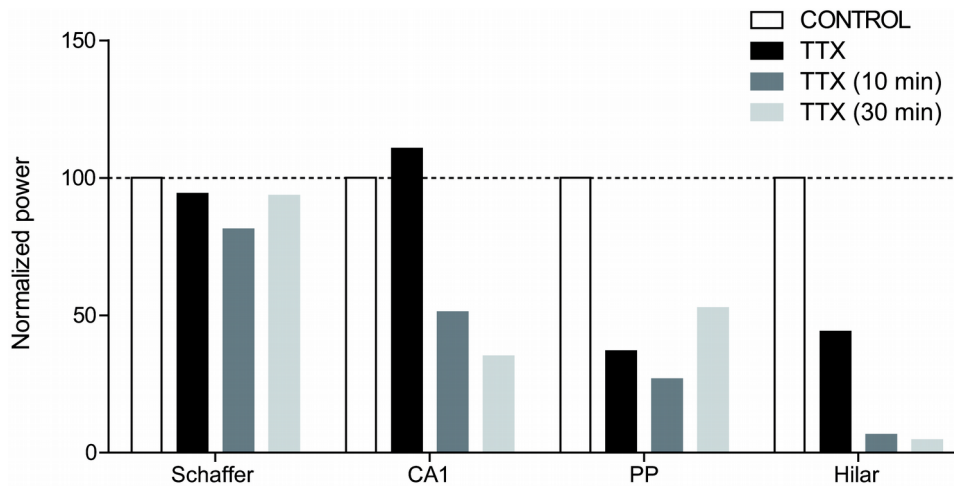


**Figure 4.2. Average power of the hippocampal LFP-generators during the injection of TTX in the perforant path**, normalized with respect to control. The power of the generators is shown before the injection (white), immediately after injecting TTX in the perforant path (black), 10 minutes later (dark gray) and 30 minutes later (light gray). The LFP-generators affected firstly and mainly by TTX treatment are the PP and the Hilar.

More details on pharmacological and electrophysiological characterization of the generators are provided below, where the ICA of the evoked potentials is dealt with.

#### **4.2. Induction of Long-Term Potentiation (LTP)**

The results from the analysis of the “Input-Output curves” revealed a strong and consistent potentiation of the entorhinal synapses onto the granule cells after the electrical tetanization of the perforant path (Figure 4.3)(see *Methods: LTP induction* for details about the stimulation protocols). The EPSP was significantly potentiated after tetanization with respect to control at all stimulation intensities and remained significantly potentiated three hours later, although not detectable for the lowest intensities. The magnitude of EPSP potentiation was maximal immediately after induction and accommodated to a level of lower potentiation with time, as previously described in LTP experiments (Bliss et al., 2007). Similarly, the PS underwent a very significant increase sfter LTP induction that lasted at least for three hours. We observed as well EPSP-to-Spike (E-S) facilitation of the perforant path input to the dentate gyrus.

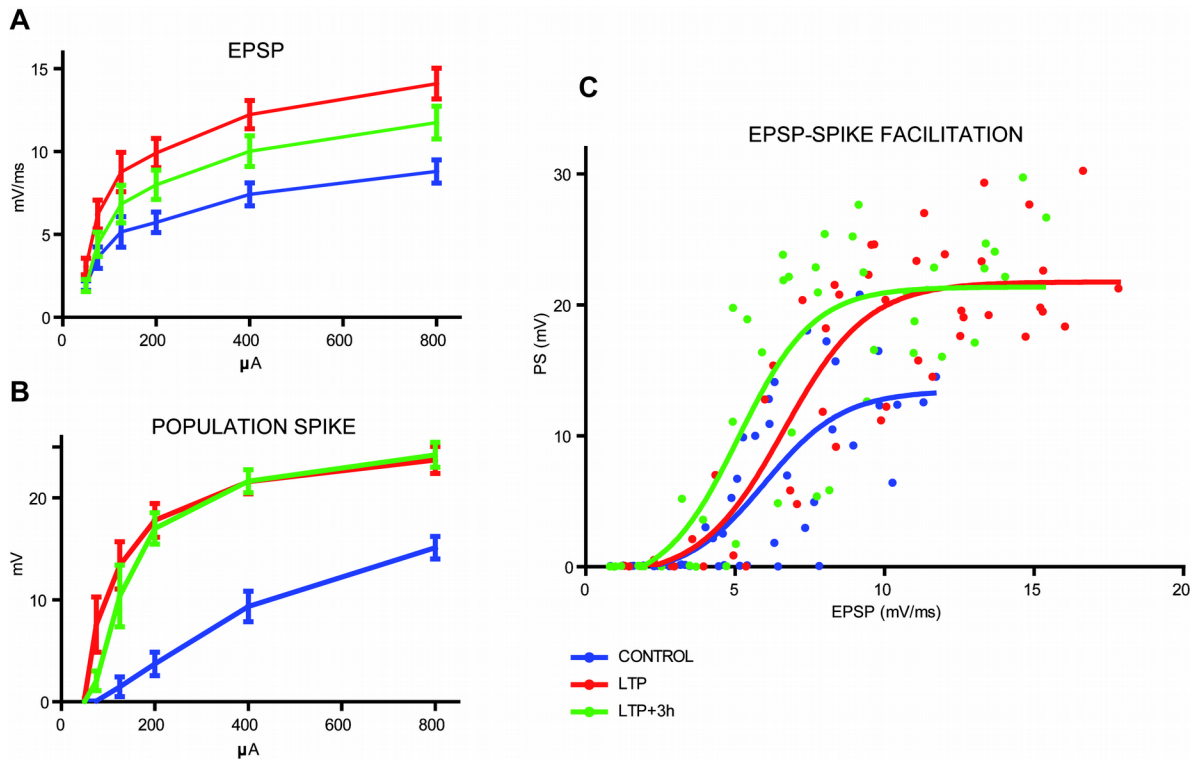


**Figure 4.3. Effects of LTP induction on the perforant path evoked-LFPs recorded in the DG.** Input-output curves showing the maximal slope of the EPSP (A) and the amplitude of the PS (B) evoked by different current intensities (x-axis) before (control), after LTP induction (LTP) and three hours later (LTP+3h). (C) shows curves for those conditions confronting the EPSP with the corresponding PS evoked by the same stimulus. In all panels symbols represent mean  $\pm$  SEM. LTP enhances EPSP and PS with LTP (red symbols and tracings) and 3 hours (green) after induction, as compared to control neurotransmission (blue). Panel (C) evidences the EPSP-to-Spike facilitation after induction of LTP. STATISTICS: (A)  $n=9$ , 2-way repeated measures ANOVA, Interaction  $F_{(10,80)}=8.86$ ,  $p<0.0001$ ; Condition  $F_{(2,80)}=227.77$ ,  $p<0.0001$ ; Intensity  $F_{(5,40)}=21.30$ ,  $p<0.0001$ . (B)  $n=9$ , 2-way repeated measures ANOVA, Interaction  $F_{(10,80)}=17.0$ ,  $p<0.0001$ ; Condition  $F_{(2,80)}=214.92$ ,  $p<0.0001$ ; Intensity  $F_{(5,40)}=52.24$ ,  $p<0.0001$ . (C)  $n=9$ , logarithmic regression (Control  $R^2=0.59$ , LTP  $R^2=0.77$ , LTP+3h  $R^2=0.69$ ); comparison of curve fits (extra sum-of-squares F test),  $F_{(8,126)}=4.197$ ,  $p=0.0002$ .

#### 4.3. LTP induction changes the spontaneous activity of the hippocampal local circuits

Studying the spontaneous activity of the LFP generators before and after LTP induction we found modifications in their temporal activations. Because generators are provided in arbitrary units after ICA, we analyzed the corresponding virtual-LFP, a realistic representation of the voltage of the LFP contributed by a specific individual generator (see *Methods* for details). The power of the reconstructed virtual-LFP was used as an approximation to the amount of activation of a generator, and we calculated it for both the whole-spectrum and specific bands of frequencies (see *Methods*). First, the PP generator had a tendency to increase its power after LTP (Figure 4.4) that was significant only for the Delta band (Figure 4.5), the fundamental band contained by this generator. Interestingly, we found a consistent decrease in the power of the Hilar generator ( $82\pm 4\%$  of control), that was significant as well in the higher frequency bands. Schaffer generator showed a decrease in its power in the Beta band three hours after LTP induction, and CA1 didn't undergo any significant change with respect to control. Three hours after the induction of LTP, all generators (except Schaffer, as mentioned) were again at control level of activation. Additionally, we calculated the ratio between the power of the PP generator and the power of the Hilar generator. Due to the fact that the former is an

excitatory generator and the latter is primarily inhibitory (see *Introduction*, and *Discussion* below), we considered this measure as the expression of the excitation-inhibition balance in the dentate gyrus network. This ratio increased significantly from control to LTP condition ( $152.5 \pm 17.9\%$ ) (Figure 4.4); three hours later there was no significant difference with control conditions. It is important to note again that synaptic transmission in the perforant path in these animals and during the evaluated periods was highly potentiated, suggesting that these synaptic changes are largely compensated in the circuit with the exception of an initial and transient time window.

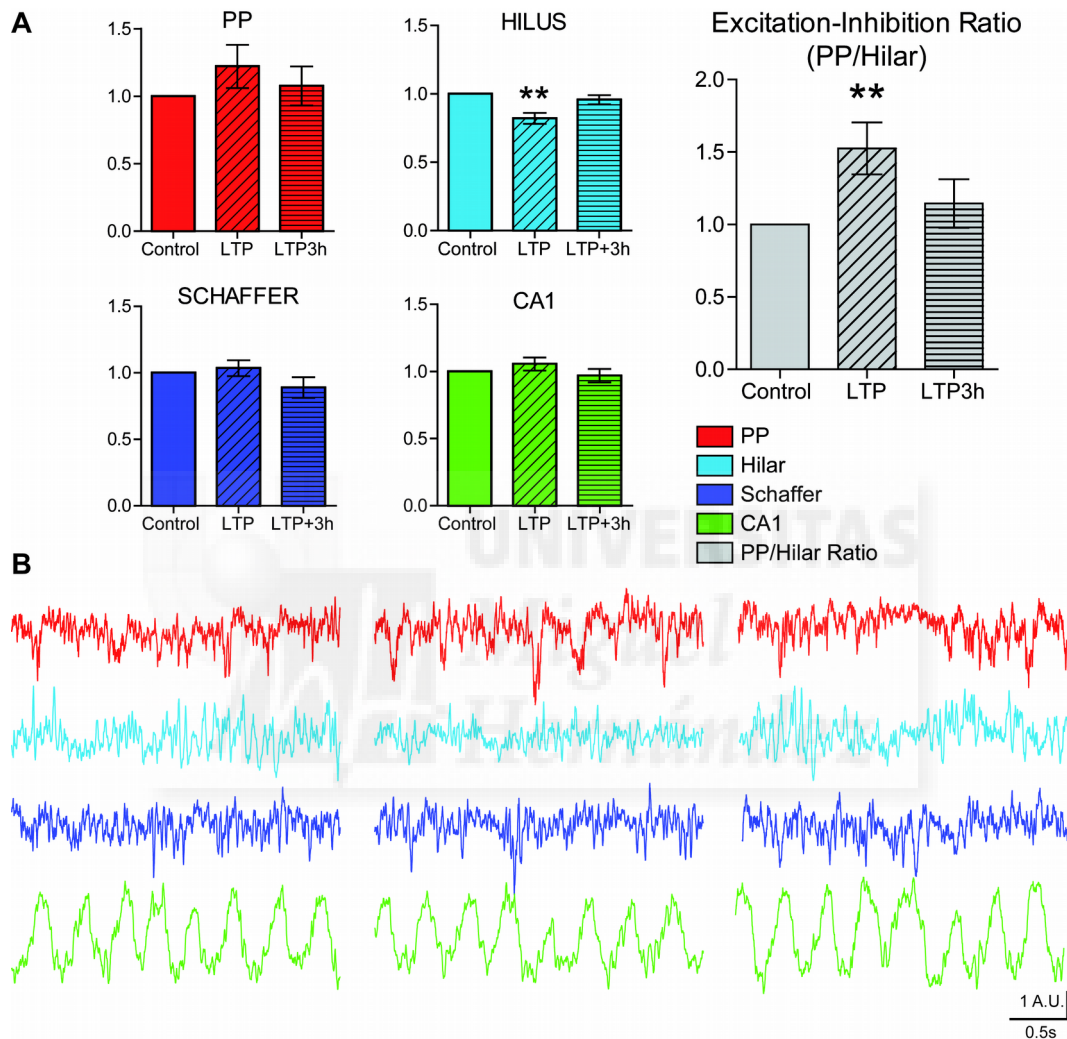


**Figure 4.4. Changes in the power of the generators with LTP.** (A) Power (normalized to control condition) of the hippocampal LFP-generators before (control) LTP induction in the perforant path, immediately after (LTP) and three hours later (LTP+3h), together with the excitation-inhibition ratio in the dentate gyrus. Bars represent mean  $\pm$  SEM. A significant decrease can be observed in the power of Hilar generator, with a corresponding increase in the excitation-inhibition ratio. (B) Representative example traces of the hippocampal generators at the aforementioned time points (control-left, LTP-middle, LTP+3h-right). STATISTICS: (A)  $n=13$ , One sample t-test ( $t$  statistic, for Gaussian distributions); Hilar:  $t_{(11)}=4.44$ ,  $p=0.001$ . Ratio:  $t_{(11)}=2.931$ ,  $p=0.0137$ .

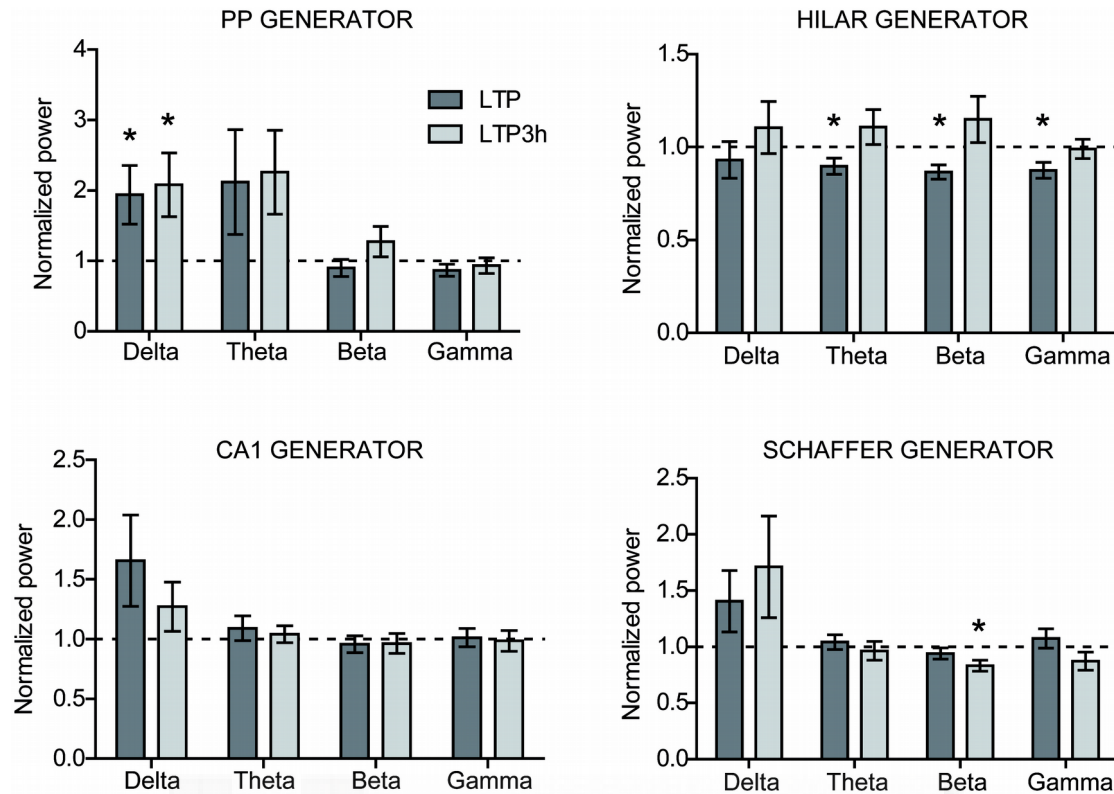


**Figure 4.5. Changes in the band-power of the generators with LTP.** (A) Power (normalized to control condition) of the hippocampal LFP-generators before (control) LTP induction in the perforant path, immediately after (LTP) and three hours later (LTP+3h). The power at control condition is represented as horizontal line at 1. Bars represent mean  $\pm$  SEM. STATISTICS: One sample t-test (t statistic, for Gaussian distributions) or Wilcoxon Signed Rank test (W statistic, for non-Gaussian distributions). Schaffer (LTP+3h, Beta):  $t_{(9)}=3.419$ ,  $p=0.0076$ ; Hilar (LTP, Theta):  $t_{(9)}=2.366$ ,  $p=0.0422$ ; Hilar (LTP, Beta):  $t_{(9)}=3.476$ ,  $p=0.007$ ; Hilar (LTP, Gamma):  $t_{(9)}=2.906$ ,  $p=0.0174$ ; PP (LTP, Delta):  $t_{(9)}=2.308$ ,  $p=0.0464$ ; PP (LTP+3h, Delta):  $W=39.0$ ,  $p=0.0488$ .

To evaluate the functional connectivity between generators and its possible modulation with LTP, we analyzed the cross-correlation in consecutive time-windows (500 ms) of the compared signals, as described in *Methods*. We then segregated the results according to the sign of the correlation coefficient and the sign of the delay, so that the data were divided into four groups (represented in the corresponding four quadrants of the graphics in Figure 4.7) and averaged across subjects. The following Figure 4.6 gives an illustration of how this process was carried out (see *Methods* for more details on this analysis).

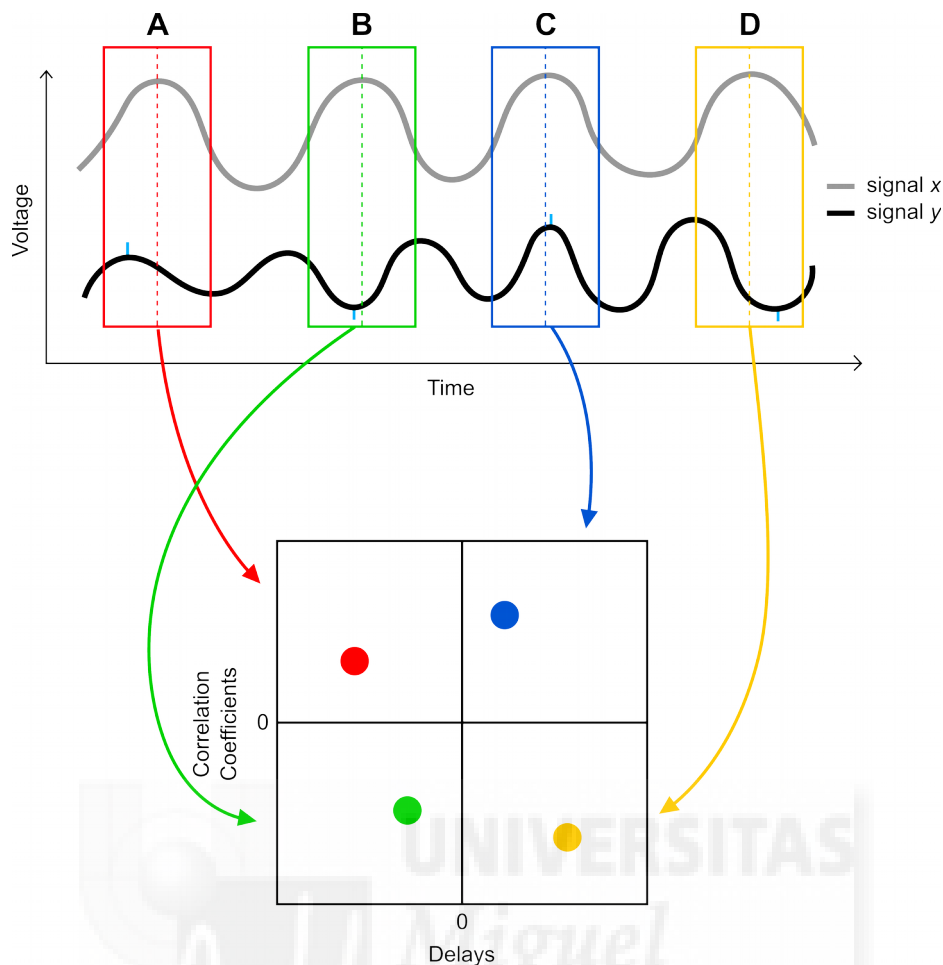


**Figure 4.6. Simplified illustration of cross-correlation analysis and representation of the results.** In the upper panel there are two schematic oscillating signals (traces in gray and black, x and y respectively). The four rectangles in colors represent possible analysis time-windows for calculating the cross-correlation between those two signals. With the real data we used actual consecutive time-windows; in this example they are placed to illustrate different possible results. Note that in each window (A-D) the relation between x and y is different and the corresponding results map into a different quadrant of the figure (example in the lower panel). Some maximal and minimal amplitudes of signal 'y' are marked by cyan ticks. Together the different combinations of positive or negative correlation coefficients and delays actually reflect different forms of engagement, as illustrated in this figure, and as reflected in the segregation of the results among the four quadrants of our graphics. Furthermore, the amount of time-windows that correspond to each of the four groups of results in each quadrant, reflect the relative dominance in time of the engaging mode represented by a quadrant.

As shown in Figure 4.7, we observed a significant change in the delay between CA1 and PP generators immediately after potentiation, increasing the delay with positive correlation coefficients and decreasing with negative coefficients. There was also a different distribution of time windows among the four quadrants during LTP condition; whereas the proportion of windows with positive coefficients and delays decreased with the potentiation, in turn there was an increase in the proportion of windows with negative coefficients and delays.

We found as well an increase in the negative delay and an associated decrease in the negative correlation coefficient between PP and Hilar generators during LTP. Since it corresponds to the quadrant with the most time-windows in it, this change seems to be consistent and it could be relevant.

Finally, there was a moderate but significant decrease in the amount of windows with negative

coefficients and positive delays between CA1 and Hilar generators. This quadrant contains the minority of all time-windows for this pair of generator, and therefore it's possible that this change does not have a strong effect on the network.

Additionally, we looked for possible changes in the amount of time that two generators were significantly correlated (Figure 4.7), and we observed a tendency to decrease that time between PP and Hilar generators, although this difference was not statistically significant.

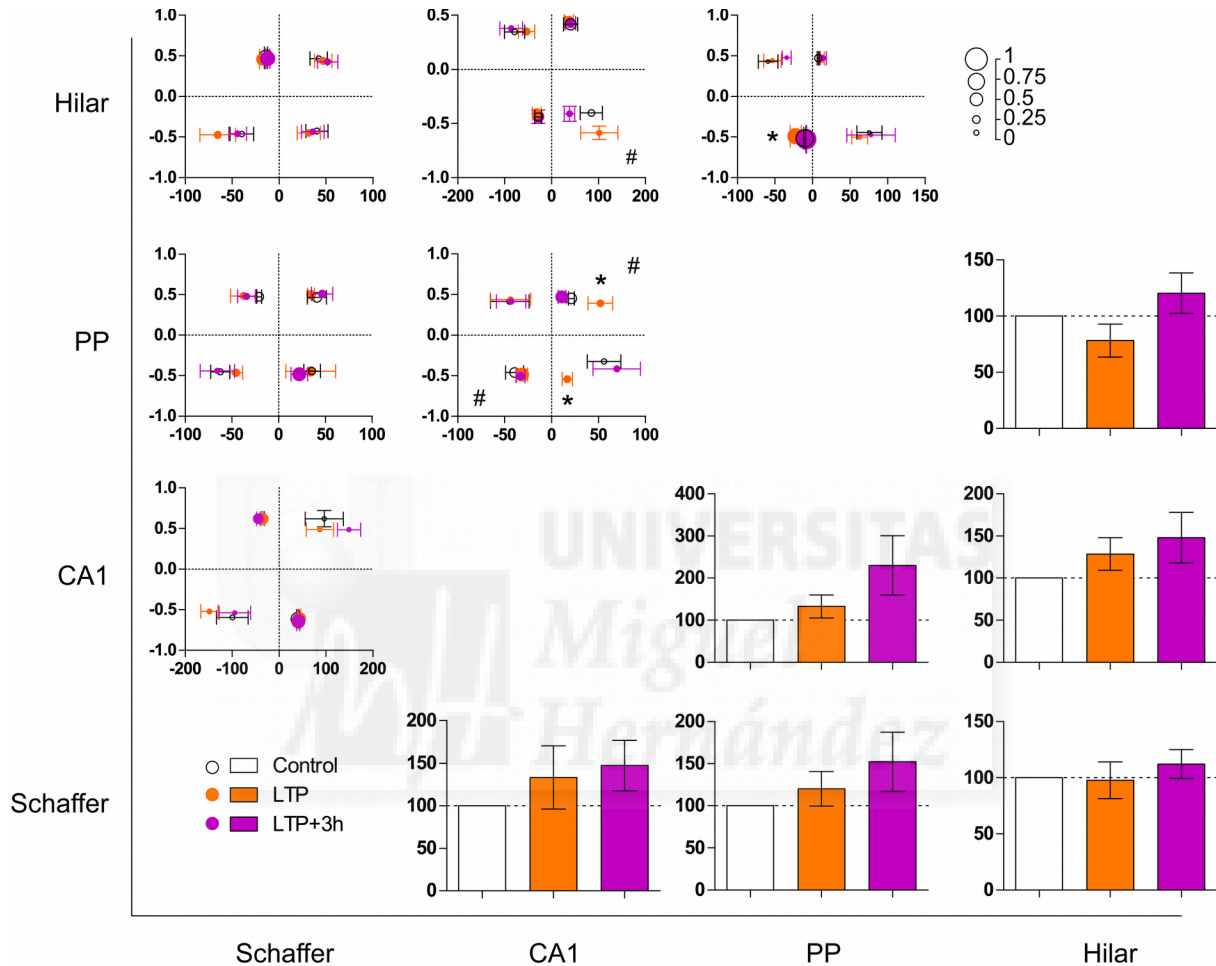


**Figure 4.7. Functional coupling between generators measured by cross-correlation before and after potentiation of the perforant path.** The upper-left subset of figures represents correlation-coefficients and delays in milliseconds (they are 2-dimensional coordinate panels; dots represent mean  $\pm$  SEM; colors represent conditions, following the legend at the lower-left corner; asterisks represent statistical significance, and hashes represent statistical significance specific for the proportion of time-windows). Each of the panels correspond to a generator pair, indicated in the axes. Results are segregated in quadrants depending on the sign of both the correlation-coefficient and the delay (as explained before in Figure 4.6 and in *Methods*), and averaged for all subjects. In addition, the relative size of the dots represents the proportion of time-windows that corresponds to each quadrant; the legend at the upper-right corner illustrates the correspondence between that proportion and the size of the dots. The lower-right subset of figures (bars representing mean  $\pm$  SEM, colors representing conditions) shows in which proportion of the total time analyzed were two generators actually significantly correlated. The amount of time is normalized with respect to the control condition. STATISTICS:  $n=10$ , repeated measures ANOVA (F statistic, for Gaussian distributions) or Kruskal-Wallis (K statistic, for non-Gaussian distributions) or Friedman test (Q statistic, for non-Gaussian distributions). Correlation coefficients: PP-Hilar (lower-left)  $F_{(2,18)}=5.105$ ,  $p=0.0016$ . Delays: CA1-PP (upper-right)  $K=10.2$ ,  $p=0.0061$ ; CA1-PP (lower-right)  $K=6.862$ ,  $p=0.0324$ ; PP-Hilar (lower-left)  $Q=9.6$ ,  $p=0.0075$ . Proportion of time-windows in quadrants: CA1-PP

(upper-right)  $F_{(2,18)}=4.745$ ,  $p=0.0221$ ; CA1-PP (lower-left)  $F_{(2,18)}=3.846$ ,  $p=0.0407$ ; CA1-Hilar (lower-right)  $F_{(2,18)}=4.575$ ,  $p=0.0247$ .

#### **4.4. Independent components of sub-threshold evoked potentials**

It has already been anatomically described by Ramón y Cajal (1904), and physiologically as well (Andersen et al., 1966; Buzsáki, 1984), that the entorhinal input to the dentate gyrus does not only contact granule cell dendrites but also hilar and molecular layer interneurons. This feed-forward inhibitory circuit has a prominent role in controlling dentate gyrus output activity (see *Discussion* below). Therefore, we investigated the possible contribution of this circuit to our functional reorganization findings (see above; see also Álvarez-Salvado et al., 2013). To this end we used low current intensity stimulation of the perforant pathway (with currents ranging from 30 to 100  $\mu$ A) to produce evoked potentials with amplitudes comparable to the average peak-to-peak amplitude of the spontaneous signal oscillation recorded in the same electrodes (hilus recordings)(Figure 4.8). This sub-threshold potentials, similar to the ones used to characterize the origin of some generators (see above; see also Korovaichuk et al., 2010), do not critically violate the signal stationarity assumption imposed by ICA analysis (Makarov et al., 2010). Typically, we recorded the spontaneous activity for periods of several minutes, while stimulating the perforant path at a very low frequency (0.1 Hz).

The typical positive sub-threshold evoked-LFP at the hilus of the dentate gyrus (hereafter referred to as simply “e-LFP”) reaches maximal amplitude with a latency of  $6.27\pm 0.04$  ms ( $n=8$ )(Figure 4.8-B). The simultaneously recorded EPSP at the molecular layer, known to represent the dendritic depolarization of the granule cells in response to the perforant pathway input (Andersen et al., 1966), has its onset at approximately 2 ms, and maximal amplitude at a latency of  $4.55\pm 0.02$  ms ( $n=8$ ). The sub-threshold evoked-LFP could be separated with ICA into two generators, the PP and the Hilar (Figure 4.8-A)(hereafter called, when referring to evoked potentials, “e-PP” and “e-Hilar”, respectively). The e-PP has a faster onset (approximately 2 ms) and maximal amplitude at  $5.09\pm 0.03$  ms ( $n=8$ ). The e-Hilar is characterized by a slower onset and maximal amplitude at  $7.35\pm 0.05$  ms ( $n=8$ ). Interestingly, the peak latency of the e-LFP (6.27 ms) is practically the same as the average of the peak latencies of the two generators that compose it (6.22 ms), which supports the notion of the summation of the two components as simultaneous but parallel potentials.

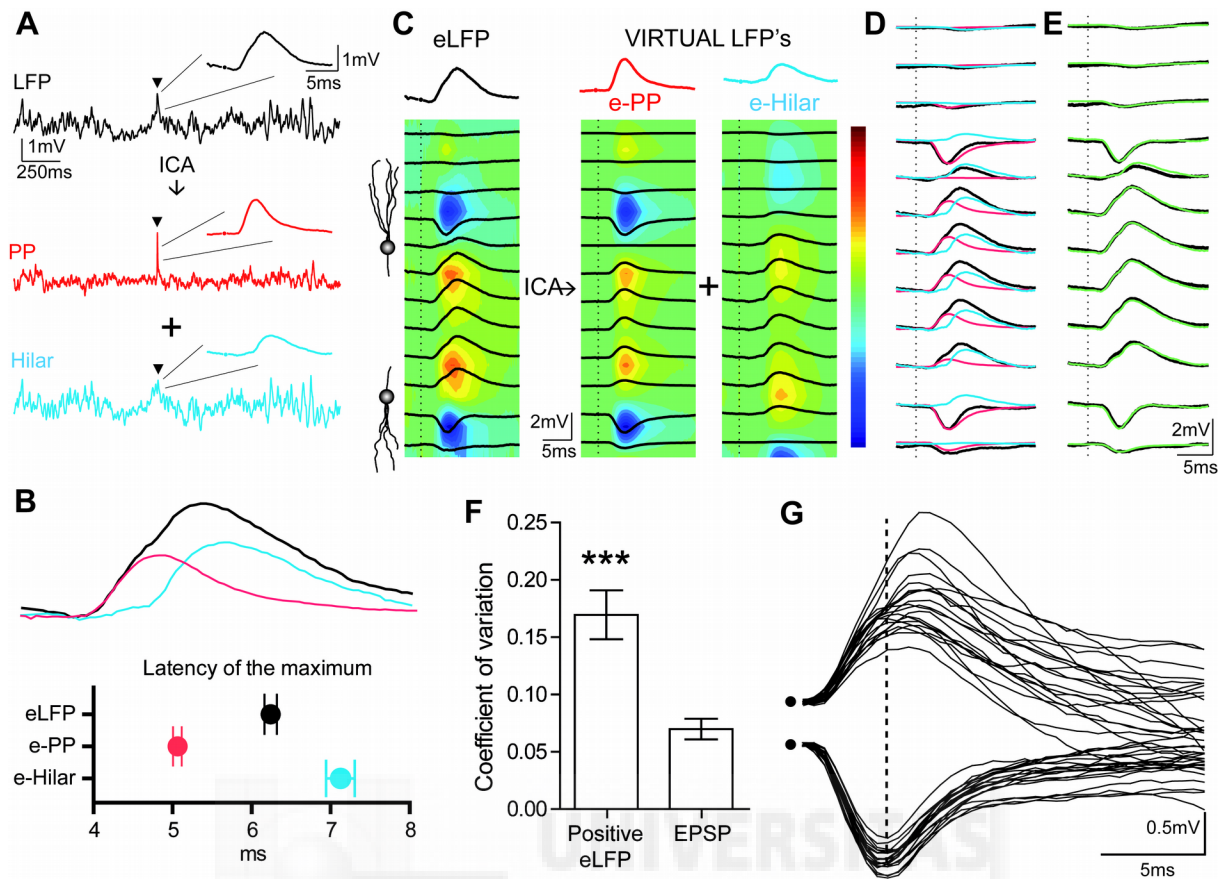


**Figure 4.8. Characterization and separation of the sub-threshold evoked-LFP into independent components.** (A) Representative example traces of spontaneous and evoked-LFP in the dentate gyrus, and the corresponding LFP-generators in which it was separated with ICA. Note that the amplitude of the e-LFP is similar to the surrounding spontaneous activity. (B) Same example traces of evoked responses as in (A) superimposed (upper panel), and group averages of their respective peak latencies (mean  $\pm$  SEM)(lower panel). (C) Traces of the same potentials shown in every recording channel at the dentate gyrus and some from overlying stratum lacunosum-moleculare (CA1), superimposed with the corresponding CSD maps (dotted lines mark the time of electrical stimulation). On the left panel, the evoked-LFP traces, and on the right the two components of that potential (PP and Hilar), represented by their reconstructed virtual-LFP. The CSD of e-PP matches perfectly the sinks at the e-LFP's CSD, but doesn't completely account for the sources. The e-Hilar presents sources at the hilus, closer to the granule cell layer, and sinks more distant into the molecular layer. (D) Evoked-LFP channels (black) superimposed with the virtual-LFP of its components (e-PP [red] and e-Hilar [cyan]). (E) Evoked-LFP channels (black) superimposed with the summation of the virtual-LFP of its components (green); note the practically complete coincidence of both groups of traces. (F) Group average of the Coefficient of Variation of the positive evoked-LFP from the hilus and the EPSP from the molecular layer (bars represent mean  $\pm$  SEM), and representative example traces of those two potentials (G), marked with dashed line at 4 ms latency. Note that the most inconstant part of the e-LFP is the peak where it exceeds the latency of the maximum of the EPSP; this is the part of the e-LFP mostly contributed by the e-Hilar component. STATISTICS: (F)  $n=8$ , paired t-test (t statistic, for Gaussian distribution),  $t_{(7)}=5.495$ ,  $p=0.0009$ .

When we performed the current source density analysis (CSD) of the generators, we found a very good correspondence between the negative EPSP in the molecular layer and the e-PP. It presents a sink at the level of the molecular layer -produced by the dendritic depolarization- and a source below the granule cell layer -resulting from the passive current propagation-, matching perfectly with the anatomy of the medial entorhinal afferent to the dentate gyrus, and with the CSD of the e-LFP. However, looking at the potential produced by the e-PP at the hilar layer, it lasts shorter than the

e-LFP, therefore evidencing the lack of a second, slower part; the e-Hilar appears to contribute with such a component. The CSD of e-Hilar's virtual LFP shows a current source below and closer to the granule cell layer than the e-PP, and a sink more distal in the molecular layer. The superimposition of both virtual LFP of the generators and the raw LFP (Figure 4.8-D) shows the different contributions of the two generators to the e-LFP. In Figure 4.8-E there is an example of how the summation of both components allows a practically perfect reconstruction of the evoked raw LFP signal.

An additional observation was that the variability in the amplitude of the e-LFP at the hilus is significantly higher than that of the EPSP at the molecular layer (Figure 4.8-F); for the former, the average coefficient of variation is  $0.169 \pm 0.021$ , while for the latter is  $0.069 \pm 0.008$ . This is well illustrated by the example shown in Figure 4.8-G. These findings suggest that the e-Hilar potential represents a feed-forward inhibition recruited by the perforant pathway with an active source in the granular layer and the variability attributable to a di-synaptic input.

In order to further investigate the relation between the Hilar generator and the local ongoing activity, we compared its magnitude with the phase of the ongoing oscillations in the Gamma (30-100 Hz) and Theta (3-10 Hz) frequency bands recorded in hilus and CA1, respectively. We observed that the amplitude of the e-Hilar was significantly bigger at the through phase of the local ongoing Gamma oscillation compared to the peak phase (Figure 4.9-A). When studying the relation between e-Hilar and Theta oscillations in CA1 generator we didn't observe any significant differences. However, we found a robust modulation of the power of the spontaneous activity of Hilar generator during the Theta cycle, showing a significantly increased power during the through phase (Figure 4.9-B).

To illustrate the modulation of the e-Hilar with the Gamma oscillations, we divided the e-Hilar traces in bigger and smaller ones, and represented separately for the two groups a fragment of Hilar and PP generators' signals around the electrical stimulation. The resulting graphics (Figure 4.9-C) evidence a different phase of Gamma for the two sizes of e-Hilar potentials. In Figure 4.9-D are shown traces of raw LFP signals from recording channels at the hilus and the molecular layer that are simultaneous to those in panel C. Interestingly, the changes observed in the Hilar generator traces can be seen as well in the LFP traces from the hilus layer.

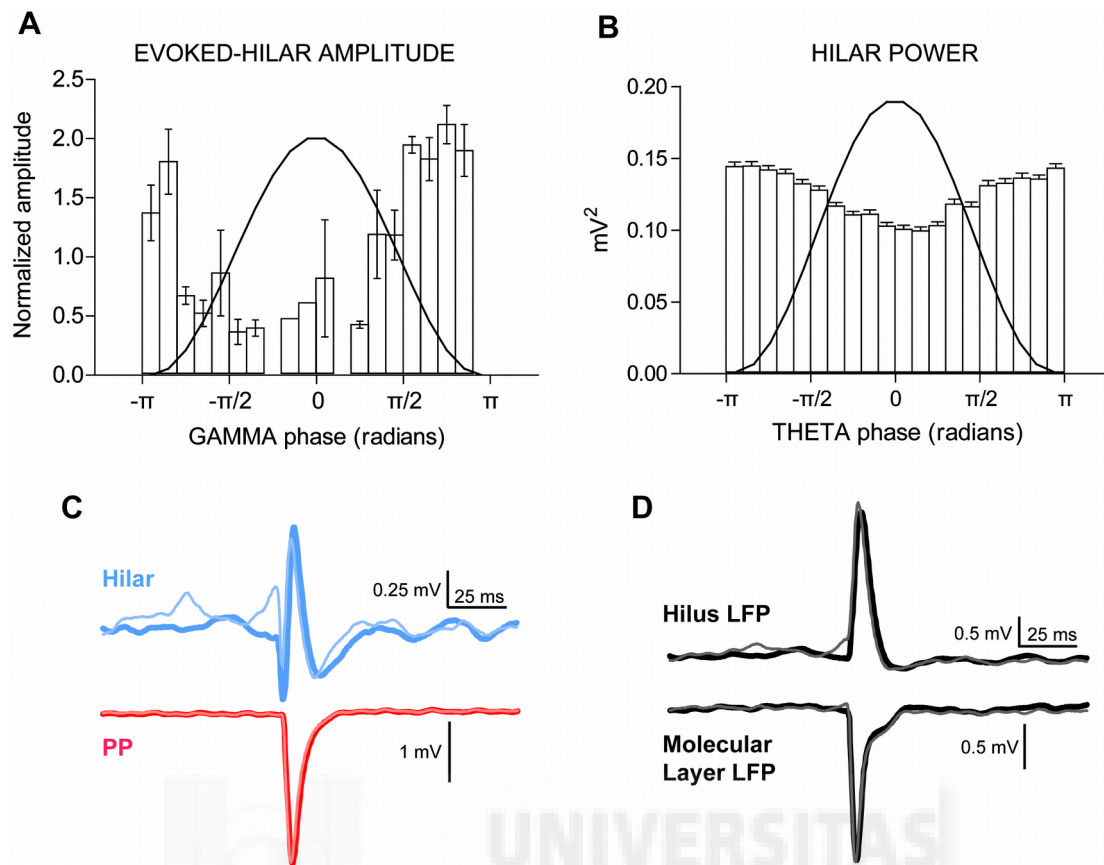


**Figure 4.9. Modulation of the Hilar generator by spontaneous Gamma and Theta oscillations.** (A) Amplitude of the e-Hilar in different phases of the gamma-cycle at the dentate gyrus, normalized to the mean amplitude of the eHilar in each experiment. Bars represent mean  $\pm$  SEM; the superimposed black trace shows a schematic Gamma oscillation corresponding to the phase values of the x-axis (in radians). (B) Power of the spontaneous activity of the Hilar generator at different phases of the theta-cycle at the CA1 generator. Power was calculated dividing the signal in 75 ms-long time-windows. Bars represent mean + SEM; superimposed black trace represents a schematic Theta oscillation like in (A). (C) Superimposed group average of virtual-LFP of Hilar (cyan) and PP (red) generators, taking only the signals around the evoked-LFP. In the corresponding lighter colors are shown the averages of the traces corresponding to smaller e-Hilar, and in darker colors the traces corresponding to bigger e-Hilar. (D) Superimposition of averaged traces equivalent to the ones in (C) taken instead from the raw LFP channels from hilus (upper traces) and molecular layer (lower traces). Gray traces represent average of the signals corresponding to the smaller e-Hilar, and black traces correspond to the bigger e-Hilar. STATISTICS: (A)  $n=6$ , Kruskal-Wallis test (K statistic, for non-Gaussian distributions),  $K=42.46$ ,  $p=0.001$ . (B)  $n=6$ , Kruskal-Wallis test,  $K=782.1$ ,  $p<0.0001$ .

#### 4.5. Pharmacological and electrophysiological characterization of the generators

To identify more accurately the nature and origin of the Hilar generator, we carried out pharmacological experiments in which we injected drugs locally in the hilus (see *Methods*). We studied the different parameters of sub-threshold evoked-LFP (and its components) during a local injection of Gabacine and Bicuculine (both antagonists for GABA<sub>A</sub> type receptors; Figures 4.10 and 4.11, respectively).

The injection of Gabacine with a concentration of 1 mM produced a significant decrease in the amplitude the e-Hilar and a corresponding increase in the excitation-inhibition ratio (measured as the ratio e-PP/e-Hilar)(Figure 4.10) Also, we observed the decrease of e-LFP that usually occurs with the

reduction of e-Hilar, as mentioned before. Gabacine has a very slow washout, so the potentials were never actually recovering back to the initial state in the duration of the experiments, as could be observed in the evoked supra-threshold potentials, that showed multiple population-spikes during the whole time of these experiments. In Figure 4.10 there is an example of different parameters of the sub-threshold evoked potential during 30 minutes, with an injection of Gabacine at approximately 5 minutes.

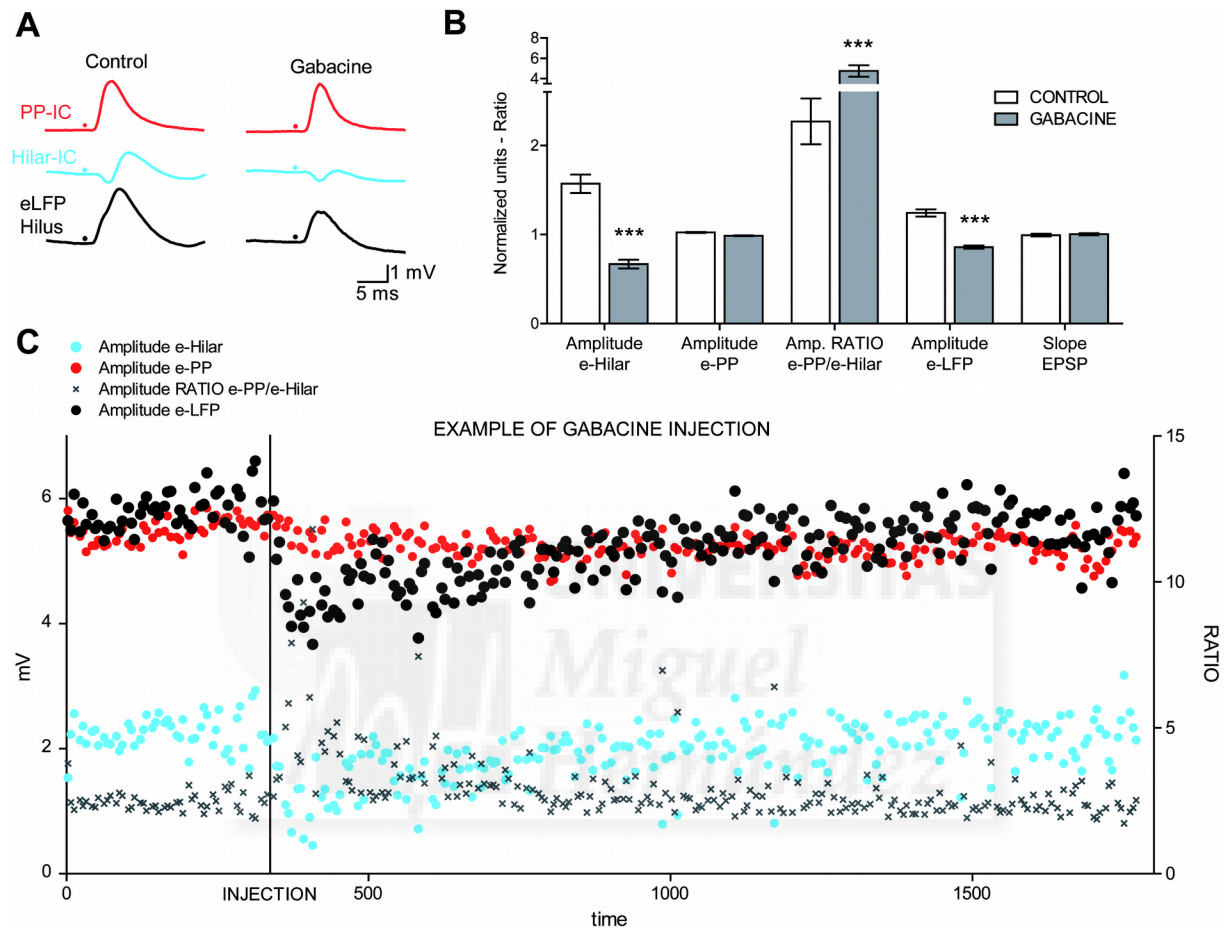


**Figure 4.10. Effect of Gabacine on sub-threshold evoked-LFP.** (A) Representative example traces of the raw e-LFP (black traces) and its components (e-PP: red; e-Hilar: cyan) before and after local injection of Gabacine in the Hilus. Note the selective reduction of the e-Hilar potential. (B) Parameters of the evoked-LFP and its components in the dentate gyrus before and after the Gabacine, normalized (except for the ratios) to the average value in each experiment. Bars represent mean  $\pm$  SEM. Some of those parameters from an example injection are represented on a timeline in (C). Time is expressed in seconds; black vertical line over "INJECTION" (at x-axis) marks the moment of the injection of Gabacine; the left y-axis plots mV, and the right y-axis shows ratio. STATISTICS:  $n=3$ , t-test (t statistic, for Gaussian distributions) or Mann Whitney test (U statistic, for non-Gaussian distributions). e-Hilar Amplitude:  $U=318$ ,  $p<0.0001$ ; Amplitude ratio e-PP/e-Hilar  $U=889$ ,  $p<0.0001$ ; e-LFP Amplitude  $U=308$ ,  $p<0.0001$ .

When we injected Bicuculine with a concentration of 100  $\mu$ M we found the same changes in the subthreshold evoked potentials than with Gabacine, and additionally a moderate but significant increase in the slope of the EPSP (Figure 4.11).

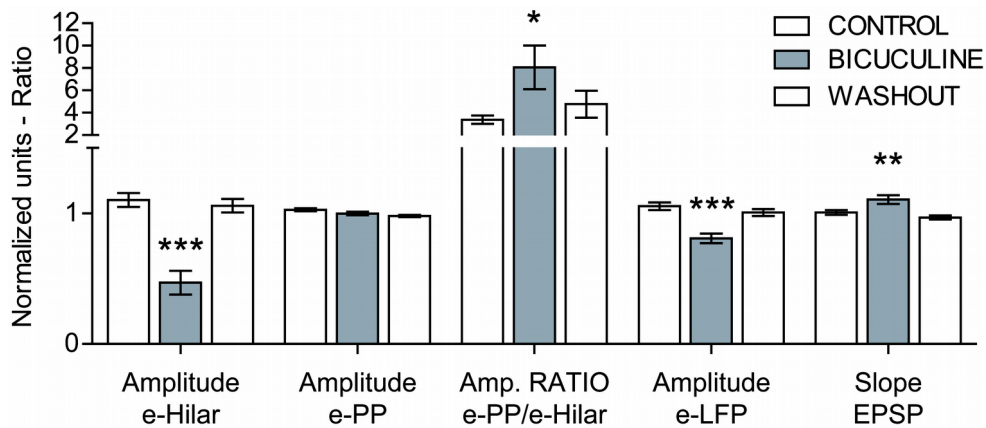


**Figure 4.11. Effect of Bicuculine on sub-threshold evoked-LFP.** Parameters of the evoked-LFP and its components in the dentate gyrus, recorded before and after local injection of Bicuculine in the Hilus. The parameters (except for the ratios) were normalized to the average value in each experiment. Bars represent mean  $\pm$  SEM. A consistent decrease of the e-Hilar (and associated changes) can be observed. STATISTICS:  $n=3$ , Kruskal-Wallis (K statistic, for non-Gaussian distributions); e-Hilar Amplitude:  $K=22.53$ ,  $p<0.0001$ ; Amplitude ratio e-PP/e-Hilar:  $K=7.557$ ,  $p=0.0229$ ; e-LFP Amplitude  $K=17.51$ ,  $p<0.0002$ ; EPSP Slope  $K=11.24$ ,  $p<0.0036$ . Dunn's multiple comparison test:  $p<0.05$  (\*),  $p<0.01$  (\*\*),  $p<0.001$  (\*\*\*)

To further investigate the cellular mechanisms behind the Hilar generator, we carried out as well paired-pulses recordings and studied how they modulated the evoked-LFP. We delivered an initial sub-threshold stimulus to record a “control” potential; two seconds later a supra-threshold stimulus was delivered, and then 150 ms later another sub-threshold evoked-LFP was recorded as a test (“paired” pulse). The following figure illustrates this stimulation protocol.

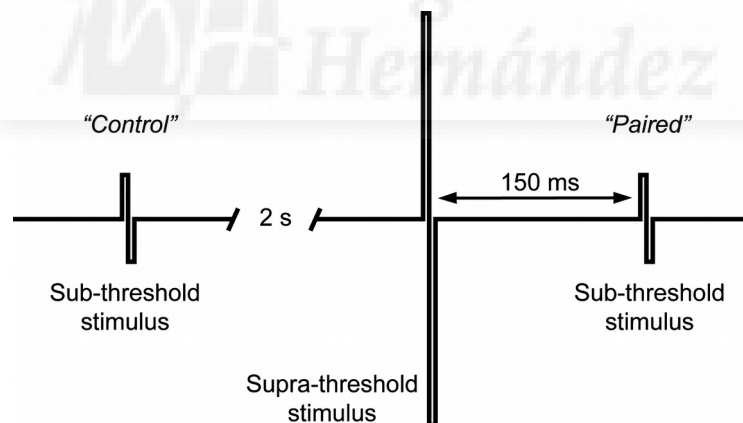


**Figure 4.12. Schematic illustration of paired-pulses stimulation protocol.** The black trace represents the current introduced with the stimulation (vertical size of the potentials is arbitrary). In the horizontal axis is represented time.

We compared the control potential with the paired potential. By choosing a 150 ms latency we aimed at modulating the GABAergic system, since 150 ms after a population spike there is a peak in the activity of GABA<sub>B</sub> receptors, that in turn reduce presynaptically the release of GABA (Davies et al., 1990). We tested the protocol by pairing two supra-threshold stimuli, and we observed a significant increase in the PS of the second evoked-LFP, thus confirming the disinhibitory effect of using 150 ms latencies (Figure 4.13-A, B). Accordingly, in the sub-threshold paired-pulses we observed a significant decrease in the magnitude of e-Hilar with respect to control, supporting a GABAergic origin of this

generator (Figure 4.13-C). We found as well a corresponding increase in the excitation-inhibition ratio, and a decrease in the amplitude of the positive e-LFP, that appears most of times and just reflects the decrease of the e-Hilar. Also we observed a decrease in the size of both e-PP and EPSP. This was due to the pairing effect on the EPSP, that resulted in a moderate but consistent decrease of its slope in supra-threshold evoked-LFP (Figure 4.13-A).

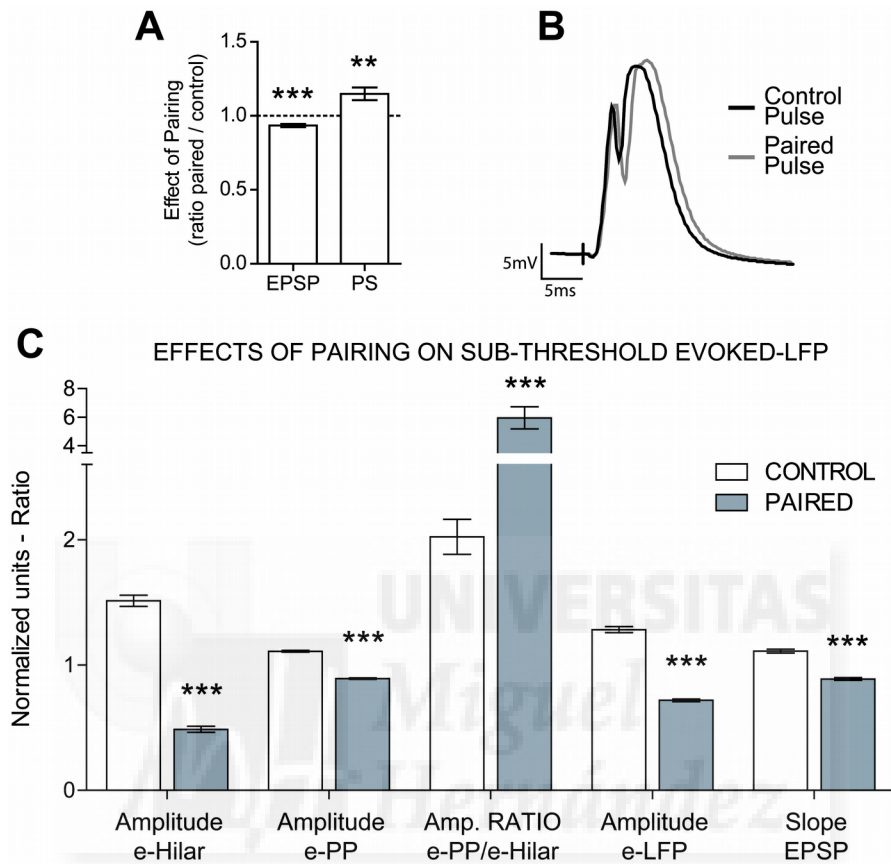


**Figure 4.13. Effect of pairing on sub-threshold e-LFP.** (C) Parameters of the sub-threshold evoked-LFP and its components, recorded in control condition (white) and after a supra-threshold stimulation (gray). The parameters (except for the ratios) were normalized to the average value in each experiment. Bars represent mean  $\pm$  SEM. Pairing provoked a consistent reduction of the evoked-LFP and its components, specially in the e-Hilar. (A) Effect of pairing on supra-threshold evoked-LFP's EPSP and PS, expressed as a paired/control ratio. The "1" value is marked with a dashed line to represent the hypothetical no-change level. Bars represent mean  $\pm$  SEM. They illustrate a significant decrease of the EPSP with pairing and an increase of the PS. (B) Representative examples of a couple of paired supra-threshold evoked-LFP, superimposed. Paired potential (gray trace) was evoked 150 ms after the control potential (black trace). Note the bigger PS of the paired potential. STATISTICS: (A)  $n=3$ , One sample t-test (t statistic, for Gaussian distributions). EPSP:  $t_{(28)}=5.983$ ,  $p<0.0001$ ; PS:  $t_{(28)}=3.482$ ,  $p=0.0017$ . (C)  $n=3$ , Wilcoxon matched-pairs signed rank test (W statistic, for non-Gaussian distributions); e-Hilar Amplitude:  $W=903.0$ ,  $p<0.0001$ ; e-PP: Amplitude  $W=903.0$ ,  $p<0.0001$ ; Amplitude ratio e-PP/e-Hilar:  $W=-901$ ,  $p<0.0001$ ; e-LFP Amplitude:  $W=903$ ,  $p<0.0001$ ; EPSP Slope:  $W=835$ ,  $p<0.0001$ .

Because the observed effects of pairing were theoretically due to the action of GABA<sub>B</sub> receptors, we wanted to test it and thus we checked if they could be prevented by pharmacologically blocking those receptors with a local injection of CGP (especific GABA<sub>B</sub> receptors antagonist drug) in the hilus. We found that indeed CGP completely prevented the facilitation of the PS observed in the supra-threshold evoked-LFP (Figure 4.14-A, B). Regarding the sub-threshold evoked-LFP, the decrease of the e-Hilar

and the associated increase in the excitation-inhibition ratio were partially prevented too (Figure 4.14-C).

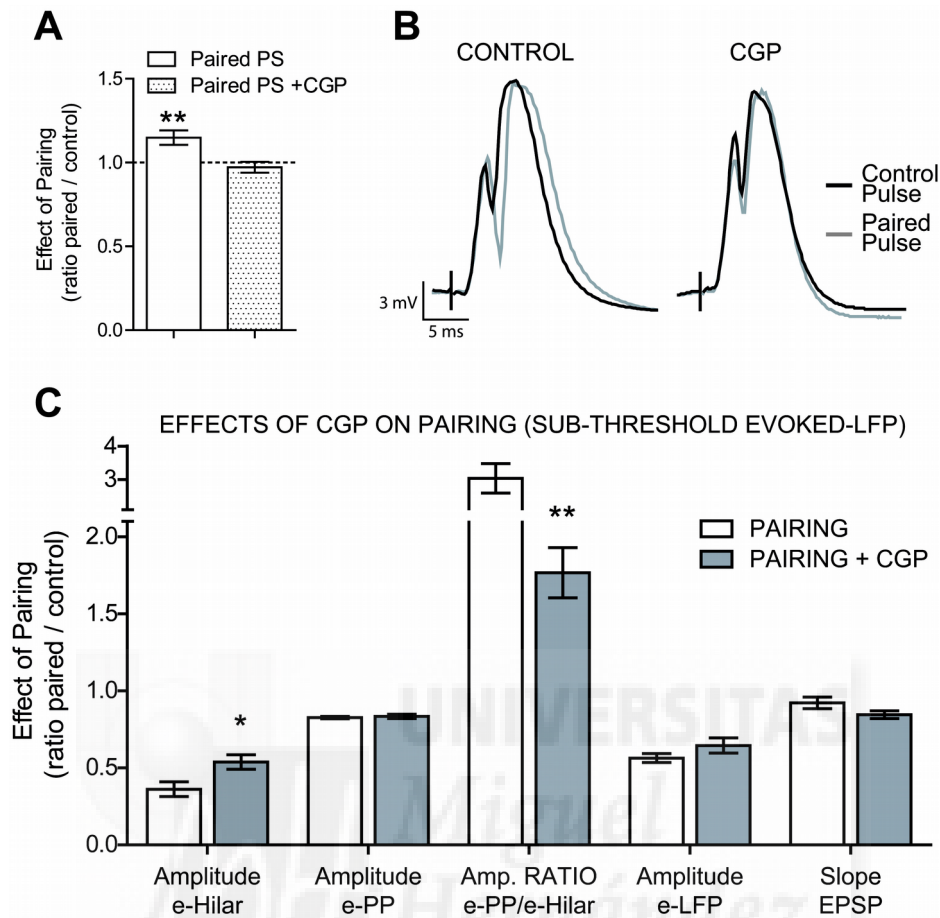


**Figure 4.14. Pharmacological reversal of the effect of pairing on sub-threshold evoked-LFP.** (C) Effect of the pairing on those parameters (measured as the ratio of the value after the pairing by the value before pairing), in control conditions (white) and in the presence of CGP (gray). Bars represent mean  $\pm$  SEM. (A) Effect of pairing on PS (expressed as a paired/control ratio) before and after local injection of CGP in the hilus. The “1” value is marked with a dashed line to represent the hypothetical no-change level. Bars represent mean  $\pm$  SEM. Note that in the presence of CGP, pairing has no effect on the PS. (B) Superimposed representative examples of a couple of paired supra-threshold evoked-LFP before and after injecting CGP. Paired potential (gray trace) was evoked 150 ms after the control potential (black trace). Note that CGP completely avoided the facilitation of PS. STATISTICS: (A)  $n=3$ , One sample t-test (t statistic, for Gaussian distributions). PS:  $t_{(28)}=3.482$ ,  $p=0.0017$ . (C)  $n=3$ , t-test (t statistic, for Gaussian distributions) or Mann Whitney test (U statistic, for non-Gaussian distributions). e-Hilar Amplitude:  $t_{(34)}=2.645$ ,  $p=0.0123$ ; Amplitude e-PP/e-Hilar ratio:  $U=77$ ,  $p=0.0075$ .

All these results pointed to a fundamental contribution of the GABAergic local network to the Hilar generator, although they leave some gaps of information for a full explanation of the cellular and molecular mechanisms of the generators. However, it is not possible to go further with the methods employed in the present work.

#### 4.6. Changes in the sub-threshold evoked potentials with LTP

Having demonstrated that the recorded e-Hilar represents inhibitory GABA<sub>A</sub> currents in granular cells (probably recruited by feed-forward connections from the entorhinal cortex), we asked whether this

inhibitory network is involved in the LTP-triggered functional reorganization of dentate gyrus output activity. When we compared the sub-threshold evoked-LFP between control and LTP, we observed a clear change in the waveform of the e-LFP in the hilus; more specifically, the latency of its amplitude peak and the amplitude itself decreased significantly after the potentiation (Figure 4.15-A). Similarly to what we observed in the pharmacological experiments, these changes in the e-LFP were a reflection of a reduction of the e-Hilar component, as illustrated in Figure 4.15-A. We found as well a corresponding increase in the excitation-inhibition ratio. Moreover, LTP was reflected in an increase in the amplitude of the e-PP and the slope of the EPSP. The quantification of these changes is shown in Figure 4.15-C. Three hours after LTP induction, the modifications observed were still persistent.

Curiously, after LTP we could observe a direct correlation between the slope of the EPSP and the amplitude of the positive e-LFP (Figure 4.15-B) that was absent in control conditions. This evidences the fact that normally the e-LFP is produced by the summation of e-PP and e-Hilar components, and thus it is only in absence of the latter (with LTP) that the EPSP contributes by itself the whole amplitude of the positive e-LFP through electro-tonic propagation. Actually, three hours after LTP, the correlation disappeared again.

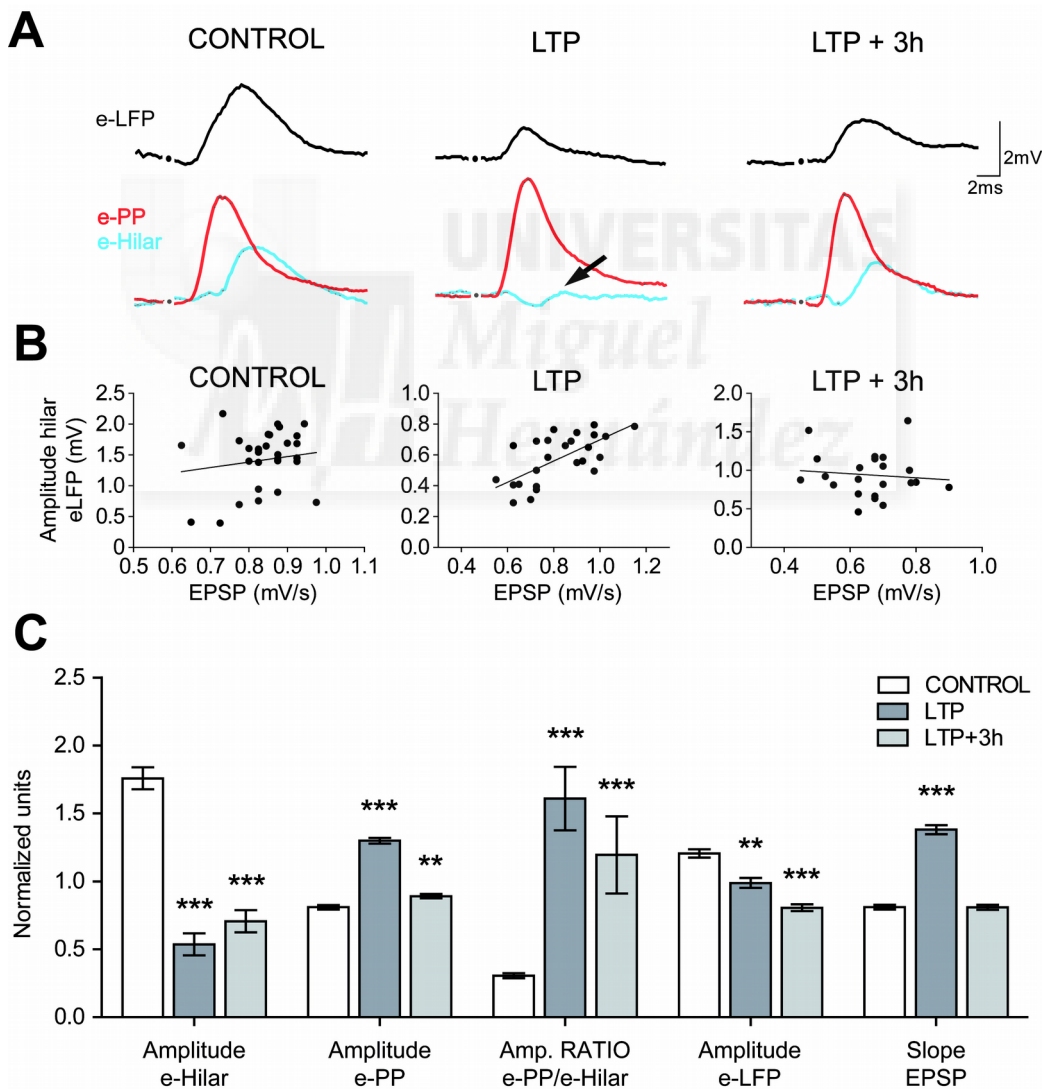


**Figure 4.15. Changes in the sub-threshold evoked-LFP with LTP.** (A) Representative example traces of the e-LFP (black) and its components (e-PP: red; e-Hilar: cyan), recorded before (control), immediately after

potentiation (LTP) and three hours later (LTP+3h). Arrow points out the nearly complete disappearance of e-Hilar component with LTP. (B) Representative example of correlation between the EPSP slope (measured at the molecular layer; mV/ms) and the maximal amplitude of the positive e-LFP (measured at the hilus; mV) in one subject during potentiation (same three conditions as in [A]). The black lines are the linear regression of the dots populations. Note that in control and LTP+3h conditions the lines are horizontal, evidencing the lack of correlation (see statistics below). (C) Parameters of the evoked-LFP and its components in the dentate gyrus, recorded in the same three conditions as in (A). Parameters were normalized to the average value in each experiment; bars represent mean  $\pm$  SEM. STATISTICS: (B)  $n=6$ , linear regression (test for goodness of fit and non-zero slope). Control:  $R^2=0.0002$ ,  $F_{(1,119)}=0.02885$ ,  $p=0.8654$ ; LTP:  $R^2=0.37$ ,  $F_{(1,166)}=99.93$ ,  $p<0.0001$ ; LTP+3h:  $R^2=0.0076$ ,  $F_{(1,108)}=0.831$ ,  $p=0.364$ . Slopes of regression lines are significantly different ( $F_{(2,393)}=10.744$ ,  $p<0.0001$ ). (C)  $n=6$ , One-way ANOVA (F statistic, for Gaussian distributions) or Kruskal-Wallis test (K statistic, for non-Gaussian distributions). e-Hilar Amplitude:  $K=45.12$ ,  $p<0.0001$ ; e-PP Amplitude:  $F_{(2,71)}=213.0$ ,  $p<0.0001$ ; Amplitude e-PP/e-Hilar ratio:  $K=44.19$ ,  $p<0.0001$ ; e-LFP Amplitude:  $K=39.22$ ,  $p<0.0001$ ; EPSP Slope:  $F_{(2,71)}=190.9$ ,  $p<0.0001$ . Bonferroni (for Gaussian distributions) or Dunn (for non-Gaussian distributions) multiple comparison tests:  $p<0.01$  (\*\*),  $p<0.001$  (\*\*\*)).

In order to approach the possible molecular mechanisms responsible for the modifications observed in the dentate gyrus with LTP, we carried out additional pharmacological experiments injecting the NMDA receptors antagonist AP5 in the hilus (see *Methods.Pharmacological experiments*). It demonstrated to block effectively the potentiation induced by electrical stimulation (Figure 4.16-A). For some of the stimulation intensities studied there was still a moderate but statistically significant change caused by LTP; however, there was a big difference between those changes and the potentiation induced in normal conditions (Figure 4.16-A), and indeed the curves obtained with AP5 were not significantly potentiated for most of the EPSP slopes. Furthermore, AP5 blocked the effect of LTP on the e-PP component of the sub-threshold evoked-LFP, but it failed to prevent the associated reduction of the e-Hilar component (Figure 4.16-B). This evidences that AP5 is effectively blocking the potentiation dependent of NMDA receptors; therefore, the mechanisms underlying the reduction of the inhibition after LTP are, at least in part, independent of the activation of NMDA receptors.

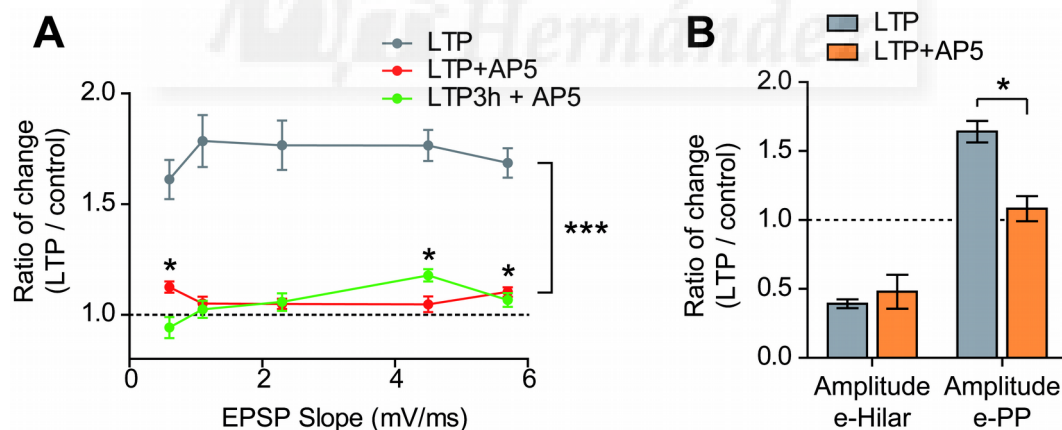


**Figure 4.16. Blockade of the effects of LTP on evoked-LFP with AP5.** (A) Input-output curves showing de ratio of potentiation induced by LTP in different magnitudes of slope of the electrically evoked EPSP (x-axis; mV/ms); the potentiation is expressed as a ratio between the slope of the EPSP after and before LTP (y-axis). Thus the curves represent different profiles of potentiation in different conditions: the usual level of potentiation in our LTP experiments (gray); and in the presence of AP5, immediately after LTP induction (red) and three hours later (green). Although red and green curves are significantly potentiated in two and one EPSP slope values (respectively), they mainly show no significant potentiation and are at the level of no-change (ratio of 1). (B) Ratio of change (LTP/control) induced by LTP in the amplitude of e-Hilar and e-PP components of the sub-threshold evoked-LFP. Conditions are LTP in normal conditions (gray) and in the presence of AP5 (orange). While the e-Hilar experiences the same degree of change with LTP in both conditions, the e-PP component is

unaffected by potentiation in the presence of AP5, going back to the no-change level of ratio 1 (marked with a horizontal dashed line). STATISTICS: (A)  $n=3$ . Differences from ratio=1, one sample t-test (t statistic, for Gaussian distributions). LTP+AP5, smallest slope:  $t_{(11)}=4.967$ ,  $p=0.0004$ ; biggest slope:  $t_{(11)}=4.904$ ,  $p=0.0017$ ; LTP3h+AP5:  $t_{(7)}=6.340$ ,  $p=0.0004$ . Differences with usual LTP, two way ANOVA (F statistic, for Gaussian distributions). Condition  $F_{(2, 118)}=230.3$ ,  $p<0.0001$ . Bonferroni multiple comparison test:  $p<0.001$ (\*\*\*). (B)  $n=3$ , Mann Whitney test (U statistic, for non-Gaussian distributions). e-PP, LTP vs LTP+AP5:  $U=0.0$ ,  $p=0.0357$ . e-PP at LTP+AP5 not significantly different from 1 (one sample t-test).

#### **4.7. Local supression of the GABAergic activity affects ongoing activity and information propagation**

To study the role of Hilar generator in the modulation of the spontaneous activity observed with LTP, we studied the effects of an injection of Gabacine in the hilus on the spontaneous activity of the generators ( $n=3$ ). We measured the power of their time courses before and after the injection. Interestingly, the power of the Hilar and PP generators showed a tendency to mimic the effects produced by the LTP, i.e. a decrease and an increase in the power, respectively; however, this effect was not statistically significant. This could be due to the fact that the spontaneous LFP recorded near the electrodes is contributed by a much larger network than an evoked sub-threshold potential recorded at the same electrode, which originating network might be much more circumscribed to the local region around the electrode. Considering that, a very localized dose of drug would possibly allow the unaffected ongoing activity in the surrounding volume of tissue to partially mask and compensate for the effect of the drug at the local level, so the total activity recorded would be hardly changed. Accordingly, Benito and colleagues (2013) could modulate significantly the activation of the hippocampal generators with GABA<sub>A</sub> receptors antagonists, using doses aproximately 5 times higher than ours.

We analyzed as well the cross-correlation between generators during the effect of Gabacine, and we didn't observe any significant change in correlation coefficients, delays or distribution of time-windows among the different connectivity patterns (see *Methods* for details on this analysis). The amount of time that generators were correlated only changed significantly between Schaffer and Hilar, decreasing after the injection of Gabacine ( $n=3$ , one sample t-test [t statistic, for Gaussian distributions],  $t_{(2)}=5.243$ ,  $p=0.0345$ ). This could be explained by the overall reduction in the activation of Hilar generator; the fact that this effect is significant only between Hilar and Schaffer generators might be due to the fact that their anatomical origins are closer than others (notice that an equivalent change occurs between PP and Hilar, although it is not statistically significant). The lack of clear observable effects on the correlations might have the same cause mentioned in the previous paragraph.

In order to test our hypothesis that a GABAergic local network in the hilus (the Hilar generator) could be fundamentally involved in the functional reorganization observed in past work (Canals et al., 2009) and supported by our own results, we carried out a similar experiment combining a local pharmacological manipulation and functional magnetic resonance imaging (for details on this technique, see *Methods*). The recordings inside the magnet showed reliably the effect of the Gabacine when it was injected: the appearance of multiple subsequent population spikes in the supra-threshold evoked-LFP in the dentate gyrus, whereas the physiological response involves exclusively one population spike (an example of this is shown in Figure 4.17-D). This is the reflection of the lack of inhibitory mechanisms, while the fact that the initial slope of the rising potential doesn't change with Gabacine (arrow in Figure 4.17-D) evidences that the input from the perforant path is not altered.

Regarding the maps of BOLD activation, we found significant differences between before and after the Gabacine injection. The ipsilateral hippocampal network was more activated in the presence of the drug, and the activity actually propagated remarkably to the contralateral hippocampus (Figure 4.17). We observed as well activations in distant extrahippocampal, cortical and subcortical areas, that were

not active with the stimulation before the Gabacine administration, namely the ventral striatum and the frontal cortex (Figure 4.17-A, arrows in colors are marking the inactive areas in control condition). These findings are in perfect agreement with those observed by Canals et al. (2009), where it was already described how LTP can open specific channels of information in the hippocampus and facilitate its propagation through this structure and to distant areas of the brain. Our results further support this notion, and add evidence that the local GABAergic network is involved in such functional reorganization and preferential information processing.

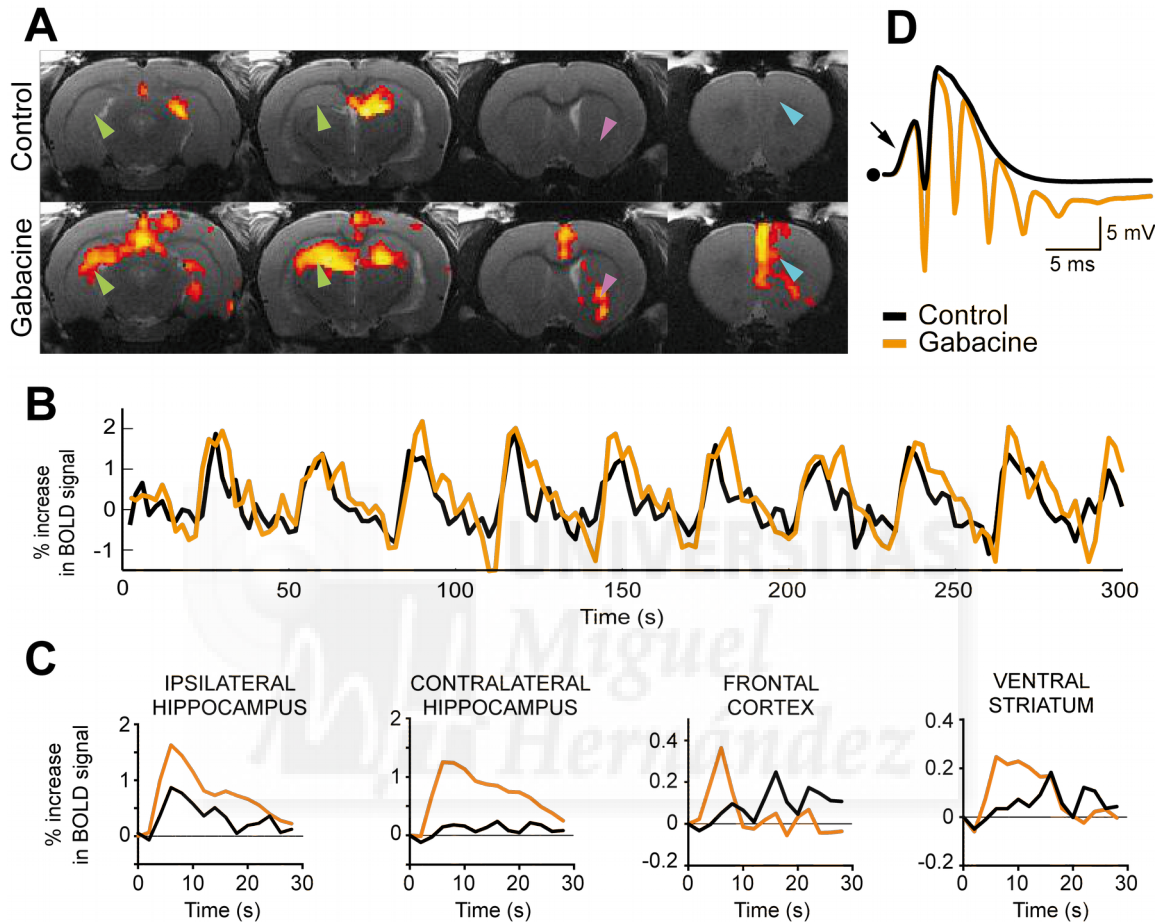


**Figure 4.17. Effects of Gabacine on BOLD signal maps across the brain.** (A) Magnetic resonance anatomical images (in gray scale) at selected rostro-caudal levels of the brain, with colors marking the voxels significantly correlated to the electrical stimulation. The upper row of images were recorded before Gabacine injection, and the lower row during the effect of the drug. Marked with arrows in colors are the hippocampus contralateral to the injection hemisphere (green), the ventral striatum (pink) and the frontal cortex (blue). Note that the activation of these areas with electrical stimulation occurs only in the presence of Gabacine in the hilus. (B) Representative example of BOLD activation of the ipsilateral hippocampus during the time of stimulation (trains were delivered every 30 seconds; see *Methods* for details); control trace in black, Gabacine trace in orange. (D) BOLD response to the stimulation in the selected areas of interest (averaged from 10 consecutive trains), before (black trace) and during Gabacine effect (orange trace). (D) Representative example of supra-threshold evoked-LFP in the hilus, recorded in the magnet during the experiment, before (black traces) and during the Gabacine effect (orange traces). Note the multiple population-spikes that appear with Gabacine, and an equal initial slope in the two traces (marked with black arrow).

#### 4.8. Learning modulates the generators' spontaneous activity

In the previous sections we have demonstrated that a change in the excitation-inhibition balance of the dentate gyrus, operated by local LTP, is responsible for a functional reorganization at the level of both the hippocampal formation and the whole brain, in good agreement with previous work (Canals et al., 2009; Álvarez-Salvado et al., 2013). We have used the same preparation to prove that a decrease in feed-forward inhibition at the dentate gyrus is indeed sufficient to trigger changes in the functional connectivity between the hippocampus and distant brain areas. We hypothesize that this could represent a mechanism for selective channeling of information –for instance novel or relevant information–, and thus in the context of memory such mechanism could be closely associated to learning. However, in order to state this, we considered as a priority to find more physiologically relevant proofs; therefore, we carried out experiments replicating the electrophysiological recording-stimulating setup in non-anesthetized, freely moving animals (see *Methods* for details on this preparation).

During these experiments, we recorded the spontaneous and sub-threshold evoked-LFP and analyzed them with ICA. We used a simple task in which the animal was repeatedly exposed to an open field (Figure 4.18-A), so that it became a familiar environment (referred to as “control” in this task), until a novel stimulus was presented. The reason of this experiment is that the animal unexpectedly confronted with a novelty in an otherwise well-known environment will activate hippocampal circuits to encode salient information in the spatial representation of the familiar environment. Our prediction was that this novelty would shift the excitation-inhibition balance towards a less inhibited state. The novel stimulus was achieved by introducing the animal in a transparent methacrylate box (referred to as “novelty box”) placed inside the familiar open field (Figure 4.18-B). This novelty session was compared with a subsequent session of 10 minutes in the familiar open field where the novelty stimulus was removed (see *Methods* for details on this task).

We used a video tracking program to obtain the spatial information of the animals' movement during the task (Figure 4.18-C), and we used that information in order to check whether the movements could be the cause of any changes observed in the LFP. For the present task, we quantified the average velocity of the animals during control and novelty conditions, and we found no significant difference (Figure 4.18-D).

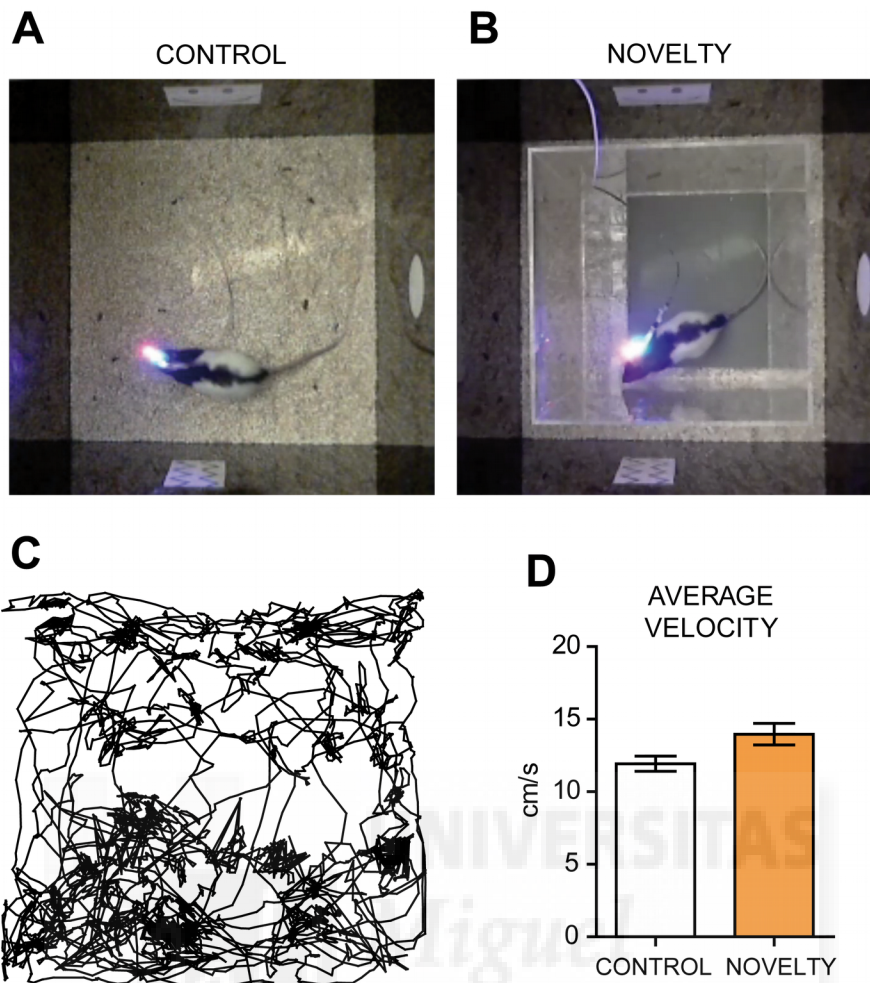


**Figure 4.18. Illustration of the Novelty task and trajectory of the animals.** (A) Picture showing an animal during a Novelty task, in the familiar open field and (B) in the novel box. Note the LED lights installed in the recording pre-amplifiers, that facilitate the video tracking of the animals. (C) Example representation of the trajectory of an animal during a session of habituation in the familiar environment, obtained with the video tracking software. (D) Group average velocity of the rats during the control (blank) and novelty (orange) sessions of the Novelty task.  $n=7$ ; bars represent mean  $\pm$  SEM.

We analyzed the power of the generators with the whole frequency spectrum and for specific frequency bands, and compared it between the two conditions of the task, both averaged (Figures 4.19 and 4.20) and over time (Figure 4.21). Regarding the averaged power, we found a significant increase of the PP generator (that corresponded to an increase of the Theta band power) with a concomitant decrease in the Hilar generator (in Delta and Gamma bands), in good agreement with previous results in anesthetized animals after LTP induction (compare to Figures 4.4 and 4.5). The excitation-inhibition ratio consequently increased. In comparison to the anesthetized preparation the freely-moving animal showed a small but more consistent decrease in the mean power of the Schaffer generator (Delta and Beta bands) and an increase in the CA1 generator selective for the Beta band.

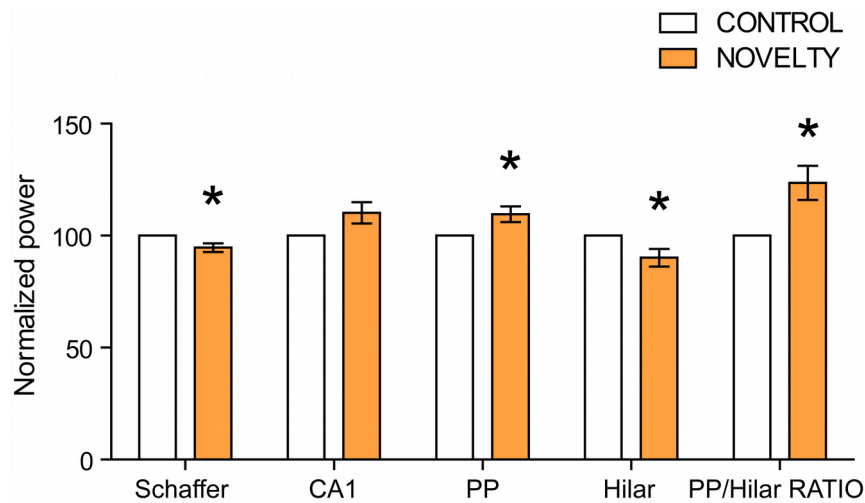


**Figure 4.19. Average power of the generators during a novelty.** Mean power of the hippocampal LFP-generators (and excitation-inhibition ratio in the dentate gyrus) in the control (blank) and novelty (orange) sessions, normalized to the average value in the control session. Bars represent mean  $\pm$  SEM. STATISTICS:  $n=7$ , One sample t-test (t statistic, for Gaussian distribution). Schaffer:  $t_{(6)}=2.729$ ,  $p=0.0342$ ; PP:  $t_{(6)}=2.722$ ,  $p=0.0345$ ; Hilar:  $t_{(6)}=2.475$ ,  $0.481$ ; Ratio:  $t_{(6)}=3.082$ ,  $p=0.0216$ .

Statistics of Novelty Task mean power of the LFP-generators					
Frequency band	SCHAFFER	CA1	PP	HILAR	Exc.-Inh. RATIO
$\delta$	Green	Grey	Grey	Green	Yellow
$\theta$	Grey	Grey	Yellow	Grey	Yellow
$\beta$	Green	Yellow	Grey	Grey	Yellow
$\gamma$	Grey	Grey	Grey	Green	Yellow

**Figure 4.20. Average frequency bands-power of the generators during a novelty.** Table illustrating statistically significant changes of the generators in specific frequency bands (Delta [ $\delta$ ], Theta [ $\theta$ ], Beta [ $\beta$ ] and Gamma [ $\gamma$ ]). Colors of the cells mean statistical significance (yellow-increase; green-decrease). STATISTICS:  $n=7$ , one sample t-test (t statistic, for Gaussian distributions). Delta band; Schaffer:  $t_{(6)}=3.917$ ,  $p=0.0078$ ; Hilar:  $t_{(6)}=2.792$ ,  $p=0.0315$ ; Ratio:  $t_{(6)}=2.611$ ,  $p=0.0401$ . Theta band; PP:  $t_{(6)}=5.524$ ,  $p=0.0015$ ; Ratio:  $t_{(6)}=3.463$ ,  $p=0.0134$ . Beta band; Schaffer:  $t_{(6)}=2.553$ ,  $p=0.0433$ ; CA1:  $t_{(6)}=2.576$ ,  $p=0.0420$ ; Ratio:  $t_{(6)}=2.803$ ,  $p=0.0310$ . Gamma band; Hilar:  $t_{(6)}=3.356$ ,  $p=0.0153$ ; Ratio:  $t_{(6)}=2.539$ ,  $p=0.0442$ .

The power of the generators was also analyzed over time during the two sessions of the task. The observations just described with the averaged power could be found as well in the power represented in a timeline, and the changes triggered by the novel stimulus were especially evident during the first tens of seconds of the novelty session (Figure 4.21), where they were statistically significant as well. On the other hand, the power of each generator was close to control values to the end of the session.

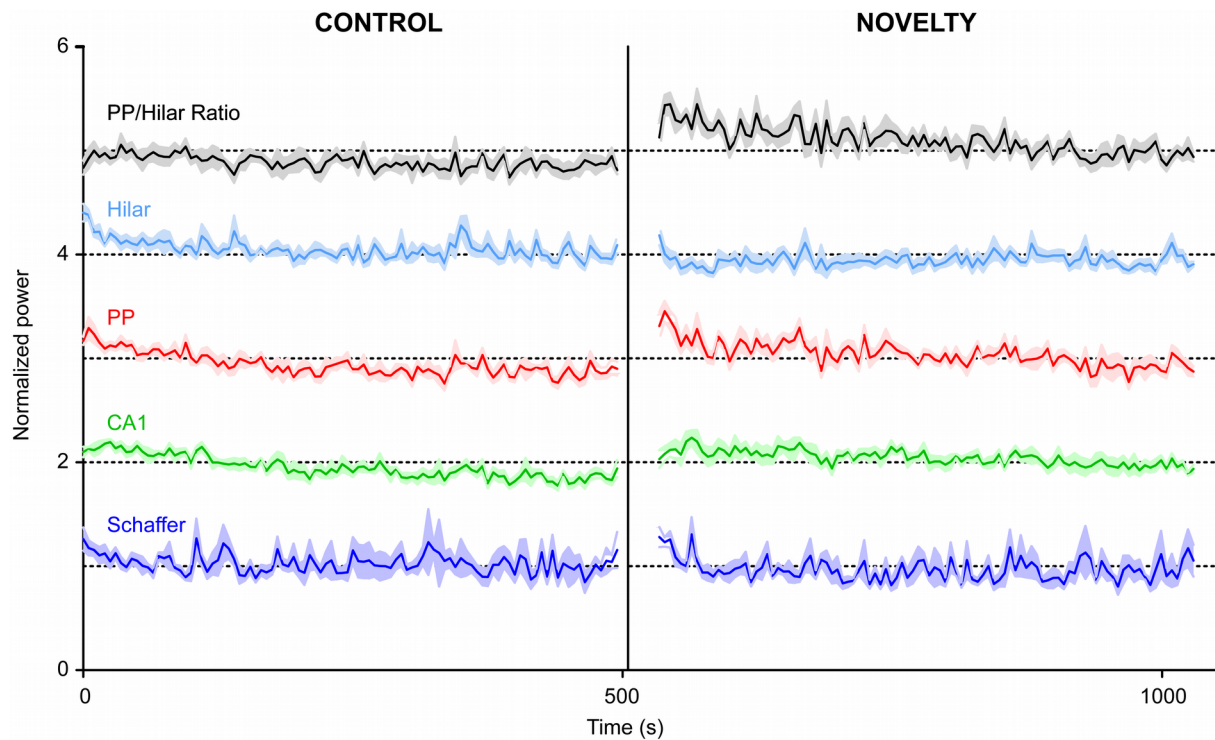


**Figure 4.21. Time course of the power of the generators during a novelty.** Power of the hippocampal LFP-generators (and excitation-inhibition ratio in the dentate gyrus), normalized to the average value in each experiment. The traces were separated in the y-axis to facilitate visualization, y-axis shows normalized units; the two sessions were represented consecutively over time, with a blank gap in the middle that corresponds to the change of session (marked with a vertical black line too). Lines and underlying lighter shades represent mean  $\pm$  SEM. Dashed horizontal black lines behind each trace marks the normalization value for each trace, representing the level of no-change. STATISTICS:  $n=7$ , Friedman test (Q statistic, for non-Gaussian distributions). Schaffer:  $Q=278.98$ ,  $p=0.0002$ ; CA1:  $Q=458.88$ ,  $p<0.0001$ ; PP:  $Q=498.09$ ,  $p<0.0001$ ; Hilar:  $Q=337.88$ ,  $p<0.0001$ ; Ratio:  $Q=404.88$ ,  $p<0.0001$ .

In order to investigate whether the functional connectivity between generators changed during a novelty, and to test our prediction that it could represent a mechanism related to learning, we analyzed the cross-correlation between generators –and processed and organized the results– as was done for the experiments with anesthetized animals (see Figure 4.6 before; we recommend to see also *Methods.Analysis of spontaneous signals*). We found that novelty actually caused significant differences in the functional connectivity between hippocampal LFP-generators (Figure 4.22).

We observed changes in the correlation coefficients and in the delays between generators. Between Schaffer and CA1, the positive coefficients associated with negative delays decreased with novelty. Conversely, between PP and Hilar we found an increase in the negative correlation coefficients, both with negative and positive delays, evidencing an increased inverse relation. Finally, between CA1 and PP there was a bigger positive correlation coefficient when it was associated with positive delays.

Regarding the delays between signals, we only observed significant changes between Schaffer and CA1 generators; there was an increase in the negative delays associated with positive coefficients.

We quantified as well the total time that the generators were significantly correlated, and found a difference again between Schaffer and CA1, that decreased significantly this amount of time.

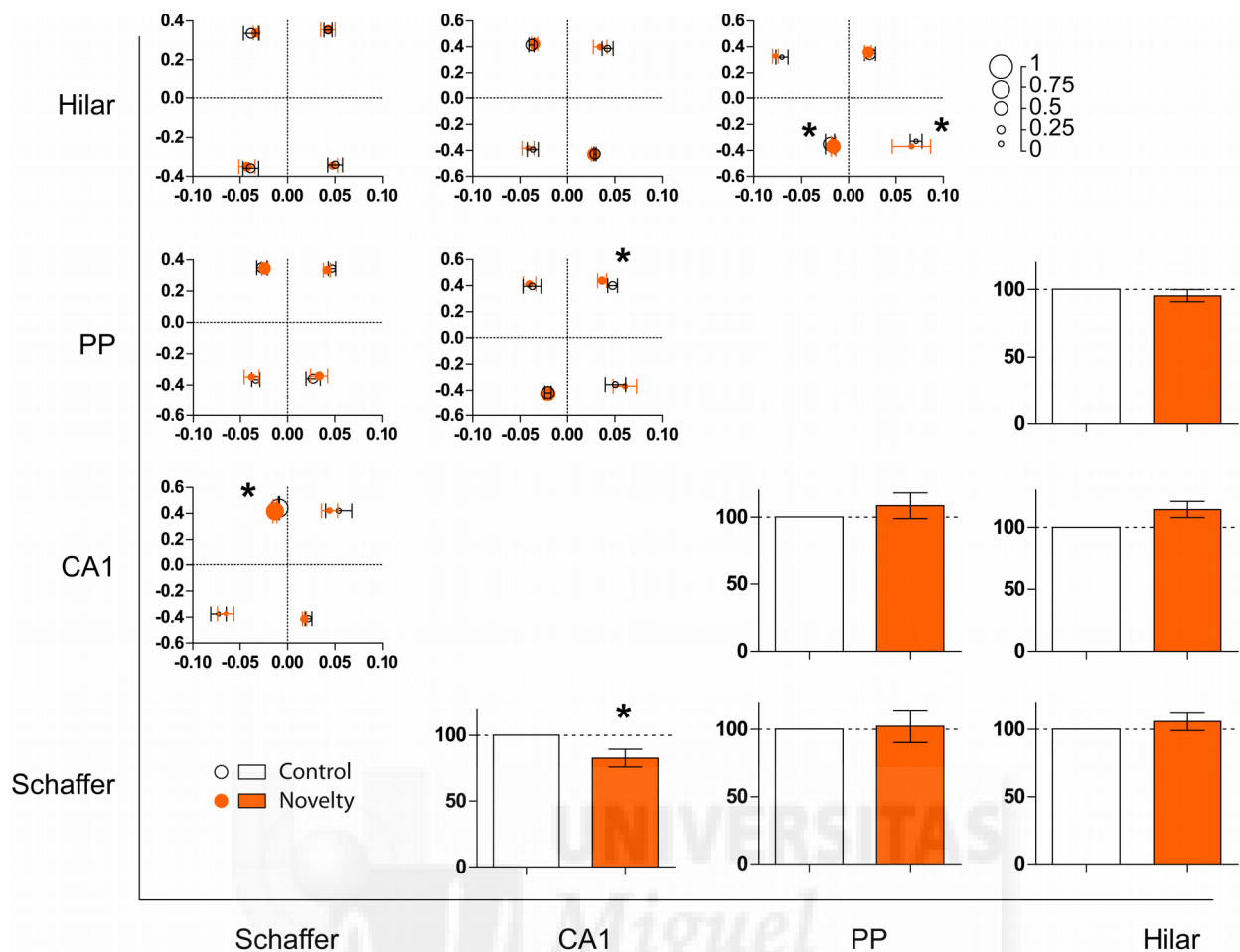


**Figure 4.22. Functional coupling between generators measured by cross-correlation during a novelty.** The upper-left subset of figures represents correlation-coefficients and delays in milliseconds (they are 2-dimensional coordinate panels; dots represent mean  $\pm$  SEM; colors represent conditions, following the legend at the lower-left corner; asterisks represent statistical significance). Each of the panels correspond to a generator pair, indicated in the axes. Results are segregated in quadrants depending on the sign of both the correlation-coefficient and the delay (as explained before in Figure 4.6 and in *Methods*), and averaged for all subjects. In addition, the relative size of the dots represents the proportion of time-windows that corresponds to each quadrant; the legend at the upper-right corner illustrates the correspondence between that proportion and the size of the dots. The lower-right subset of figures (bars representing mean  $\pm$  SEM, colors representing conditions) shows in which proportion of the total time analyzed were two generators actually significantly correlated. The amount of time is normalized with respect to the control condition. STATISTICS:  $n=7$ , paired t-test (t statistic, for Gaussian distributions) or Wilcoxon matched-pairs signed rank test (W statistic, for non-Gaussian distributions). Correlation coefficients; Schaffer-CA1: (upper-left)  $t_{(6)}=3.378$ ,  $p=0.0149$ ; CA1-PP: (upper-right)  $W=-28$ ,  $p=0.0156$ ; PP-Hilar (lower-left)  $t_{(6)}=3.879$ ,  $p=0.0082$ ; PP-Hilar (lower-right)  $t_{(6)}=3.799$ ,  $p=0.009$ . Delays; Schaffer-CA1 (upper-left)  $W=28$ ,  $p=0.0156$ . Total correlated time; Schaffer-CA1:  $t_{(6)}=2.583$ ,  $p=0.0416$ .

Surprisingly, when we studied the subthreshold evoked potentials, we found no significant changes in its parameters (Figure 4.23) during the novelty task. The evoked-LFP seemed to be stable over time. This is in opposition to findings in anesthetized animals described before in this chapter.

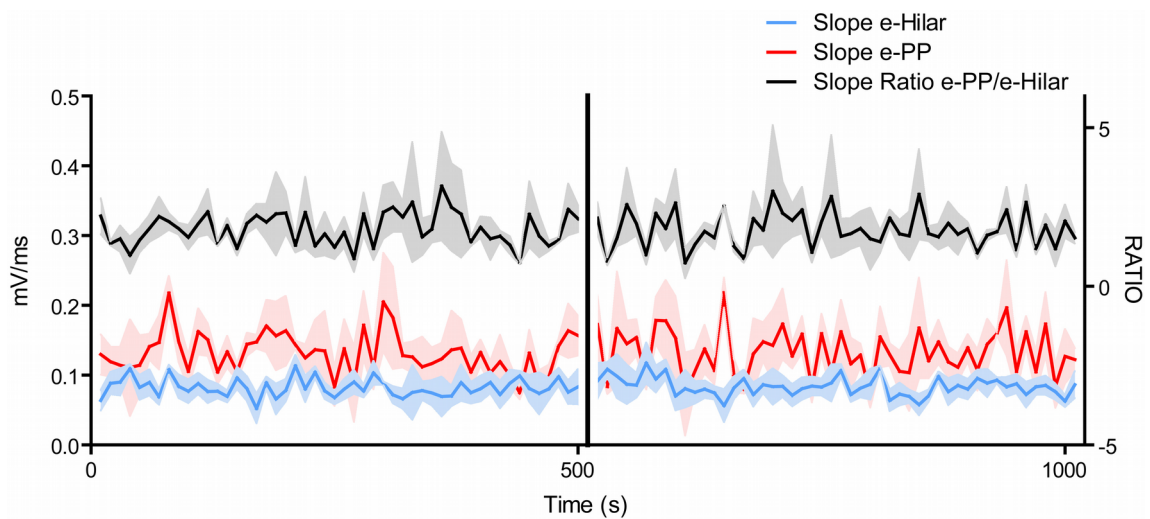


**Figure 4.23. Effects a novelty on the time course of the sub-threshold evoked-LFP.** Maximal slope of the components of the sub-threshold evoked-LFP (e-PP:red; e-Hilar:cyan) and corresponding ratio (black trace) represented in a timeline during the novelty task, with the control and novelty sessions represented consecutively (the blank gap and the black vertical line in the middle mark the change of condition). Traces and underlying shades represent mean  $\pm$  SEM; the values are the average of all subjects ( $n=7$ ); left y-axis represents slope (mV/ms) and right y-axis represents ratio. Note that there is no significant change in any of the parameters over time.





## V. DISCUSSION

### ***5.1. LFP-Generators are a reliable representation of hippocampal Local Field Potentials***

In this work, independent component analysis (ICA) was used as a source separation method to analyze individually the electrophysiological activity of the different sub-areas of the hippocampus. This activity was recorded as an extracellular LFP and therefore was mixed together in the raw signals. The application of this method to study LFP has been already investigated and its reliability tested (Makarov et al., 2010; Makarova et al., 2011). Although in anesthetized animals some of the generators studied (i.e. PP and Schaffer) might have a small relative contribution to the total variance of the LFP (Korovaichuk et al., 2010), they were consistently obtained with every ICA calculation, suggesting that despite their small voltage, they are produced by actual local neuronal populations. Equivalent generators were found in the extensive work that the group of Óscar Herreras and Valeri Makarov have developed, using ICA and very similar methods (Korovaichuk et al., 2010; Makarova et al., 2011; Benito et al., 2013).

We were particularly interested in the dentate gyrus and its generators, and the changes they might undergo during LTP or during learning (based on Canals et al., 2009). One of the two main generators found contributing to the LFP in this region was the perforant path generator (PP); it corresponded to the dendritic depolarizations caused by the perforant path axon terminals on the granule cells, as we demonstrated by (1) electrically stimulating that pathway and recovering the corresponding evoked-LFP in this generator, and (2) largely decreasing the power of the generator by TTX injection in either the entorhinal cortex or directly on the perforant pathway, in accordance with previous work (Korovaichuk et al., 2010; Makarova et al., 2011; Benito et al., 2013). The other main generator producing the LFP of the dentate gyrus was the Hilar generator. This generator, that also receives perforant path input as it was demonstrated in the TTX experiments mentioned, is of large amplitude (actually dominates the LFP in the dentate gyrus) and mainly of an inhibitory (GABAergic) nature. We could demonstrate this with a combination of electrophysiological and pharmacological experiments (discussed below); our data strongly support that the Hilar generator reflects the activity of the local interneuronal network and, more specifically, of the synaptic activity exerted by that network on granule cells, in good agreement with previous results (Benito et al., 2013). The features of both dentate gyrus generators and their functional reorganization under long-term synaptic plasticity are discussed below.

### ***5.2. Hilar generator reflects local feed-forward inhibition***

Using sub-threshold evoked-LFP and pharmacological manipulations we attempted to characterize the Hilar generator. We arrived at the conclusion that it is produced by an interneuronal population that exerts GABAergic inhibition on granule cells through feed-forward connections in the somatic-perisomatic domain. We found in our results several different evidences supporting this

conclusion as follows.

In the first place, when studying subthreshold evoked-LFP we can rule out the possibility of observing feed-back activity, for it would require an action potential in granule cells, and its occurrence is rather unlikely when we are not observing a population spike (PS). Therefore, the fact that we consistently observe a contribution from this generator to the sub-threshold evoked-LFP implies that such contribution is not due to feedback connections. In this regard, the different variability of the maximal peaks of the sub-threshold positive evoked-LFP from the hilus ("e-LFP") and of the negative EPSP from the molecular layer ("EPSP") reflected the variability of the Hilar component of the evoked-LFP ("e-Hilar") which is the potential that mainly contributes to its maximal peak. This evidences that the e-Hilar is more variable than the e-PP from one stimulus to another, and suggests that the reason of that is a difference in the connectivity behind both potentials; while e-PP originates from the direct excitatory input of the perforant path, the e-Hilar is most probably due to a feed-forward connection, because it displays a less constant and reliable response, and additionally accumulates a delay of approximately 2 ms with respect to the e-PP, which is well explained with the idea of a di-synaptic circuit (Andersen et al., 1966). Moreover, we studied the current source density (CSD) maps of the Hilar generator to locate topographically the origin of its signal. The CSD reveals a current source right under and in the granule cell layer of the dentate gyrus, and a current sink on the outer molecular layer. The source could be active and represent an hyperpolarizing perisomatic connection onto granule cells (and so the sink would be passive due to electro-tonic propagation), in accordance with the connectivity of local interneurons that inhibit the perisomatic domain (reviewed by Houser, 2007). This interpretation was also suggested by Benito and collaborators (2013), since they found identical CSD maps for an equivalent generator.

Also, we were able to selectively modulate the e-Hilar through a paired-pulse protocol. As mentioned already in the introduction chapter, after a stimulation provokes the activation of an inhibitory feed-forward connection with a neuron, the subsequent release of GABA neurotransmitter affects not only the target neuron, but also the interneuron itself through activation of GABA<sub>B</sub> auto-receptors. It has been shown that this produces a disinhibition that is maximal from 100 to 200 ms after the original stimulus (Davies et al., 1990). We took advantage of this physiological phenomenon to differentiate excitatory and inhibitory effects elicited by the same sub-threshold stimulation. If e-Hilar reflects feed-forward inhibition recruited by the perforant pathway, then we should expect that paired-pulses delivered at a 150 ms interstimulus interval –which increase the PS of granule cells– would significantly decrease the amplitude of the e-Hilar component. Therefore, we compared sub-threshold evoked-LFP recorded before and 150 ms after a supra-threshold stimulus and observed that paired stimuli were consistently accompanied of a decrease of the e-Hilar (in both amplitude and slope), suggesting that GABA<sub>B</sub> autoreceptors in dentate gyrus interneurons were preventing GABA neurotransmitter release at synapses on granule cells. Consistent with this idea, the GABA<sub>B</sub> antagonist CGP partially prevented paired-pulse disinhibition at 150 ms, both in the PS and in the sub-threshold e-Hilar potential. Although we also found a decrease in the magnitude of the EPSP and the e-PP due to the persistent hyperpolarization of the granule cells resulting from the supra-threshold stimulation (Lopantsev & Schwartzkroin, 1999), the fact that the PS increases with the second pulse demonstrates the lack of feed-forward inhibitory mechanisms, because an equal input current is capable of producing a bigger output, even though it evokes a slightly smaller EPSP.

In the same line, we found a consistent decrease of the magnitude of the e-Hilar when applied GABA<sub>A</sub> and GABA<sub>B</sub> receptors antagonists locally in the hilus. Generally, this supports the idea that this population is fundamentally produced by GABAergic activity, but more importantly, it also supports that the activity observed in the Hilar generator is not the membrane potential of the feed-forward interneurons themselves, but the resulting activity that they exert on the granule cells. A comparable pharmacological characterization of the spontaneous activity of an equivalent generator -with identical spatial distribution and CSD- was carried out by Benito and colleagues (2013).

We found interesting relations between spontaneous activity and Hilar generator. First, the broad-band power of the Hilar generator is significantly higher at the through phase of the Theta-band oscillations of the CA1 generator, at the level of the *stratum lacunosum-moleculare*. This means that the overall Theta rhythm generated in the hippocampus somehow involves and affects too the interneuronal network at the dentate gyrus. In this regard, it is known that interneurons are responsible for regular hyperpolarization of principal cells in the hippocampus during the through phase of Theta oscillations (Ylinen et al., 2004; reviewed by Buzsáki, 2002). Importantly, it has been shown that induction of LTP is facilitated during the peak phase, both in anesthetized and awake animals, in CA1 and in dentate gyrus (Pavlidis et al., 1988; Hölscher et al., 1997; Orr et al., 2001; Hyman et al., 2003). This evidence supports the idea of an increased inhibition during the through phase of hippocampal Theta oscillations affecting incoming inputs. Second and regarding the sub-threshold evoked-LFP, it is also modulated by the Gamma-oscillations measured from the Hilar generator; the e-Hilar component increases its amplitude during the through phase of the local Gamma cycle, and decreases towards the peak. It has been proved that Gamma oscillation can be produced and sustained by local networks of mutually connected interneurons that receive excitatory drive (Jefferys et al., 1996; reviewed by Fries et al., 2007; Bartos et al., 2007), and it has been suggested that basket-cells exerting somatic inhibition onto principal cells are best suited for this function (Bartos et al., 2007). Considering that, it seems probable that Hilar generator consists in a local network of interneurons, possibly basket-cells (Benito et al., 2013), that oscillate and actually produce the high-frequency activity typically observed in the LFP of the hilus and in the Hilar generator.

Considering the evidence presented in the previous chapters, we conclude that perisomatic feed-forward inhibition in the dentate gyrus is represented in the so-called Hilar generator, and thus by studying it we may understand better the local inhibitory network, its role in the propagation of neuronal signals and its modulation by synaptic plasticity and actual learning.

### ***5.3. LTP in the dentate gyrus decreases local inhibition and changes the excitation-inhibition balance***

The induction of LTP caused a significant decrease in the activation of the Hilar generator and an increase of the PP generator. Therefore, we found as well an increase in the excitation-inhibition ratio (measured as the ratio between PP and Hilar generators). We observed these changes both in the spontaneous activity (in the form of changes in the power of the signals), and in the sub-threshold evoked-LFP (as changes in amplitude or slope of the e-PP and e-Hilar components).

The decrease in the power of Hilar generator was found too in the high frequencies, in line with the idea that this generator is mainly produced by interneurons (see before), since this cell type has been recurrently associated with the pacing of gamma oscillations (Fries et al., 2007; Bartos et al., 2007). Conversely, the increase in signal power recorded in the PP generator occurred at slower frequency bands (reaching statistical significance in the Delta band), which comes as no surprise since this generator predominantly contains mid-low frequencies, in accordance with our own and also previous observations (Korovaichuk et al., 2010). No additional statistically significant changes in the power of the hippocampal generators were found after LTP induction but a modest reduction of the Schaffer generator three hours after LTP, specific for high frequencies. Although we did not investigate this alteration in detail, there is evidence showing that higher activation of granule cells may develop an overall reduction of CA3 pyramidal cells' activity (Bragin et al., 1995; Penttonen et al., 1997), partly because mossy fibers contact approximately 10 times more CA3 feed-forward inhibitory interneurons than pyramidal neurons (Acsády et al., 1998). Therefore, it is plausible that this occurs more frequently after plasticity in the dentate gyrus and may help to reach a homeostasis in the system, preventing an excessive excitability.

In line with the evidence just mentioned, there is as well the possibility that the changes in the power of the generators can not only be accounted for by the different dominance of frequency bands, but by specific synaptic mechanisms, such as effects of LTP on different sub-populations of ion channels (even channels with subtle differences in their composition of proteic subunits, like the different subtypes of NMDA receptors) or synaptic properties that make them act as filters for certain frequencies and might be affected by plasticity.

An important piece of evidence that may help us to interpret these results is that, besides a potentiation of the EPSP and PS after induction of LTP, we also observed EPSP-to-Spike potentiation (E-S potentiation) when we analyzed the supra-threshold evoked-LFP; this phenomenon has been typically linked to changes in the excitation-inhibition balance, and more specifically in feed-forward inhibition (Lu et al., 2000; Laezza et al., 1999), thus further supporting our hypothesis of the Hilar generator as a local inhibitory population.

Whereas the mechanisms underlying the potentiation of the excitatory synapses following high frequency stimulation have been extensively studied (Bliss et al., 2007), relatively much less is known about depression of synaptic inputs under the same stimulating conditions. It has been described that tetanic stimulations able to inducing LTP on principal cells, can produce different forms of plasticity on interneurons (Tomasulo & Steward, 1996; McMahan & Kauer, 1997; Maccaferri et al., 1998). There are some possible molecular mechanisms that could explain a decrease of inhibitory activity associated with LTP in the perforant path in our experiments.

First, there is the possibility that the perforant path terminals, while producing a potentiation on granule cells, may cause a concomitant depression of the inputs to interneurons. In this regard, it is possible that a given afferent pathway exerts different effects in the synapses at different target cells; different studies with rat brain slices described mechanisms by which this might take place. Maccaferri and collaborators (1998), found that mossy fiber terminals in CA3, after undergo tetanic stimulation, produced either potentiation or sometimes depression depending on whether they contact pyramidal neurons or interneurons, respectively; they observed that this effect was mediated by presynaptic mGluR receptors. Laezza and colleagues (1999), in turn, stimulated directly CA3 pyramidal layer in hippocampal slices and observed that local interneurons would undergo LTD in a NMDA receptor-independent manner and mediated by presynaptic mGluR and postsynaptic AMPA receptors with high permeability to  $Ca^{2+}$ . Recent evidence also showed that these AMPA receptors mediate long-lasting changes in the intrinsic excitability of hilar interneurons after local stimulation at 30 Hz (Dasgupta & Sikdar, 2014).

An alternative account for our results would be that the axon terminals of the interneurons recruited by inputs from the entorhinal cortex –and impinging onto granule cells– undergo depression following LTP of the perforant path. Evidence supporting this possibility was provided in the CA1 region by Lu and collaborators (2000), who found in *in vitro* preparation an LTD of inhibitory synapses on pyramidal neurons with a concomitant LTP of the excitatory inputs after tetanic stimulation of the Schaffer collateral. This mechanism operates through a postsynaptic, NMDA receptor-dependent activation of the  $Ca^{2+}$ -sensitive phosphatase Calcineurin, that causes the dephosphorylation and desensitization of GABA<sub>A</sub> receptors on the pyramidal neuron. Another possible signaling pathway for the above mechanisms involves a special form of heterosynaptic plasticity, mediated by endocannabinoids, that has been first described by Chevaleyre and Castillo (2003) in hippocampal slices. The authors found that LTP induction on CA1 pyramidal neurons provoked an LTD on nearby synapses from interneurons contacting the same pyramidal cells. The change was NMDA-independent and initiated by activation of mGluR on the postsynaptic excitatory neuron that triggers the synthesis and release of endocannabinoid 2-arachidonoylglycerol (2-AG) to the synaptic cleft, and activates type 1 cannabinoid receptors (CB1R) on the presynaptic GABAergic terminals; that will lead to a long-term decrease of the release of GABA neurotransmitter. Interestingly, this mechanism was reported to mediate *in vitro* a depression of GABAergic afferents contacting mossy cells in the hilus of the dentate

gyrus (Hofmann et al., 2006; Nahir et al., 2010).

While none of the studies reviewed in the paragraphs above fit the experimental conditions in the present work, they help us suggest a cellular mechanism or mechanisms to explain our results. Further experiments, however, will be required to clarify the issue. We have demonstrated a differential sensitivity to AP5 (NMDA receptor antagonist) of the excitatory and inhibitory (feed-forward) components of the entorhinal input; while the facilitation of the excitatory input was prevented by AP5 administered before LTP induction, the depression of the inhibition was unaffected. This result, together with the different time courses of both components (facilitation being long-lasting and depression more transient) suggests a differential mechanistic origin of both phenomena.

Nonetheless, we cannot say which of the mechanisms explained is (or are) responsible for the changes we observe with LTP. Concerning the depression of excitatory synapses on interneurons mediated by mGluR, it has been demonstrated that presynaptic receptors of this type are located at perforant path terminals (Macek et al., 1996; Bradley et al., 1996) and are known to be responsible of NMDA-independent LTD in excitatory synapses on granule cells (Camodeca et al., 1999; Pöschel & Manahan-Vaughan, 2005; Naie & Manahan-Vaughan, 2005). Therefore it seems feasible that the same or similar molecular machinery could serve to produce as well LTD in excitatory synapses on hilar interneurons. On the other hand, a mechanism depressing inhibitory synapses on granule cells could be operating too, and we actually favor this possibility because Hilar generator is actually produced by the inhibitory drive on granule cells, and not by the excitatory activity on interneurons (as discussed before in section 5.2). Moreover, this mechanism has already been reported to happen in interneurons in the dentate gyrus, and it is known that, at least in CA3, presynaptic inhibitory terminals express CB1 receptors (Hájos et al., 2000). Nevertheless, both types of mechanisms are not mutually exclusive, and thus we must as well consider that they could be acting simultaneously.

In any case, regardless of the cellular mechanism, a transient depression of inhibition may have a far reach effect on activity propagation due to the large territories in which hilar interneurons extend their axons (Buckmaster & Schwartkroin., 1995; Miles et al., 1996; reviewed by Houser, 2007). Since perisomatic inhibition controls the output of the inhibited neurons, release of this “break” may translate into an enhanced transmission to downstream hippocampal subfields and, eventually, to extrahippocampal targets.

#### ***5.4. Decreases in inhibition in the dentate gyrus are sufficient to induce a functional reorganization in the brain***

We have previously shown that the impact of local synaptic plasticity in the perforant pathway is not restricted to the synaptic relay at which it is induced, as it is so usually studied, but may open up the regulation of activity propagation at the system level (Canals et al., 2009; Álvarez-Salvado et al., 2013). The electrophysiological investigation presented here points to a synaptically controlled mechanism that operates the excitation-inhibition balance in the dentate gyrus to gate activity propagation. In order to provide further evidence in support of such gating mechanism, we combined for the first time fMRI with electrophysiological recordings, electric microstimulation of the perforant pathway and local pharmacological manipulation. As shown in the *Results* chapter, pharmacological blockade of GABA<sub>A</sub> receptors in the hilus was sufficient to induce a change in the long-range functional connectivity of the hippocampus. Under GABA<sub>A</sub> blockade, depolarization of entorhinal axons propagated ipsi- and contralaterally across the hippocampus and reached distant brain areas, like prefrontal, retrosplenial and perirhinal cortices, and nucleus accumbens (Figure 4.17). This result matched extremely well that obtained by Canals and collaborators (2009), in which activity propagation towards the very same structures was observed only after LTP induction (see also Álvarez-Salvado et al., 2013). The fact that these changes were induced only by blocking GABA<sub>A</sub>

receptors demonstrates that a decrease of the inhibitory activity in the dentate gyrus is sufficient in order to modify functional connectivity.

When we examined the spontaneous electrophysiological activity of the LFP-generators of the hippocampus, we found as well significant changes in their correlation after induction of LTP.

The most remarkable was a decrease in the correlation between PP and Hilar generators. In control conditions they show a consistent inverse correlation with a very short delay ( $\sim 10$  ms), and after LTP induction they temporarily decrease their cross-correlation, becoming less engaged. Together with the decrease in hilar power, and considering the inhibitory nature of that generator, we interpret this result as a decrease in the inhibitory control over granule cells, thus facilitating that incoming activity is transferred to downstream hippocampal areas.

We observed as well that CA1 and PP increase their interdependency after LTP induction. The positive delays changed close to the equivalent of  $90^\circ$  of a Theta cycle, and moreover there was a bigger amount of time-windows with negative correlation and a similar negative delay. This could happen as a consequence of an increased engagement in a specific phase relation between these two generators, therefore suggesting the possibility of an enhanced propagation of activity across hippocampal subfields after LTP. This notion is coherent with the fact that transfer of information from dentate gyrus to CA3 pyramidal neurons depends almost exclusively on the firing of granule cells (Henze et al., 2002), and therefore inhibitory control over action potential output gains relevance in controlling information flow in the dentate gyrus.

Taken together, the modifications of the functional connectivity due to LTP evidence a functional reorganization of the hippocampus as a whole, and suggest that the overall processing of information is facilitated from dentate gyrus to CA1. In line with these ideas, Maccaferri and McBain have demonstrated that different local plasticity among CA1 pyramidal neurons and interneurons can strongly affect the processing of incoming information by the local circuit (Maccaferri & McBain, 1995, 1996). Moreover, it has been proved that synaptic potentiation of an afferent pathway actually changes functional connectivity in the local network of CA3 (Yun et al., 2007), and changes in the excitation-inhibition balance were suggested as a putative mechanism behind that functional reorganization. The necessity of this balance for optimal signal processing has already been suggested (Willshaw & Dayan, 1990). In this context, our results could indicate that LTP triggers in the hippocampus a preferential channeling –and subsequent further transfer– of information (possibly relevant or novel information).

### ***5.5. Context novelty is sufficient to change the excitation-inhibition balance in the dentate gyrus and to induce a subsequent functional reorganization***

In our electrophysiological and fMRI experiments with anesthetized animals we have described the prime role of excitation-inhibition balance in the dentate gyrus to gate activity propagation, in and outside of the hippocampal formation. With the aim of moving towards truly physiological conditions we performed electrophysiological recordings in the hippocampus of non-anesthetized animals and substituted LTP induction by ethologically relevant behavioral stimulation; for these experiments we chose a novelty task since it has been shown that exploration of a novel environment actually induces a synaptic potentiation in the perforant path (Moser et al., 1993). The task aimed at presenting a single novelty to the animals in a familiar context by introducing them in a small transparent box inside a black and bigger familiar box (see *Methods*). The novel box allowed visualization of the containing familiar box, and the rest of the environment (i.e. the room) was absolutely familiar to the animals; therefore, since it has been proved that Long-Evans rats remember purely visual scenes as familiar or novel (Delcasso et al., 2014), then behavioral stimulation consisted only on the so-called novelty itself.

At the same time, the tactile quality of the novel box (sand paper floor), along with the new olfactory information of the unknown enclosure, represent remarkable and novel stimuli.

Studying the spontaneous activity of the hippocampal LFP-generators in awake animals, we found changes comparable to those we observed in the anesthetized animals. PP generator increased its power, Hilar decreased it and subsequently the excitation-inhibition ratio consistently increased in the dentate gyrus. Curiously these changes were especially noticeable during the first minutes that the rat was exposed to the novelty, most likely due to progressive habituation to the novel and simple environment. Regarding correlations between generators, we found a slight increase of the negative correlation between PP and Hilar generators, unlike in the anesthetized animals; since during urethane anesthesia the Theta-band oscillations in the dentate gyrus are reduced in comparison to awake animals (Buzsáki et al., 1986), there could be as well differences in the coupling between the different elements of the local network in these two states. Nonetheless, we observed a higher synchronization between CA1 and PP (increase in positive correlation), suggesting again an easier transfer of information from dentate gyrus to downstream target areas.

Additional findings not observed in the anesthetized preparation after LTP induction include a decorrelation between Schaffer and CA1, and between Schaffer and PP; moreover, Schaffer generator had lower power during novelty. Besides being coherent with a lower overall activation of Schaffer collateral as a result of the increased activity of granule cells (Bragin et al., 1995; Penttonen et al., 1997), these modifications in the circuit may result also from a qualitatively different pattern of activation at CA3. The features of mossy fibers-CA3 connectivity facilitate that supra-threshold stimulation of CA3 pyramidal neurons is achieved by highly coordinated discharge of granule cells (Acsády et al., 1998). Not only does this make sense in the context of selective channeling of information, but it also matches our own observations in experiments with anesthetized animals, in which PP and Schaffer generator switched from their usual pattern of activation to have a mostly flatter waveform with occasional large events of coordinated depolarization (these data are not shown due to their preliminary state). In line with this, and finally, we observed an increased of the power of CA1 generator with novelty, that could be a consequence of a different afferent pattern of excitation from the Schaffer collateral. Take together, these results evidence that while synapses may remain potentiated over time, the network can accommodate those changes in the spontaneous activity by adjusting different features of its functional connectivity (Figure 5.2).

A striking finding in the behavioral experiments was that there were no differences in the sub-threshold evoked-LFP during the novelty task. This is certainly unexpected since we could observe robust modulation of the corresponding spontaneous activity, and the reason why such changes are not observable in the evoked-LFP is unknown. Observing previous studies in awake animals, one may find that changes in electrically evoked responses induced by behavioral manipulations were somewhat mild (Moser et al., 1993; Gruart et al., 2006) in comparison with the potentiation that can be achieved with electrical tetanization in awake and anesthetized animals (Bliss & Gardner-Medwin, 1973; Bliss and Lømo, 1973; see *Results*). Also, it could be that extensive averaging of data might be required to detect statistically significant differences in evoked-LFP with awake animals. In any case, it cannot be ruled out that modulatory systems are differently active, or that local network is differently engaged, between awake and anesthetized states, and that could indeed affect the measurement of evoked-LFP.

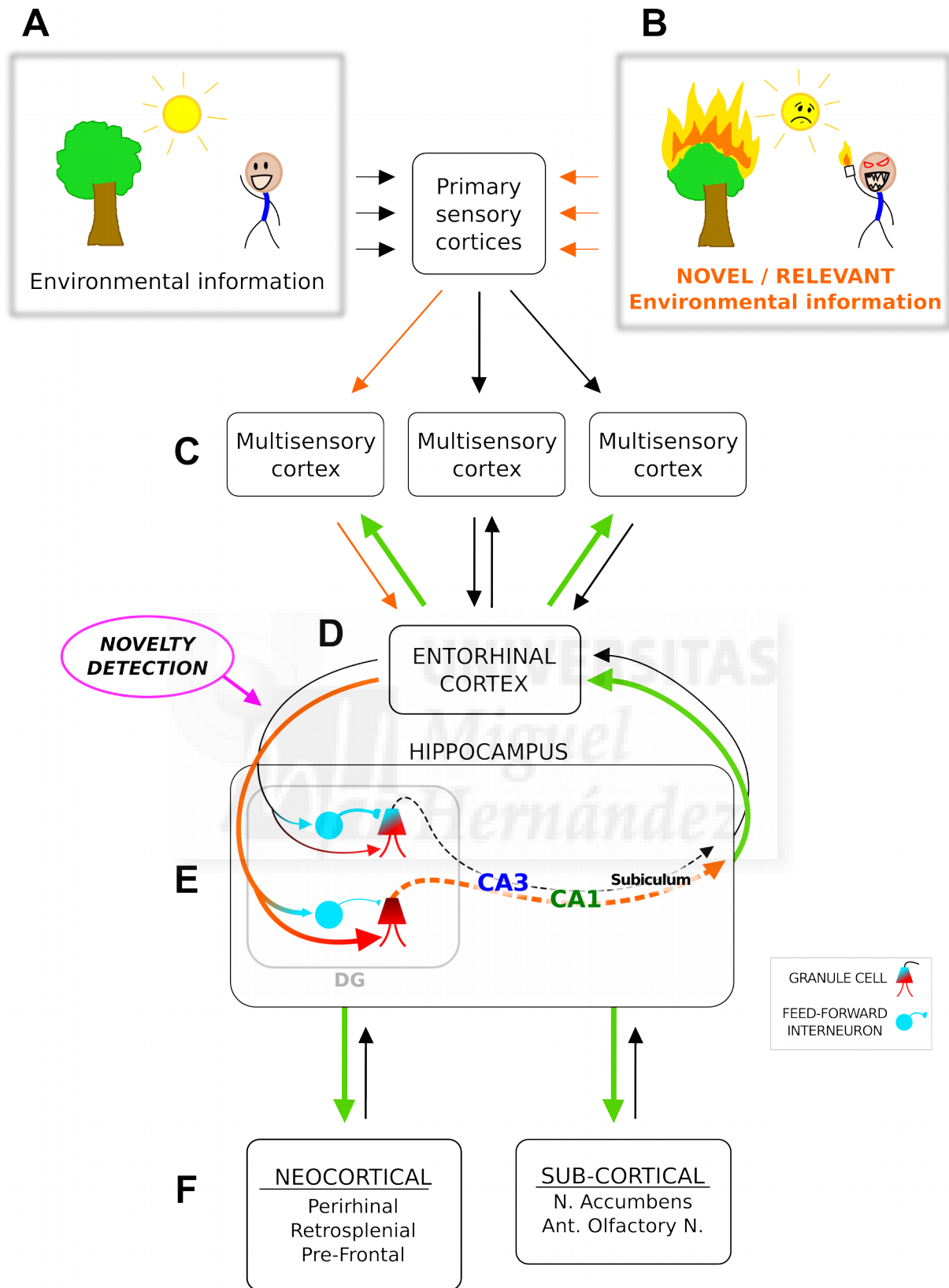


**Figure 5.1. Schematic representation of our theory.** On the upper part of the figure, two different environmental settings are illustrated: a “control” scene (A), and the same scene with novel and relevant information (B). Starting from them, the black arrows represent the normal flow of information through the brain, considering for example a completely familiar scene. The sensory information is first processed at primary

cortices and then ends in multisensory cortices (C) that process more complex information. From there it will go to entorhinal cortex (D), that in turn projects to the hippocampus (E), with a major input to the dentate gyrus (DG) (follow the black arrow starting from the left of the entorhinal cortex). This excitatory input, the perforant path, will drive both granule cells and local inhibitory feed-forward interneurons (see the legend to the right of [E]); cyan and red colors illustrate the cellular origin of the Hilar and PP generators, respectively. The subsequent output activity (dashed black line) will cross CA3, CA1 and subiculum sub-areas of the hippocampus, and then will be transferred back to cortical and subcortical areas in part through entorhinal cortex. The processing of novel information follows the same pathways (orange arrows from [B] to [E]), but is differently processed by the hippocampus, and would be detected as novel at the interface between entorhinal cortex and dentate gyrus or at the dentate gyrus itself (marked with pink arrow). Following the orange thick arrow starting from the left of the entorhinal cortex, novel information changes the local circuit in the dentate gyrus, depressing the feed-forward inhibition on granule cells and potentiating in turn the input to these neurons; this is noted in the different sizes of the synaptic elements compared to the “normal” pathway, and in the dominant red color on the granule cell. This disinhibition produces preferential processing of novel information, and will result in its propagation to distant and new cortical and subcortical areas (F) (represented in green thick arrows) that normally are not reached by the hippocampal output.

Although we cannot know the details of the exact plastic phenomena taking place at every sub-region of the hippocampal network, our results together clearly demonstrate a functional reorganization of the hippocampal network during a context novelty. Since novelty –as a quality of external stimuli– is not dissociated from learning, we hypothesize that such functional reorganization favors information transfer through the hippocampus and to distant brain areas, encoding in turn novel information into new memories (see Figure 5.1 for an illustration of this theory) This is coherent with previous work showing an increased functional connectivity between hippocampus and other brain structures associated with learning (see *Introduction*). However, to provide a causal link between learning and the network plasticity here described, different behavioral tasks should be used that demonstrate a later consolidation and recollection of information acquired with the novelty.

## **5.6. Concluding remarks**

In the present work we have proved that LFP-generators obtained by independent component analysis are a reliable and demonstrable representation of hippocampal network activity, and that they allow the study of different local neuronal networks. Combining this analysis with electrophysiological techniques we could demonstrate that LTP of the perforant path affects differently excitatory and inhibitory neuronal populations in the dentate gyrus, and that in turn this leads to a functional reorganization at the level of the hippocampal formation. In Figure 5.2 we show a summary of our main findings with anesthetized animals.

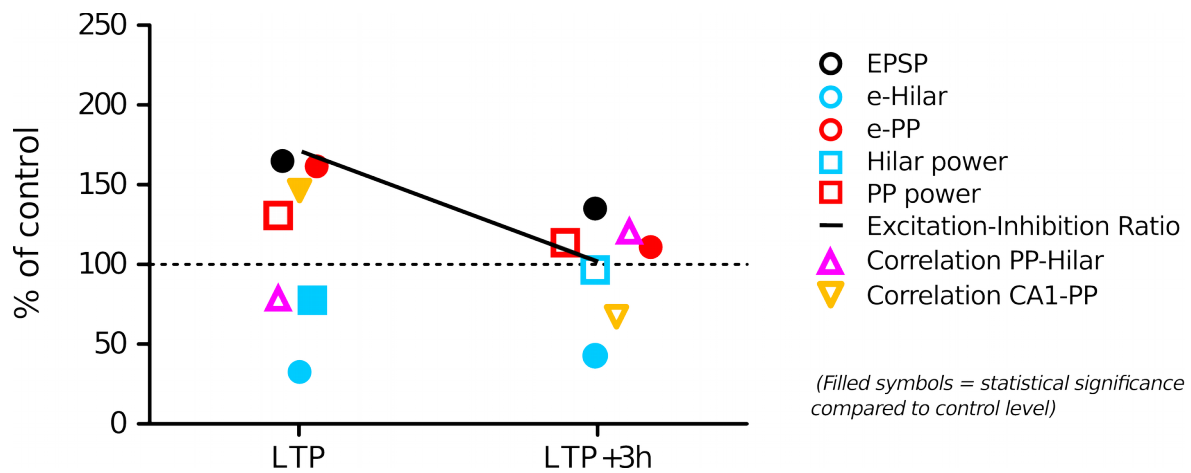


**Figure 5.2. Summary of the main results found in LTP experiments.** Group average of different parameters (related in the legend, on the right) normalized respect to control, and represented for the conditions after induction of LTP (LTP) and three hours later (LTP+3h). Note that the changes observed in the evoked-LFP (EPSP, e-Hilar and e-PP), that inform fundamentally about the state of synapses, remain altered with time; in contrast, the rest of parameters measured, that correspond to the spontaneous activity, display accommodation over time despite the persistent synaptic plasticity.

Interestingly, such changes extended into a functional reorganization at the level of the whole brain, allowing that local activation at the dentate gyrus reached distant cortical areas. Indeed this is what we believe happens during real learning in an awake animal, as it was confirmed in part by our behavioral experiments. Further work would be necessary in order to either go deeper into the cellular and molecular mechanisms underlying all the phenomena described, or to go further and explore how these changes of the hippocampus and the brain are modulated in a long-term time scale and during the different states of a learning process.

## VI. CONCLUSIONS

1. Induction of Long-Term Potentiation on the perforant path modifies the spontaneous activity of the hippocampus, as measured by independent component analysis of hippocampal Local-Field Potentials.
2. Two distinct inputs of the entorhinal cortex to the dentate gyrus can be reliably studied by decomposing the dentate gyrus Local-Field Potentials with independent component analysis; one (“PP generator”) corresponds to the excitatory input from the perforant path to the granule cells, and the other (“Hilar generator”) to the feed-forward perisomatic inhibition exerted by local interneurons that are driven as well by the perforant path excitatory terminals.
3. Both pathways are differentially affected by Long-Term Potentiation; while PP generator becomes slightly potentiated, Hilar generator decreases its activity. In this way, Long-Term Potentiation changes the excitation-inhibition balance in the dentate gyrus. Three hours after induction of Long-Term Potentiation the local network of the dentate gyrus accommodates and those changes disappear.
4. The depression observed in Hilar generator after Long-Term Potentiation is not dependent on the activation of glutamate receptors of NMDA type, unlike for the potentiation of PP generator.
5. Paralleling inhibitory depression, there is a decreased engagement between PP and Hilar generators and a concomitant enhancement of the functional coupling with CA1 generator, suggesting facilitated information flow across the trisynaptic circuit of the hippocampus.
6. Local decrease of the inhibition in the dentate gyrus is sufficient to induce a functional reorganization of the hippocampal network, enhancing activity propagation across hippocampal subfields ipsi- and contralaterally, and also recruiting extrahippocampal neocortical and subcortical structures upon perforant path stimulation.
7. Context novelty is sufficient to induce comparable modifications in the hippocampal network, suggesting a putative role in learning and memory for the mechanisms described.

## VI. CONCLUSIONES

1. La inducción de Potenciación a Largo Plazo en el tracto perforante modifica la actividad espontánea del hipocampo, según nuestros resultados con análisis de componentes independientes de Potenciales de Campo Local hipocampales.
2. Es posible estudiar de manera fidedigna dos aferencias distintas de la corteza entorrinal al giro dentado mediante descomposición de los Potenciales de Campo Local de este último con análisis de componentes independientes; uno (el “generador PP”) se corresponde con la aferencia excitatoria del tracto perforante a las células granulares, y el otro (el “generador Hilar”) con la inhibición perisomática prealimentada ejercida por interneuronas locales controladas también por las terminales excitatorias del tracto perforante.
3. Ambas rutas resultan afectadas de manera diferente por la Potenciación a Largo Plazo; mientras que el PP resulta ligeramente potenciado, el generador Hilar disminuye su actividad. De este modo, la Potenciación a Largo Plazo cambia el balance excitación-inhibición en el giro dentado. Tres horas tras su inducción, la red local del giro dentado se acomoda y los cambios desaparecen.
4. La depresión observada en el generador Hilar con la Potenciación a Largo Plazo no depende de la activación de los receptores de glutamato del tipo NMDA, al contrario de lo que ocurre con la potenciación del generador PP.
5. Al mismo tiempo que la depresión de la inhibición, hay una disminución de la coordinación entre los generadores PP e Hilar, y un correspondiente aumento del acoplamiento funcional con el generador CA1, lo que sugiere un flujo de información facilitado a través del circuito trisináptico del hipocampo.
6. La disminución local de la inhibición en el giro dentado es suficiente para inducir una reorganización funcional en la red hipocampal, aumentando la propagación de la actividad a través de las sub-áreas del hipocampo ipsi y contralateralmente, y también reclutando estructuras neocorticales y subcorticales extrahipocampales durante la estimulación del tracto perforante.
7. Una novedad contextual es suficiente para inducir cambios muy similares en la red hipocampal, lo que sugiere un posible rol de los mecanismos descritos durante los procesos de aprendizaje y memoria.

## VII. ABBREVIATIONS

**2-AG:** 2-arachidonoylglycerol; endocannabinoid molecule.  
**AP5:** (2R)-amino-5-phosphonopentanoate; NMDA receptors antagonist drug.  
**CA1:** Cornu Ammonis area 1; sub-area of the hippocampus. Also CA1 LFP-generator (see *Methods*).  
**CA3:** Cornu Ammonis area 3; sub-area of the hippocampus.  
**CB1R:** Type 1 cannabinoid receptors.  
**CGP:** CGP 52432; GABA<sub>B</sub> type receptor-specific antagonist.  
**CSD:** Current Source Density.  
**D.f.:** Degrees of freedom (statistical analysis).  
**DAPI:** 4',6-diamidino-2-phenylindole; fluorescent staining.  
**DG:** Dentate Gyrus; sub-region of the hippocampal system.  
**DiI:** 1,1'-dioctadecyl-3,3',3'-tetramethylindocarbocyanine perchlorate; a dye.  
**e-LFP:** Positive, electrically evoked potential recorded in the hilus layer.  
**e-PP:** PP component of the evoked-LFP, obtained by independent component analysis.  
**e-Hilar:** Hilar component of the evoked-LFP, obtained by independent component analysis.  
**E-S potentiation:** EPSP-to-Spike potentiation.  
**EC:** Entorhinal Cortex.  
**EPI:** Eco-Planar Image; method for acquiring images with magnetic resonance.  
**EPSP:** Excitatory Post-Synaptic Potential.  
**fMRI:** Functional Magnetic Resonance Imaging.  
**GABA:** Gamma-aminobutyric acid; a neurotransmitter.  
**GFAP:** Glial Fibrillary Acidic Protein; a protein abundant in astrocytes.  
**ICA:** Independent Component Analysis.  
**LFP:** Local Field Potential.  
**LTD:** Long-Term Depression.  
**LTP:** Long-Term Potentiation.  
**mGluRX:** Type X metabotropic glutamate receptor.  
**NMDA:** N-methyl-D-aspartate; also ionotropic receptor for glutamate ("NMDA receptor").  
**PP:** Perforant Path generator (see *Methods*).  
**PS:** Population Spike.  
**SEM:** Standard Error of the Mean.  
**TTX:** Tetrodotoxin; a blocker of voltage-gated sodium channels.



## VIII. BIBLIOGRAPHY

- Abraham, W. C., & Goddard, G. V. (1983). Asymmetric relationships between homosynaptic long-term potentiation and heterosynaptic long-term depression. Recuperado a partir de <http://www.nature.com/nature/journal/v305/n5936/abs/305717a0.html>
- Acsády, L., Kamondi, A., Sík, A., Freund, T., & Buzsáki, G. (1998). GABAergic Cells Are the Major Postsynaptic Targets of Mossy Fibers in the Rat Hippocampus. *The Journal of Neuroscience*, *18*(9), 3386-3403.
- Altman, J., & Das, G. D. (1965). Autoradiographic and histological evidence of postnatal hippocampal neurogenesis in rats. *The Journal of comparative neurology*, *124*, 319–335. doi:10.1002/cne.901240303
- Alvarez, P., & Squire, L. R. (1994). Memory consolidation and the medial temporal lobe: a simple network model. *Proceedings of the National Academy of Sciences of the United States of America*, *91*, 7041–7045. doi:10.1073/pnas.91.15.7041
- Álvarez-Salvado, E., Pallarés, V., Moreno, A., & Canals, S. (2013). Functional MRI of long-term potentiation: imaging network plasticity. *Philosophical transactions of the Royal Society of London. Series B, Biological sciences*, *369*(1633), 20130152.
- Amaral, D. G. (1978). A golgi study of cell types in the hilar region of the hippocampus in the rat. *The Journal of Comparative Neurology*, *182*(5), 851–914. doi:10.1002/cne.901820508
- Amaral, D. G., Insausti, R., & Cowan, W. M. (1984). The commissural connections of the monkey hippocampal formation. *The Journal of comparative neurology*, *224*(3), 307–36. doi:10.1002/cne.902240302
- Amaral, D., & Lavenex, P. (2007). Hippocampal neuroanatomy. *The hippocampus book*, *3*, 37–114.
- Andersen, P., Bliss, T. V. P., & Skrede, K. K. (1971). Lamellar organization of hippocampal excitatory pathways. *Experimental Brain Research*, *13*(2), 222–238.
- Andersen, P., Holmqvist, B., & Voorhoeve, P. E. (1966). Entorhinal Activation of Dentate Granule Cells. *Acta Physiologica Scandinavica*, *66*(4), 448-460. doi:10.1111/j.1748-1716.1966.tb03223.x
- Andersen, P., Sundberg, S. H., Sveen, O., & Wigström, H. (1977). Specific long-lasting potentiation of synaptic transmission in hippocampal slices. *Nature*, *266*(5604), 736–737. doi:10.1038/266736a0
- Baeg, E. H., Kim, Y. B., Kim, J., Ghim, J.-W., Kim, J. J., & Jung, M. W. (2007). Learning-Induced Enduring Changes in Functional Connectivity among Prefrontal Cortical Neurons. *The Journal of Neuroscience*, *27*(4), 909-918. doi:10.1523/JNEUROSCI.4759-06.2007
- Barnes, C. A., & McNaughton, B. L. (1985). An age comparison of the rates of acquisition and forgetting of spatial information in relation to long-term enhancement of hippocampal synapses. *Behavioral neuroscience*, *99*(6), 1040.
- Barrionuevo, G., & Brown, T. H. (1983). Associative long-term potentiation in hippocampal slices. *Proceedings of the National Academy of Sciences of the United States of America*, *80*, 7347–7351.
- Bartos, M., Vida, I., & Jonas, P. (2007). Synaptic mechanisms of synchronized gamma oscillations in inhibitory interneuron networks. *Nature Reviews Neuroscience*, *8*(1), 45-56. doi:10.1038/nrn2044
- Bell, A. J., & Sejnowski, T. J. (1995). An information-maximization approach to blind separation and blind deconvolution. *Neural computation*, *7*(6), 1129–1159.
- Benito, N., Fernández-Ruiz, A., Makarov, V. A., Makarova, J., Korovaichuk, A., & Herreras, O. (2013). Spatial Modules of Coherent Activity in Pathway-Specific LFPs in the Hippocampus Reflect Topology and Different Modes of Presynaptic Synchronization. *Cerebral Cortex*, bht022. doi:10.1093/cercor/bht022
- Bliss, Tim; Collingridge, Graham; Morris, Richard; (2007). Synaptic Plasticity in the Hippocampus. En *The hippocampus book*. Oxford University Press.
- Bliss, T. V. P., & Gardner-Medwin, A. R. (1973). Long-lasting potentiation of synaptic transmission in the dentate area of the unanaesthetized rabbit following stimulation of the perforant path. *The Journal of*

- Physiology*, 232(2), 357-374.
- Bliss, T. V. P., & Lømo T. (1973). Long-lasting potentiation of synaptic transmission in the dentate area of the anaesthetized rabbit following stimulation of the perforant path. *The Journal of Physiology*, 232(2), 331–356.
- Bontempi, B., Laurent-Demir, C., Destrade, C., & Jaffard, R. (1999). Time-dependent reorganization of brain circuitry underlying long-term memory storage. *Nature*, 400, 671–675. doi:10.1038/23270
- Bradley, S. R., Levey, A. I., Hersch, S. M., & Conn, P. J. (1996). Immunocytochemical localization of group III metabotropic glutamate receptors in the hippocampus with subtype-specific antibodies. *The Journal of neuroscience*, 16(6), 2044–2056.
- Bragin, A., Jando, G., Nadasdy, Z., Landeghem, M. van, & Buzsáki, G. (1995). Dentate EEG spikes and associated interneuronal population bursts in the hippocampal hilar region of the rat. *Journal of Neurophysiology*, 73(4), 1691-1705.
- Brewer, J. B., Zhao, Z., Desmond, J. E., Glover, G. H., & Gabrieli, J. D. (1998). Making memories: brain activity that predicts how well visual experience will be remembered. *Science (New York, N.Y.)*, 281, 1185–1187. doi:10.1126/science.281.5380.1185
- Buckmaster, P. S., & Schwartzkroin, P. A. (1995). Interneurons and inhibition in the dentate gyrus of the rat in vivo. *The Journal of Neuroscience*, 15(1), 774-789.
- Burwell, R. D., & Amaral, D. G. (1998a). Cortical afferents of the perirhinal, postrhinal, and entorhinal cortices of the rat. *The Journal of comparative neurology*, 398(2), 179–205.
- Burwell, R. D., & Amaral, D. G. (1998b). Perirhinal and postrhinal cortices of the rat: interconnectivity and connections with the entorhinal cortex. *Journal of Comparative Neurology*, 391(3), 293–321.
- Buzsáki, G. (1984). Feed-forward inhibition in the hippocampal formation. *Progress in Neurobiology*, 22(2), 131-153. doi:10.1016/0301-0082(84)90023-6
- Buzsáki, G. (2002). Theta Oscillations in the Hippocampus. *Neuron*, 33(3), 325-340. doi:10.1016/S0896-6273(02)00586-X
- Buzsáki, G., Czopf, J., Kondákor, I., & Kellényi, L. (1986). Laminar distribution of hippocampal rhythmic slow activity (RSA) in the behaving rat: Current-source density analysis, effects of urethane and atropine. *Brain Research*, 365(1), 125-137. doi:10.1016/0006-8993(86)90729-8
- Cajal, S. R. Y. (1894). The Croonian Lecture: La Fine Structure des Centres Nerveux. *Proceedings of the Royal Society of London*, 55, 444-468.
- Camodeca, N., Breakwell, N. A., Rowan, M. J., & Anwyl, R. (1999). Induction of LTD by activation of group I mGluR in the dentate gyrus in vitro. *Neuropharmacology*, 38(10), 1597-1606.
- Canals, S., Beyerlein, M., Merkle, H., & Logothetis, N. K. (2009). Functional MRI Evidence for LTP-Induced Neural Network Reorganization. *Current Biology*, 19, 398–403. doi:10.1016/j.cub.2009.01.037
- Castellucci, V., Pinsker, H., Kupfermann, I., & Kandel, E. R. (1970). Neuronal Mechanisms of Habituation and Dishabituation of the Gill-Withdrawal Reflex in Aplysia. *Science*, 167(3926), 1745–1748. doi:10.1126/science.167.3926.1745
- Chevalyere, V., & Castillo, P. E. (2003). Heterosynaptic LTD of hippocampal GABAergic synapses: a novel role of endocannabinoids in regulating excitability. *Neuron*, 38(3), 461–472.
- Dasgupta, D., & Sikdar, S. K. (2014). Calcium permeable AMPA receptor-dependent long lasting plasticity of intrinsic excitability in fast spiking interneurons of the dentate gyrus decreases inhibition in the granule cell layer. *Hippocampus*. doi:10.1002/hipo.22371
- Davies, C. H., Davies, S. N., & Collingridge, G. L. (1990). Paired-pulse depression of monosynaptic GABA-mediated inhibitory postsynaptic responses in rat hippocampus. *The Journal of Physiology*, 424(1), 513–531.
- Davis, S., Vanhoutte, P., Pagès, C., Caboche, J., & Laroche, S. (2000). The MAPK/ERK Cascade Targets Both Elk-1 and cAMP Response Element-Binding Protein to Control Long-Term Potentiation-Dependent Gene Expression in the Dentate Gyrus In Vivo. *The Journal of Neuroscience*, 20(12), 4563-4572.
- Dayan, P., & Willshaw, D. J. (1991). Optimising synaptic learning rules in linear associative memories. *Biological cybernetics*, 65(4), 253–265.
- Delcasso, S., Huh, N., Byeon, J. S., Lee, J., Jung, M. W., & Lee, I. (2014). Functional Relationships between the Hippocampus and Dorsomedial Striatum in Learning a Visual Scene-Based Memory Task in Rats. *The Journal of Neuroscience: The Official Journal of the Society for Neuroscience*, 34(47), 15534-15547. doi:10.1523/JNEUROSCI.0622-14.2014
- Delorme, A., & Makeig, S. (2004). EEGLAB: an open source toolbox for analysis of single-trial EEG dynamics including independent component analysis. *Journal of neuroscience methods*, 134(1), 9–21.
- Del Pino, I., García-Frigola, C., Dehorter, N., Brotons-Mas, J., Alvarez-Salvado, E., MartínezdeLagrán, M., ... Rico, B. (2013). Erbb4 Deletion from Fast-Spiking Interneurons Causes Schizophrenia-like Phenotypes.

- Neuron*, 79(6), 1152–1168.
- Dingledine, R., Hynes, M. A., & King, G. L. (1986). Involvement of N-methyl-D-aspartate receptors in epileptiform bursting in the rat hippocampal slice. *The Journal of physiology*, 380(1), 175–189.
- Eugenio Tanzi. (1893). I fatti e le induzioni dell'odierna istologia del sistema nervoso. *Riv Sper Fren Medi Leg*, 19, 419–472.
- Ferguson MacDonald, J., & Martin Wojtowicz, J. (1980). Two conductance mechanisms activated by applications of L-glutamic, L-aspartic, DL-homocysteic, N-methyl-D-aspartic, and DL-kainic acids to cultured mammalian central neurones. *Canadian journal of physiology and pharmacology*, 58(11), 1393–1397.
- Freund, T. F., & Buzsáki, G. (1996). Interneurons of the hippocampus. *Hippocampus*, 6, 347–470. doi:10.1002/(SICI)1098-1063(1996)6:4<347::AID-HIPO1>3.0.CO;2-I
- Fries, P., Nikolić, D., & Singer, W. (2007). The gamma cycle. *Trends in neurosciences*, 30(7), 309–316.
- Gruart, A., Muñoz, M. D., & Delgado-García, J. M. (2006). Involvement of the CA3–CA1 synapse in the acquisition of associative learning in behaving mice. *The Journal of neuroscience*, 26(4), 1077–1087.
- Hájos, N., Katona, I., Naiem, S. S., Mackie, K., Ledent, C., Mody, I., & Freund, T. F. (2000). Cannabinoids inhibit hippocampal GABAergic transmission and network oscillations. *European Journal of Neuroscience*, 12(9), 3239–3249. doi:10.1046/j.1460-9568.2000.00217.x
- Harris, E. W., & Cotman, C. W. (1986). Long-term potentiation of guinea pig mossy fiber responses is not blocked by N-methyl D-aspartate antagonists. *Neuroscience letters*, 70(1), 132–137.
- Hawkins, J., & Blakeslee, S. (s. f.). On Intelligence. 2004. *New York: An Owl Book*.
- Hebb, D. (1949). *The organization of behavior*. Wiley, New York.
- Henze, D. A., Wittner, L., & Buzsáki, G. (2002). Single granule cells reliably discharge targets in the hippocampal CA3 network in vivo. *Nature Neuroscience*, 5(8), 790–795. doi:10.1038/mn887
- Herron, C. E., Williamson, R., & Collingridge, G. L. (1985). A selective N-methyl-D-aspartate antagonist depresses epileptiform activity in rat hippocampal slices. *Neuroscience letters*, 61(3), 255–260.
- Hofmann, M. E., Nahir, B., & Frazier, C. J. (2006). Endocannabinoid-Mediated Depolarization-Induced Suppression of Inhibition in Hilar Mossy Cells of the Rat Dentate Gyrus. *Journal of Neurophysiology*, 96(5), 2501–2512. doi:10.1152/jn.00310.2006
- Hölscher, C., Anwyl, R., & Rowan, M. J. (1997). Stimulation on the positive phase of hippocampal theta rhythm induces long-term potentiation that can be depotentiated by stimulation on the negative phase in area CA1 in vivo. *The Journal of Neuroscience*, 17(16), 6470–6477.
- Houser, C. R. (2007). Interneurons of the dentate gyrus: an overview of cell types, terminal fields and neurochemical identity. *Progress in Brain Research*, 163, 217–232. doi:10.1016/S0079-6123(07)63013-1
- Hyman, J. M., Wyble, B. P., Goyal, V., Rossi, C. A., & Hasselmo, M. E. (2003). Stimulation in hippocampal region CA1 in behaving rats yields long-term potentiation when delivered to the peak of theta and long-term depression when delivered to the trough. *The Journal of Neuroscience*, 23(37), 11725–11731.
- Insausti, R., Amaral, D. G., & Cowan, W. M. (1987). The entorhinal cortex of the monkey: II. Cortical afferents. *The Journal of comparative neurology*, 264(3), 356–95. doi:10.1002/cne.902640306
- Ishizuka, N., Weber, J., & Amaral, D. G. (1990). Organization of intrahippocampal projections originating from CA3 pyramidal cells in the rat. *The Journal of Comparative Neurology*, 295(4), 580–623. doi:10.1002/cne.902950407
- Jahr, C. E., & Stevens, C. F. (1987). Glutamate activates multiple single channel conductances in hippocampal neurons. Recuperado a partir de <http://www.nature.com/nature/journal/v325/n6104/abs/325522a0.html>
- Jahr, C. E., & Stevens, C. F. (1993). Calcium permeability of the N-methyl-D-aspartate receptor channel in hippocampal neurons in culture. *Proceedings of the National Academy of Sciences*, 90(24), 11573–11577.
- Jefferys, J. G., Traub, R. D., & Whittington, M. A. (1996). Neuronal networks for induced '40 Hz' rhythms. *Trends in neurosciences*, 19(5), 202–208.
- Kelso, S. R., Ganong, A. H., & Brown, T. H. (1986). Hebbian synapses in hippocampus. *Proceedings of the National Academy of Sciences*, 83(14), 5326–5330.
- Kentros, C., Hargreaves, E., Hawkins, R. D., Kandel, E. R., Shapiro, M., & Muller, R. V. (1998). Abolition of long-term stability of new hippocampal place cell maps by NMDA receptor blockade. *Science*, 280, 2121–2126. doi:10.1126/science.280.5372.2121
- Korovaichuk, A., Makarova, J., Makarov, V. A., Benito, N., & Herreras, O. (2010). Minor Contribution of Principal Excitatory Pathways to Hippocampal LFPs in the Anesthetized Rat: A Combined Independent Component and Current Source Density Study. *Journal of Neurophysiology*, 104(1), 484–497. doi:10.1152/jn.00297.2010

- Kupfermann, I., Castellucci, V., Pinsker, H., & Kandel, E. (1970). Neuronal Correlates of Habituation and Dishabituation of the Gill-Withdrawal Reflex in Aplysia. *Science*, 167(3926), 1743–1745. doi:10.1126/science.167.3926.1743
- Laezza, F., Doherty, J. J., & Dingledine, R. (1999). Long-term depression in hippocampal interneurons: joint requirement for pre-and postsynaptic events. *Science*, 285(5432), 1411–1414.
- Lang, E. W., Tome, A. M., Keck, I. R., Gorriz-Saez, J. M., & Puntinet, C. G. (2012). Brain connectivity analysis: a short survey. *Computational Intelligence and Neuroscience*, 2012, 412512.
- Lawrence, J. J., & McBain, C. J. (2003). < i> Interneuron Diversity series</i>: Containing the detonation–feedforward inhibition in the CA3 hippocampus. *Trends in neurosciences*, 26(11), 631–640.
- Lesburguères, E., Gobbo, O. L., Alaux-Cantin, S., Hambucken, A., Trifilieff, P., & Bontempi, B. (2011). Early tagging of cortical networks is required for the formation of enduring associative memory. *Science (New York, N.Y.)*, 331, 924–928. doi:10.1126/science.1196164
- Levy, W. B., & Steward, O. (1979). Synapses as associative memory elements in the hippocampal formation. *Brain research*, 175, 233–245. doi:10.1016/0006-8993(79)91003-5
- Li, X.-G., Somogyi, P., Ylinen, A., & Buzsáki, G. (1994). The hippocampal CA3 network: An in vivo intracellular labeling study. *The Journal of Comparative Neurology*, 339(2), 181–208. doi:10.1002/cne.903390204
- Lopantsev, V., & Schwartzkroin, P. A. (1999). GABAA-Dependent Chloride Influx Modulates GABAB-Mediated IPSPs in Hippocampal Pyramidal Cells. *Journal of Neurophysiology*, 82(3), 1218–1223.
- Lu, Y. M., Mansuy, I. M., Kandel, E. R., & Roder, J. (2000). Calcineurin-mediated LTD of GABAergic inhibition underlies the increased excitability of CA1 neurons associated with LTP. *Neuron*, 26(1), 197–205.
- Lynch, G., Larson, J., Kelso, S., Barrionuevo, G., & Schottler, F. (1983). Intracellular injections of EGTA block induction of hippocampal long-term potentiation. *Nature*, 305(5936), 719–721.
- Lynch, G. S., Dunwiddie, T., & Gribkoff, V. (1977). Heterosynaptic depression: a postsynaptic correlate of long-term potentiation. *Nature*, 266, 737–739. doi:10.1038/266737a0
- Maccaferri, G., & McBain, C. J. (1995). Passive propagation of LTD to stratum oriens-alveus inhibitory neurons modulates the temporoammonic input to the hippocampal CA1 region. *Neuron*, 15(1), 137–145.
- Maccaferri, G., & McBain, C. J. (1996). Long-term potentiation in distinct subtypes of hippocampal nonpyramidal neurons. *The Journal of neuroscience*, 16(17), 5334–5343.
- Maccaferri, G., Tóth, K., & McBain, C. J. (1998). Target-Specific Expression of Presynaptic Mossy Fiber Plasticity. *Science*, 279(5355), 1368–1371. doi:10.1126/science.279.5355.1368
- MacDermott, A. B., Mayer, M. L., Westbrook, G. L., Smith, S. J., & Barker, J. L. (1986). NMDA-receptor activation increases cytoplasmic calcium concentration in cultured spinal cord neurones. Recuperado a partir de <http://www.nature.com/nature/journal/v321/n6069/abs/321519a0.html>
- Macek, T. A., Winder, D. G., Gereau, R. W., Ladd, C. O., & Conn, P. J. (1996). Differential involvement of group II and group III mGluRs as autoreceptors at lateral and medial perforant path synapses. *Journal of Neurophysiology*, 76(6), 3798–3806.
- Makarova, J., Herreras, O., & Makarov, V. A. (2013). Inferring network model from local field potentials. *BMC Neuroscience*, 14(Suppl 1), P255. doi:10.1186/1471-2202-14-S1-P255
- Makarova, J., Ibarz, J. M., Makarov, V. A., Benito, N., & Herreras, O. (2011). Parallel Readout of Pathway-Specific Inputs to Laminated Brain Structures. *Frontiers in Systems Neuroscience*, 5. doi:10.3389/fnsys.2011.00077
- Makarov, V. A., Makarova, J., & Herreras, O. (2010). Disentanglement of local field potential sources by independent component analysis. *Journal of Computational Neuroscience*, 29(3), 445–457. doi:10.1007/s10827-009-0206-y
- Manelis, A., Paynter, C. A., Wheeler, M. E., & Reder, L. M. (2013). Repetition related changes in activation and functional connectivity in hippocampus predict subsequent memory. *Hippocampus*, 23(1), 53–65. doi:10.1002/hipo.22053
- Marr, D. (1970). A theory for cerebral neocortex. *Proceedings of the Royal Society of London. Series B, Containing papers of a Biological character. Royal Society (Great Britain)*, 176, 161–234. doi:10.1098/rspb.1970.0040
- Martin, S. J., Grimwood, P. D., & Morris, R. G. M. (2000). Synaptic plasticity and memory: an evaluation of the hypothesis. *Annual review of neuroscience*, 23(1), 649–711.
- Martín-Vázquez, G., Makarova, J., Makarov, V. A., & Herreras, O. (2013). Determining the True Polarity and Amplitude of Synaptic Currents Underlying Gamma Oscillations of Local Field Potentials. *PLoS ONE*, 8(9), e75499. doi:10.1371/journal.pone.0075499

- Maviel, T., Durkin, T. P., Menzaghi, F., & Bontempi, B. (2004). Sites of neocortical reorganization critical for remote spatial memory. *Science (New York, N.Y.)*, 305, 96–99. doi:10.1227/01.NEU.0000309672.48828.06
- McBain, C. J., Freund, T. F., & Mody, I. (1999). Glutamatergic synapses onto hippocampal interneurons: precision timing without lasting plasticity. *Trends in neurosciences*, 22(5), 228–235.
- McMahon, L. L., & Kauer, J. A. (1997). Hippocampal Interneurons Express a Novel Form of Synaptic Plasticity. *Neuron*, 18(2), 295–305. doi:10.1016/S0896-6273(00)80269-X
- McNaughton, B. L., Douglas, R. M., & Goddard, G. V. (1978). Synaptic enhancement in fascia dentata: cooperativity among coactive afferents. *Brain research*, 157, 277–293. doi:10.1016/0006-8993(78)90030-6
- Miles, R., Tóth, K., Gulyás, A. I., Hájos, N., & Freund, T. F. (1996). Differences between Somatic and Dendritic Inhibition in the Hippocampus. *Neuron*, 16(4), 815–823. doi:10.1016/S0896-6273(00)80101-4
- Monfils, M. H., & Teskey, G. C. (2004). Skilled-learning-induced potentiation in rat sensorimotor cortex: A transient form of behavioural long-term potentiation. *Neuroscience*, 125, 329–336. doi:10.1016/j.neuroscience.2004.01.048
- Morris, R. G. M., Anderson, E., Lynch, G. a, & Baudry, M. (1986). Selective impairment of learning and blockade of long-term potentiation by an N-methyl-D-aspartate receptor antagonist, AP5. Recuperado a partir de <http://www.nature.com/nature/journal/v319/n6056/abs/319774a0.html>
- Moser, E. I., Krobot, K. A., Moser, M. B., & Morris, R. G. (1998). Impaired spatial learning after saturation of long-term potentiation. *Science (New York, N.Y.)*, 281, 2038–2042. doi:10.1126/science.281.5385.2038
- Moser, E., Moser, M. B., & Andersen, P. (1993). Synaptic potentiation in the rat dentate gyrus during exploratory learning. *Neuroreport*, 5, 317–320.
- Nadel, L., & Moscovitch, M. (1997). *Memory consolidation, retrograde amnesia and the hippocampal complex* (Vol. 7).
- Nahir, B., Lindsly, C., & Frazier, C. J. (2010). mGluR-mediated and endocannabinoid-dependent long-term depression in the hilar region of the rat dentate gyrus. *Neuropharmacology*, 58(4), 712–721.
- Naie, K., & Manahan-Vaughan, D. (2005). Investigations of the protein synthesis dependency of mGluR-induced long-term depression in the dentate gyrus of freely moving rats. *Neuropharmacology*, 49 Suppl 1, 35–44. doi:10.1016/j.neuropharm.2005.06.001
- Oliet, S. H., Malenka, R. C., & Nicoll, R. A. (1997). Two distinct forms of long-term depression coexist in CA1 hippocampal pyramidal cells. *Neuron*, 18(6), 969–982.
- Orr, G., Rao, G., Houston, F. P., McNaughton, B. L., & Barnes, C. A. (2001). Hippocampal synaptic plasticity is modulated by theta rhythm in the fascia dentata of adult and aged freely behaving rats. *Hippocampus*, 11(6), 647–654.
- Park, H.-J., & Friston, K. (2013). Structural and functional brain networks: from connections to cognition. *Science (New York, N.Y.)*, 342, 1238411. doi:10.1126/science.1238411
- Pavlidis, C., Greenstein, Y. J., Grudman, M., & Winson, J. (1988). Long-term potentiation in the dentate gyrus is induced preferentially on the positive phase of  $\beta$ -rhythm. *Brain research*, 439(1), 383–387.
- Penttonen, M., Kamondi, A., Sik, A., Acsády, L., & Buzsáki, G. (1997). Feed-forward and feed-back activation of the dentate gyrus in vivo during dentate spikes and sharp wave bursts. *Hippocampus*, 7(4), 437–450. doi:10.1002/(SICI)1098-1063(1997)7:4<437::AID-HIPO9>3.0.CO;2-F
- Pöschel, B., & Manahan-Vaughan, D. (2005). Group II mGluR-induced long term depression in the dentate gyrus in vivo is NMDA receptor-independent and does not require protein synthesis. *Neuropharmacology*, 49 Suppl 1, 1–12. doi:10.1016/j.neuropharm.2005.06.018
- Ranganath, C., Heller, A., Cohen, M. X., Brozinsky, C. J., & Rissman, J. (2005). Functional connectivity with the hippocampus during successful memory formation. *Hippocampus*, 15(8), 997–1005. doi:10.1002/hipo.20141
- Rempel-Clower, N. L., Zola, S. M., Squire, L. R., & Amaral, D. G. (1996). *Three cases of enduring memory impairment after bilateral damage limited to the hippocampal formation.* (Vol. 16).
- Restivo, L., Vetere, G., Bontempi, B., & Ammassari-Teule, M. (2009). The formation of recent and remote memory is associated with time-dependent formation of dendritic spines in the hippocampus and anterior cingulate cortex. *The Journal of neuroscience: the official journal of the Society for Neuroscience*, 29, 8206–8214. doi:10.1523/JNEUROSCI.0966-09.2009
- Ribot, T. (1882). *Diseases of memory: Essays in the positive psychology. The international scientific series.* Vol 43.
- Rogan, M. T., Stäubli, U. V., & LeDoux, J. E. (1997). Fear conditioning induces associative long-term potentiation in the amygdala. *Nature*, 390, 604–607. doi:10.1038/37601
- Roman, F. S., Truchet, B., Chaillan, F. A., Marchetti, E., & Soumireu-Mourat, B. (2011). Olfactory Associative

- Discrimination: A Model for Studying Modifications of Synaptic Efficacy in Neuronal Networks Supporting Long-term Memory. *Reviews in the Neurosciences*, 15(1), 1–18. doi:10.1515/REVNEURO.2004.15.1.1
- Rumpel, S., LeDoux, J., Zador, A., & Malinow, R. (2005). Postsynaptic receptor trafficking underlying a form of associative learning. *Science (New York, N.Y.)*, 308, 83–88. doi:10.1126/science.1103944
- Sacchetti, B., Scelfo, B., Tempia, F., & Strata, P. (2004). Long-term synaptic changes induced in the cerebellar cortex by fear conditioning. *Neuron*, 42, 973–982. doi:10.1016/j.neuron.2004.05.012
- Sarter, M., & Markowitsch, H. J. (1985). Convergence of intra- and interhemispheric cortical afferents: lack of collateralization and evidence for a subrhinal cell group projecting heterotopically. *The Journal of comparative neurology*, 236(3), 283–96. doi:10.1002/cne.902360302
- Scharfman, H. E., & Myers, C. E. (2013). Hilar mossy cells of the dentate gyrus: a historical perspective. *Frontiers in Neural Circuits*, 6, 106. doi:10.3389/fncir.2012.00106
- Schott, B. H., Wüstenberg, T., Wimber, M., Fenker, D. B., Zierhut, K. C., Seidenbecher, C. I., ... Richardson-Klavehn, A. (2013). The relationship between level of processing and hippocampal-cortical functional connectivity during episodic memory formation in humans. *Human Brain Mapping*, 34(2), 407–424. doi:10.1002/hbm.21435
- Schwarz, A. J., Danckaert, A., Reese, T., Gozzi, A., Paxinos, G., Watson, C., ... Bifone, A. (2006). A stereotaxic MRI template set for the rat brain with tissue class distribution maps and co-registered anatomical atlas: application to pharmacological MRI. *Neuroimage*, 32(2), 538–550.
- Scoville, W. B., & Milner, B. (1957). Loss of recent memory after bilateral hippocampal lesions. *The Journal of neuropsychiatry and clinical neurosciences*, 12, 103–113. doi:10.1136/jnnp.20.1.11
- Sevelinges, Y., Gervais, R., Messaoudi, B., Granjon, L., & Mouly, A.-M. (2004). Olfactory fear conditioning induces field potential potentiation in rat olfactory cortex and amygdala. *Learning & memory (Cold Spring Harbor, N.Y.)*, 11, 761–9. doi:10.1101/lm.83604
- Shew, T., Yip, S., & Sastry, B. R. (2000). Mechanisms involved in tetanus-induced potentiation of fast IPSCs in rat hippocampal CA1 neurons. *Journal of neurophysiology*, 83(6), 3388–3401.
- Shyu, B.-C., Lin, C.-Y., Sun, J.-J., Sylantsev, S., & Chang, C. (2004). A method for direct thalamic stimulation in fMRI studies using a glass-coated carbon fiber electrode. *Journal of neuroscience methods*, 137(1), 123–131.
- Siapas, A. G., Lubenov, E. V., & Wilson, M. A. (2005). Prefrontal phase locking to hippocampal theta oscillations. *Neuron*, 46, 141–151. doi:10.1016/j.neuron.2005.02.028
- Soriano, E., & Frotscher, M. (1989). A GABAergic axo-axonic cell in the fascia dentata controls the main excitatory hippocampal pathway. *Brain research*, 503, 170–174. doi:10.1016/0006-8993(89)91722-8
- Squire, L. R. (1992). Memory and the hippocampus: A synthesis from findings with rats, monkeys, and humans. *Psychological Review*, 99(2), 195–231. doi:10.1037/0033-295X.99.2.195
- Takashima, A., Petersson, K. M., Rutters, F., Tendolkar, I., Jensen, O., Zwarts, M. J., ... Fernández, G. (2006). Declarative memory consolidation in humans: a prospective functional magnetic resonance imaging study. *Proceedings of the National Academy of Sciences of the United States of America*, 103, 756–761. doi:10.1073/pnas.0507774103
- Takeuchi, T., Duzkiewicz, A. J., & Morris, R. G. M. (2013). The synaptic plasticity and memory hypothesis: encoding, storage and persistence. *Philosophical Transactions of the Royal Society of London. Series B, Biological Sciences*, 369(1633), 20130288. doi:10.1098/rstb.2013.0288
- Tang, J., Wotjak, C. T., Wagner, S., Williams, G., Schachner, M., & Dityatev, A. (2001). Potentiated amygdaloid auditory-evoked potentials and freezing behavior after fear conditioning in mice. *Brain Research*, 919, 232–241. doi:10.1016/S0006-8993(01)03020-7
- Teyler, T. J., & DiScenna, P. (1986). The hippocampal memory indexing theory. *Behavioral neuroscience*, 100, 147–154. doi:10.1037/0735-7044.100.2.147
- Teyler, T. J., & Rudy, J. W. (2007). *The hippocampal indexing theory and episodic memory: Updating the index* (Vol. 17).
- Tomasulo, R. A., & Steward, O. (1996). Homosynaptic and heterosynaptic changes in driving of dentate gyrus interneurons after brief tetanic stimulation in vivo. *Hippocampus*, 6(1), 62–71.
- Traub, R. D., Pais, I., Bibbig, A., LeBeau, F. E., Buhl, E. H., Garner, H., ... Whittington, M. A. (2005). Transient depression of excitatory synapses on interneurons contributes to epileptiform bursts during gamma oscillations in the mouse hippocampal slice. *Journal of neurophysiology*, 94(2), 1225–1235.
- Wang, L., Negreira, A., LaViolette, P., Bakkour, A., Sperling, R. A., & Dickerson, B. C. (2010). Intrinsic interhemispheric hippocampal functional connectivity predicts individual differences in memory performance ability. *Hippocampus*, 20(3), 345–351. doi:10.1002/hipo.20771
- Wang, S.-H., & Morris, R. G. M. (2010). Hippocampal-neocortical interactions in memory formation,

- consolidation, and reconsolidation. *Annual Review of Psychology*, 61, 49–79, C1–4. doi:10.1146/annurev.psych.093008.100523
- Weisz, D. J., Clark, G. A., & Thompson, R. F. (1984). Increased responsivity of dentate granule cells during nictitating membrane response conditioning in rabbit. *Behavioural brain research*, 12, 145–154. doi:10.1016/0166-4328(84)90037-8
- Whitlock, J. R., Heynen, A. J., Shuler, M. G., & Bear, M. F. (2006). Learning induces long-term potentiation in the hippocampus. *Science (New York, N.Y.)*, 313, 1093–1097. doi:10.1126/science.1128134
- Willshaw, D., & Dayan, P. (1990). Optimal plasticity from matrix memories: What goes up must come down. *Neural Computation*, 2(1), 85–93.
- Ylinen, A., Soltész, I., Bragin, A., Penttonen, M., Sik, A., & Buzsáki, G. (1995). Intracellular correlates of hippocampal theta rhythm in identified pyramidal cells, granule cells, and basket cells. *Hippocampus*, 5(1), 78–90. doi:10.1002/hipo.450050110
- Yun, S. H., Lee, D. S., Lee, H., Baeg, E. H., Kim, Y. B., & Jung, M. W. (2007). LTP induction modifies functional relationship among hippocampal neurons. *Learning & Memory*, 14(3), 190–194. doi:10.1101/lm.466307





**IX. ANNEX**





[rstb.royalsocietypublishing.org](http://rstb.royalsocietypublishing.org)



## Research

**Cite this article:** Álvarez-Salvado E, Pallarés V, Moreno A, Canals S. 2014 Functional MRI of long-term potentiation: imaging network plasticity. *Phil. Trans. R. Soc. B* **369**: 20130152. <http://dx.doi.org/10.1098/rstb.2013.0152>

One contribution of 35 to a Discussion Meeting Issue 'Synaptic plasticity in health and disease'.

### Subject Areas:

neuroscience, systems biology

### Keywords:

long-term potentiation, fMRI, neurophysiology, dentate gyrus, prefrontal cortex, mossy cells

### Author for correspondence:

Santiago Canals  
e-mail: [scanals@umh.es](mailto:scanals@umh.es)

# Functional MRI of long-term potentiation: imaging network plasticity

Efrén Álvarez-Salvado, Vicente Pallarés, Andrea Moreno and Santiago Canals

Instituto de Neurociencias, Consejo Superior de Investigaciones Científicas, Universidad Miguel Hernández, Sant Joan d'Alacant 03550, Spain

Neurons are able to express long-lasting and activity-dependent modulations of their synapses. This plastic property supports memory and conveys an extraordinary adaptive value, because it allows an individual to learn from, and respond to, changes in the environment. Molecular and physiological changes at the cellular level as well as network interactions are required in order to encode a pattern of synaptic activity into a long-term memory. While the cellular mechanisms linking synaptic plasticity to memory have been intensively studied, those regulating network interactions have received less attention. Combining high-resolution fMRI and *in vivo* electrophysiology in rats, we have previously reported a functional remodelling of long-range hippocampal networks induced by long-term potentiation (LTP) of synaptic plasticity in the perforant pathway. Here, we present new results demonstrating an increased bilateral coupling in the hippocampus specifically supported by the mossy cell commissural/associational pathway in response to LTP. This fMRI-measured increase in bilateral connectivity is accompanied by potentiation of the corresponding polysynaptically evoked commissural potential in the contralateral dentate gyrus and depression of the inactive convergent commissural pathway to the ipsilateral dentate. We review these and previous findings in the broader context of memory consolidation.

## 1. Introduction

Brains are modular structures implementing highly distributed and efficient coding [1–4]. Sensory systems like vision, for instance, process multiple features of a complex scene in parallel, such as motion, colour and orientation among others [5] and integrate these features in one coherent, unitary perception [3,6]. Integration occurs at all levels in the hierarchy of the central nervous system, and memory is a prime example of the highest level integration. In an episode of our every-day life experience, highly processed multi-sensory information from all modalities is combined with emotions, motivation and previous experience and encoded in the form of memories for its long-term use as the basis for learning [7–10]. Given the central role of memory in cognition, unveiling the mechanisms supporting integration and storage of information is a major challenge for neuroscience. Research over recent years suggests that these processes depend on the interaction of molecular, cellular and systems-level mechanisms.

In this context, a global description of the functional connectivity between cortical and subcortical structures supporting memory is fundamental to understand integration in distributed brain networks. How and when does a brain structure interact with its many partners in the broader network of anatomically connected regions? In the hippocampus, a region well known to play a critical role in the acquisition of declarative memory [11,12], the local circuits are highly stereotypic and similar across different septo-temporal levels, while the extrahippocampal connectivity is heterogeneously distributed in this axis [13]. Several lines of evidence, mainly arriving from behavioural experiments in lesioned animals, indicate that, in parallel with the distribution of long-range connections, there exists a segregation of functions along the septo-temporal axis of the hippocampus [14,15]. This suggests that the broad

function supported by a particular hippocampal level is given by its characteristic—anatomically defined—inputs and outputs and their dynamic properties, the latter being determined by context-dependent processes, such as short- and long-term synaptic plasticity and neuromodulation. The combination of both static and dynamic network descriptions is what we refer to here as functional connectivity.

Although conceptually appealing, a mechanistic link between the dynamic properties of synapses and those of activity propagation in the neuronal network in which they are embedded is not yet established. In this article, we review in a broader context some recent findings from our laboratory performing combined functional magnetic resonance imaging (fMRI)-electrophysiological experiments that suggest a functional reorganization of long-range hippocampal circuits controlled by synaptic plasticity and discuss their possible implication for the systems consolidation of memory. Furthermore, we present new results on the effects of synaptic plasticity on interhemispheric hippocampal communication.

### (a) Cellular and systems consolidation of memories

In 1973, Bliss & Lømo [16] reported the first demonstration of a use-dependent strengthening of synaptic connections, a phenomenon known as long-term potentiation (LTP). They showed that neurons in the hippocampal formation can in fact undergo plastic changes in their synaptic inputs when stimulated repeatedly above a certain frequency threshold. This finding and others that followed were considered the experimental demonstration of Hebb's postulate on synaptic strength and learning [17], and since then LTP has been widely accepted as the prevalent model of an experience-dependent modification of brain circuits [18,19]. This notion, recently referred to as *cellular consolidation* [20], has received support in experiments in which LTP induction by direct electric stimulation was replaced by learning processes, not only in the hippocampus [21–24] but also in cortical and subcortical areas such as the amygdala or the olfactory and sensorimotor cortices [25–31]. Similarly, impairment of hippocampal-dependent learning has been reported in experimental manipulations that either prevent LTP pharmacologically with NMDA (*N*-methyl-D-aspartate) receptor antagonists [32,33] or occlude synaptic plasticity by LTP overinduction [34].

Important functional interactions between the hippocampus and other brain regions, however, are required in order to encode episodic information into long-term memories. Classic experiments by Penfield had already demonstrated that electrical stimulation of a number of structures in the medial temporal lobe (MTL) in humans elicited reports of multimodal imagery and mnemonic features, a phenomenon of memory reactivation also triggered by seizures in patients with temporal lobe epilepsy [35,36]. More direct evidence came from brain-damaged humans [11,37] and lesion studies in animals [38–40] which demonstrated that memory storage and retrieval engage a distributed network of reciprocal connections. MTL lesions impair the formation of new memories and often debilitate those acquired before the damage. The severity of this retrograde amnesia varies with the precise locus of temporal lobe injury, with hippocampal-restricted lesions mainly affecting new memory formation and sparing older ones [37]. Further implication of a distributed network of memory-related

structures came from electrophysiological and fMRI studies showing, for instance, an important link between the MTL and the prefrontal cortex (PFC). Co-activation of the parahippocampal and the PFC in human fMRI experiments was found to predict subsequent memory performance [41,42], while in animals enhanced correlated firing and increased coupling in the theta frequency range between hippocampus and medial PFC were found when rats successfully used spatial memory [43], to mention one example.

A widely accepted view supports that the connections of the hippocampus with other MTL structures, and in turn their connections with more distributed areas, provide the former with an input representation of the environment. This spatio-temporally distributed, complex pattern of activity representing external events is processed to become a simplified, indexed new pattern of output activity that goes all the way back to the corresponding areas of the cortex. The connections within the hippocampal formation would be the ones undergoing the cellular consolidation process, setting and stabilizing in that way the engagement between the involved cortical areas [44]. The reactivation of this index, and the subsequent activation of the retrieved sites, would take place repeatedly over time making the specific memory stable and independent from the hippocampus. After this process, known as 'systems consolidation' [20,45,46], the PFC is believed to take over the role initially fulfilled by the hippocampus, indexing and binding information stored in distributed cortical networks to retrieve remote memories [47].

However, while the evidence supporting the link between synaptic plasticity in the hippocampus and memory encoding is robust, little is known about how experimentally measured regional synaptic modifications alter the activity of more global, widespread networks supporting system consolidation of memory.

### (b) Synapse to network transformations: the use of combined fMRI–electrophysiology experiments

In an attempt to link the cellular and system levels of memory consolidation, that is to relate synaptic plasticity to widespread network dynamics, we simultaneously combined fMRI and *in vivo* electrophysiology in rats [48] and investigated the global functional consequences of LTP [49]. In these acute experiments, urethane-anaesthetized rats are implanted in the perforant pathway (PP) and dentate gyrus (DG) with MRI-compatible stimulating and recording electrodes, respectively. Blood oxygenation-level-dependent (BOLD) imaging allows us to record activity-related signals simultaneously over the entire brain, and in combination with microstimulation [48,50] represents a very powerful tool for the study of highly distributed networks. On the other hand, the simultaneously recorded electrophysiological signals let us unequivocally relate BOLD signals with the underlying neuronal activity [51]. In this way, functional connectivity in widely distributed brain networks as well as local synaptic potentials can be longitudinally followed in the same subject across, for instance, an experimental modification of synaptic strength.

It is important to note that the fMRI maps generated with this technique reflect a measure of functional connectivity between brain regions that is essentially different from that obtained from resting state fMRI, an imaging modality in which subjects are not stimulated by any external input or

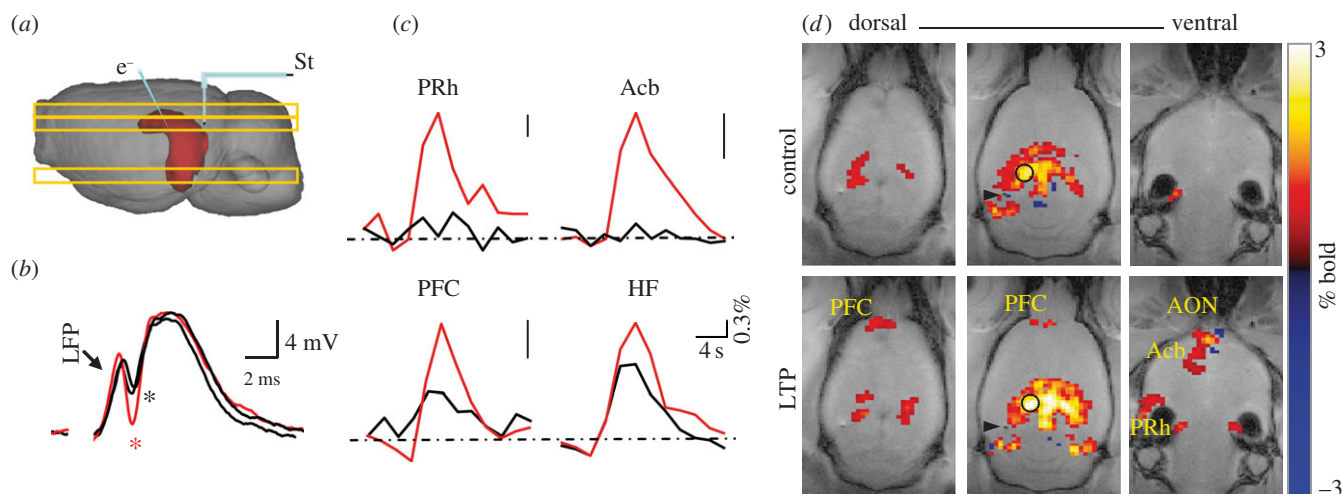


**Figure 1.** LTP of synaptic strength in the perforant pathway changes the hippocampal long-range functional connectivity. (a) Schematic of the experimental preparation. The placement of the stimulating (St) and recording electrodes is shown in a three-dimensional reconstruction of the rat brain. The hippocampal surface is displayed in red. The location of the MRI slices shown in (d) is also illustrated. (b) Evoked local field potentials (LFP) and (c) BOLD signal time course recorded in the hippocampus (HF), prefrontal cortex (PFC), nucleus accumbens (Acb), the anterior olfactory nucleus (AON) and the perirhinal cortex (PRh), during perforant pathway stimulation, before (black) and after (red) induction of LTP. Arrow points towards the EPSP and asterisks mark the population spike. (d) Functional maps thresholded ( $p < 0.001$  uncorrected) and overlaid on horizontal FLASH anatomical scans, showing brain active areas during perforant path stimulation before (control) and after synaptic potentiation (LTP). The colour-coded scale represents positive and negative BOLD response in per cent change from baseline. The position of the tip of the stimulation electrode is marked by the black arrowhead. Adapted with permission from [49].

cognitive tasks [40,52]. In electric-stimulation fMRI, the activated brain regions are causally related through the stimulation site, helping the interpretation of the results in terms of activity propagation. Using this technique, we showed—perhaps not surprisingly—that electric stimulation of the medial perforant tract produces fMRI maps that spatially correlate with the characteristic pattern of terminal fields of its axons [53–56]. Activations were found in the DG, CA3 and CA1 regions, subiculum, entorhinal cortex and the septum [48]. The BOLD signal amplitude was a good predictor of the underlying electrophysiological responses as measured in combined fMRI–electrophysiology experiments in the DG (see below), very stable under urethane anaesthesia and robust across animals [48,49]. These characteristics conferred a quantitative value to the BOLD signal in long-term experiments as those required to investigate the systems-level consequences of LTP.

In the first study [48], by systematically varying frequency and intensity of the stimulating current, we concluded that (1) a certain level of activity, in an approximately constant population of neurons, must be reached in order to start a detectable BOLD signal; (2) the activity threshold for BOLD elicitation can be reached by applying trains of pulses at relatively low frequencies (approx. 4 Hz); (3) once the threshold is surpassed, the BOLD signal (magnitude and extension of the activation) is linearly correlated with the stimulating current; and (4) at current intensities evoking a half-maximal population spike in the electrophysiology and frequencies between 10 and 20 Hz, the activity spreads through the ipsi- and contralateral hippocampal formations, whereas at frequencies lower than 5 Hz and higher than 20 Hz, the activity is restricted to the ipsilateral hippocampus. Interestingly, previous electrophysiological investigations of anaesthetized animals had demonstrated that the relative strength of monosynaptic and multi-synaptic entorhinal inputs to the hippocampus is frequency-dependent. Yeckel & Berger [57] have shown that at frequencies lower than 5 Hz

or higher than 20 Hz the pyramidal neurons in the hippocampus are preferentially stimulated monosynaptically. By contrast, frequencies of 10–15 Hz greatly enhance polysynaptic excitation of pyramidal neurons through the intrinsic pathways. Our fMRI results were in perfect match with the above electrophysiological result and consistent with a frequency-dependent activity transfer between and within hippocampal formations. As an important added value, fMRI experiments offered a spatial representation of the consequences of such synaptic frequency filtering.

### (c) Long-term potentiation induces a functional reorganization of long-range brain networks

Together with the information channels established by the specific axonal projections, sometimes referred to as the wiring diagram of the network, the plastic properties of synapses at different timescales is most likely the major determinant of activity propagation in the brain. While it is clear that synaptic strength determines the functional coupling between pre- and postsynaptic neurons, the polysynaptic impact of potentiating or depressing specific sets of synapses on the dynamic properties of wider networks is not yet understood. We used the combined electrophysiology–fMRI technique to investigate this issue in the hippocampus [49]. We first recorded activation maps in response to electric stimulation of the PP with test protocols not altering synaptic plasticity, and then induced LTP with a high-frequency stimulation paradigm [16]. The functional maps obtained with the test stimulation after LTP induction revealed three major findings. First, the magnitude of the BOLD signal in the tetanized DG was potentiated proportionally to the simultaneously recorded excitatory postsynaptic potential (EPSP), in agreement with previous findings showing that fMRI signals best correlate with synaptic activity [49,51,58] (figure 1). Second, activation after LTP spread across broader and bilateral regions of the MTL, including the hippocampus

proper, the subiculum and entorhinal cortex. The result suggests an unanticipated increase in the bilateral coupling of both hippocampal formations as a consequence of unilateral synaptic potentiation (see below). Third, in a proportion of animals (67% of cases), we found that PP stimulation after LTP activates a number of extrahippocampal structures, such as the PFC, nucleus accumbens (Acb) and perirhinal cortex (PRh). All these effects were observed immediately after LTP induction and lasted for the duration of the experiment (2–3 h after potentiation).

The reported synaptically driven functional reorganization was not associated with global increases in excitability because only a subset of the numerous hippocampal outputs [13,59] were activated. Extrahippocampal activations were entirely contingent on LTP induction, as stimulation of the PP with saturating current intensities (up to 1.0 mA) in controls never produced activations in those regions [48,49]. The results were well supported by anatomical findings demonstrating important monosynaptic and bidirectional connectivity between the hippocampus and all identified extrahippocampal structures in our study [13]. Interestingly, the newly recruited structures by hippocampal activation after LTP have been repeatedly involved in memory processing over the years [11,13,41,43,60–64].

#### (d) Considerations on the origin of fMRI signals

Functional MRI signals are mainly produced by the increase in cerebral blood flow (CBF) induced by vasoactive compounds released during neuronal activation, although brain blood volume does also contribute (for a review, see [65]). An important matter for neuroimaging is therefore to understand which aspects of neuronal work are reflected in increased CBF. Experiments simultaneously combining fMRI and electrophysiological recordings in the primary visual cortex of anaesthetized monkeys showed that the imaging signal evoked by visual stimulation maximally correlates with the local field potential (LFP), an aggregate measure of synaptic and active dendritic currents [51]. Although the correlation of the BOLD signal was only slightly higher towards LFP compared with spiking activity (multiunit and single unit activity), the LFP signal was the only predictor of the haemodynamic response when long stimulation protocols that habituate spiking activity were used. Consistent with these findings were studies in the rat cerebellar cortex which convincingly showed that local CBF can indeed be dissociated from spiking activity while strongly correlated with LFPs [66–68].

Based on the above results, it is believed that neuroimaging signals reflect the local processing of incoming neuronal activity to a particular area, rather than the output message being sent in outgoing efferent neuronal activity. The demonstration that local synaptic plasticity modulates the amplitude of the BOLD signal in the LTP experiment [49] reinforces this view. Of note, in the hippocampus, the axial organization of the cellular elements, with a rather precise alignment of dendritic shafts and somas, minimizes the cancellation of current sources from the LFP generators and facilitates the neurophysiological interpretation of the electrically evoked field potentials, such as synaptic currents reflected in the EPSP and spiking activity in the population spike. Using this preparation, we were able to unequivocally show that the EPSP slope was a precise predictor of BOLD signal amplitude,

better than either the population spike or the electrical current used for stimulation [48,49]. This result has recently been confirmed in experiments combining electrophysiological recordings with hippocampal CBF measurements based on Laser-Doppler flowmetry [69]. Overall, fMRI with BOLD contrast offers quantitative and reliable measures of local synaptic processing.

#### (e) Theoretical considerations of long-term potentiation-fMRI experiments for memory formation

The described results demonstrated that activity patterns previously thought to primarily induce synaptic plasticity locally in the ipsilateral DG, in fact altered subsequent activity across a wide network of interconnected brain regions. Both synaptic potentiation in the DG and network reorganization were blocked by MK801 suggesting that the same NMDA-dependent mechanism attributed to memory encoding in the hippocampus may also explain the kind of network interactions required for systems consolidation. This view departs from the classical model [12] in that hippocampal–neocortical interaction would not be a progressive and necessary consequence of cellular consolidation, but rather, triggered by an active gating mechanism operated by synaptic plasticity. These findings suggest a potential mechanism to efficiently route activity propagation and information channelling in parallel distributed neuronal networks. Whether this mechanism generalizes across brain regions will require further investigation. For the moment, it is interesting to note that visual perceptual learning [59] in humans modifies the synchrony of spontaneous BOLD signals between visual and frontal–parietal networks in a way that predicts the degree of learning [70,71].

Reorganization of hippocampal and PFC networks in humans has already been demonstrated in fMRI studies during memory recall [42], in line with lesion and imaging (2-deoxyglucose) data in rodents [72,73] and consistent with the idea of a hippocampal to neocortical shift in memory consolidation. A progressive decrease in hippocampal activity and increase of that in the medial PFC were observed at recall over a three-month period. The initial shift from hippocampal to PFC activation was detected as fast as 24 h after the initial encoding [42]. These results pointed towards a systems consolidation of memory faster than that initially considered in the classical consolidation theory [12,74], although alternative interpretations of PFC activation as a consequence of a more effortful recall could not be ruled out [75,76]. In the same experiment, slow-wave sleep (SWS) duration after encoding correlated with memory performance and hippocampal deactivation suggesting a causative link. During SWS, a replay of neuronal firing sequences associated with earlier learning occurs and is predominantly found during high-frequency oscillatory events in the hippocampus, the so-called ripples [76–78], and concomitantly in the medial PFC [79,80]. Disruption of ripple sequences during SWS interferes with memory consolidation [81]. It is important to note that neuronal activity during ripples is capable of inducing LTP at CA1 synapses [82], and therefore a similar network reorganization and information channelling as the one described in our fMRI-LTP experiments [49] may also help to explain the information transfer from the

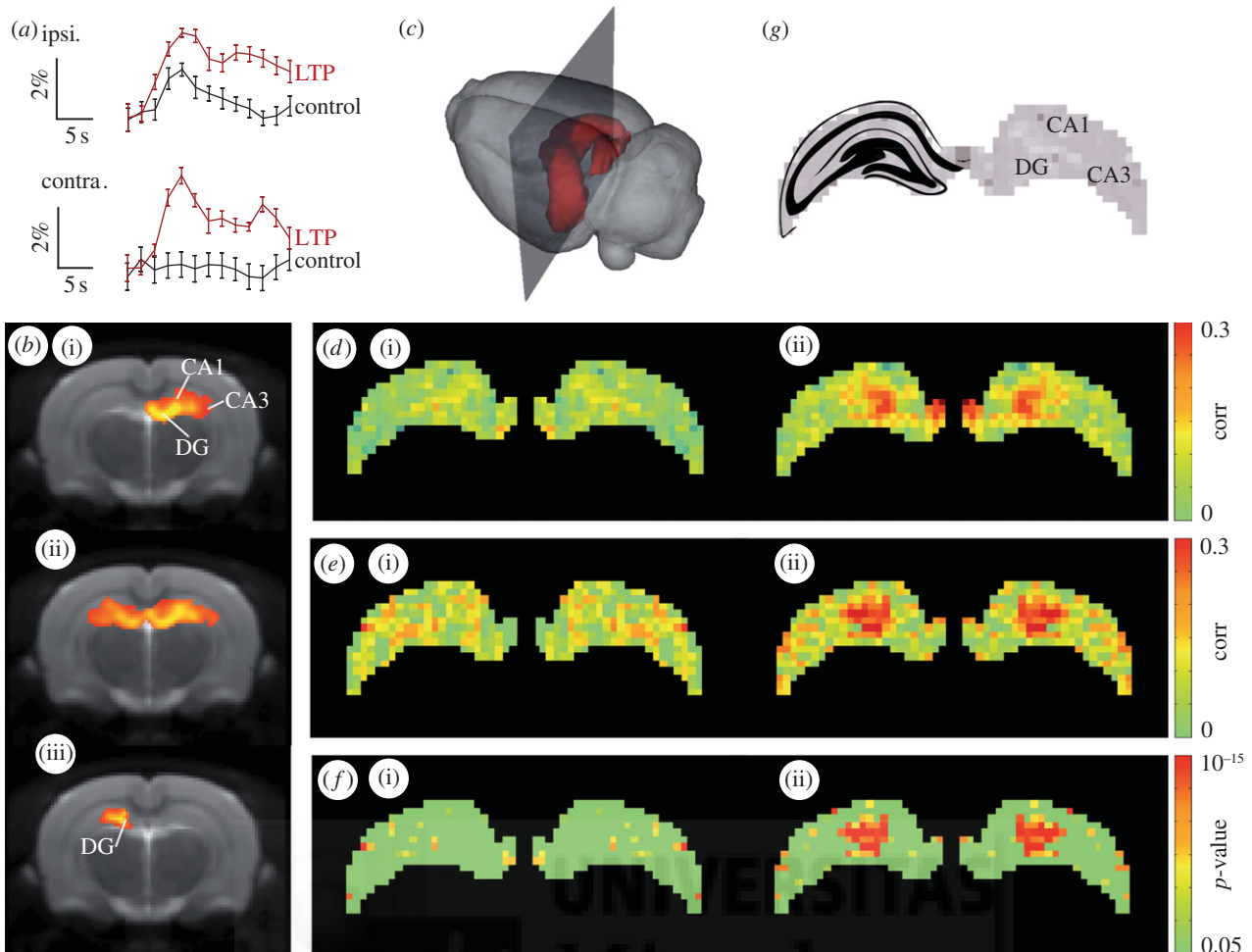


**Figure 2.** Enhanced bilateral coupling in the hippocampus after LTP is supported by the mossy cell commissural system. (a) BOLD signal time courses recorded in the dorsal ipsilateral and contralateral hippocampus before (black) and 3 h after (red) LTP induction. (b) Electric-stimulation fMRI maps ( $n = 4$ ,  $p < 0.001$ ) obtained before (i) and after (ii) LTP induction. The statistical comparison between pre- and post-LTP conditions ( $p < 0.01$ ) is also shown (iii). Extrahippocampal activity is masked. (c) The septo-temporal level of the coronal slices shown in all panels is illustrated on a three-dimensional reconstruction of the rat brain in which the hippocampal surface has been coloured in red. The dorsal hippocampus at the indicated level was segmented and the bilateral cross-correlation of the BOLD time courses was calculated for homotopic voxels (d,e). Cross-correlations before (i) and 3 h after (ii) LTP induction are shown for the group ( $n = 4$ ) (d) and one individual subject (e), as well as the statistical significance map (f). Correlation values and statistical significance are colour coded and scales are shown on the right. (g) The hippocampal territories in the corresponding septo-temporal level are overlaid on the cross-correlation map (in greyscale for clarity) of panel (di).

hippocampus to the PFC during memory consolidation in rest/sleep periods. Our data also suggest, however, that hippocampal–PFC interactions may take place even earlier, during memory encoding.

Enhanced coupling of the hippocampus with the PFC, PRh and Acb was found in fMRI data immediately after LTP induction, paralleling the timing of synaptic strength potentiation in the DG [49]. What could be the relevance of this functional reorganization for the first stages of memory encoding? We believe that early network interactions triggered by synaptic plasticity may optimize the coordination of two memory buffers for systems consolidation, one in the hippocampus and another in PFC. In experiments using a hippocampal-dependent pair-associate task for rats, it was elegantly demonstrated that systems consolidation can occur very rapidly when information is assimilated in a previously stored ‘schema’ in the neocortex [83]. In these cases, encoding is hippocampus-dependent but quickly consolidates in neocortex, reflecting an influence of prior knowledge on the rate of consolidation [84]. Coordination between the hippocampus and the prelimbic regions of the medial PFC were required not only for retrieval but also during memory encoding [64]. In this view [85], parallel encoding in cortex and hippocampus

would establish the relevant associative links (orchestrated by the hippocampus) between objects and events initially disconnected but already represented in the cortex. Additional support of hippocampal–PFC interaction during encoding comes from early human fMRI studies showing that activations in right PFC and bilateral parahippocampal cortex during memory encoding are predictive of how well a visual experience will be remembered [41].

The above results suggest a parallel encoding of memories working cooperatively. Interestingly, our fMRI results indicate that PFC–hippocampal interactions can be driven in a bottom-up manner by synaptic plasticity in the hippocampus. This interpretation contrasts with the ‘classical’ view of memory formation in that an early and hippocampal-dependent participation of the PFC would be required at encoding.

### (f) Enhanced interhemispheric communication

An unanticipated consequence of LTP induction found in the above fMRI experiments was the large increase in the recruitment of contralateral hippocampal subfields (figures 1d and 2). In fact, the relative potentiation of fMRI signals was significantly higher in the contralateral formation (figure 2).

In line with this result, bilateral changes in the expression of neurotrophins and trk receptor mRNA were found as a consequence of unilateral LTP [86]. We interpreted these findings as an enhanced commissural communication based on unilateral strengthening of synaptic weights. This conclusion was supported by previous findings demonstrating the absence of LTP in the crossed monosynaptic entorhinal projection to the contralateral hippocampus [87], and therefore discarding a direct effect of tetanization. A polysynaptic spread of the stimulation protocol used to induce LTP (200 Hz) was similarly discarded based on the filtering of high frequencies reported in the hippocampus (see above) [48,57]. As the low-frequency stimulation used as test stimulus is able to propagate trans-synaptically, the polysynaptic activation of brain areas after LTP is most probably the result of potentiated synaptic currents elicited by a test stimulus delivered at a frequency that spreads multi-synaptically. Contralateral activation may therefore reflect increased commissural–associational communication.

Although some reports start to show an intriguing bilateral asymmetry in rat hippocampus [88–91], little is known about its functional relevance. Two commissural systems connect the hippocampus, the CA3 contralateral projection to CA1, CA2 and CA3, and the contralateral DG projection mainly formed by hilar mossy cells (MCs). The CA3 network is thought to operate as an autoassociative memory with capability to selectively retrieve a specific pattern of firing activity (from among several possible patterns) when provided with a partial environmental cue [92,93]. The MC network, on the other hand, implements heteroassociative connections with granule cells (GCs) in more rostral and caudal positions relative to the MC soma location and with homotopic positions of the contralateral DG. Based on this divergent architecture, it has been suggested that the MC associational systems would be important in pattern separation and sequence learning (for a review, see [94]). In principle, the enhanced bilateral coupling observed after LTP induction in our fMRI experiments could be the result of either increased CA3 commissural output, or an increased hilar commissural pathway, or both. A different engagement of each of the commissural/associational loops will thus be most probably associated with different computational meanings. In the following paragraphs, we present new data on LTP-induced network reorganization focusing on the bilateral hippocampal crosstalk.

## 2. Methods

A total of 14 male Sprague-Dawley rats (250–350 g) were used in electrophysiology and fMRI studies. All experiments were approved by the local authorities (IN-CSIC) and were performed in accordance with Spanish (law 32/2007) and European regulations (EU directive 86/609, EU decree 2001-486).

### (a) Electrode implantation, microstimulation and recording

For all experiments, electrophysiology-only or combined fMRI–electrophysiology experiments, the animals were anaesthetized with urethane (1.2–1.5 g kg<sup>-1</sup>, i.p.) and secured in a stereotaxic device. Stimulating electrodes were implanted using standard surgical and stereotaxic procedures, as described previously [48,49]. A twisted platinum-iridium Teflon-coated bipolar electrode (200 mm diameter, 10–15 kW: A-M Systems, WA, USA) was positioned in the medial PP (from  $\lambda$ : 0 mm anteroposterior and

4.1–4.5 mm lateral, 2.5–3 mm ventral to the dural surface) for orthodromic stimulation of the DG and the hippocampus proper [95]. Charge balanced biphasic 0.1 ms duration pulses were delivered with a constant current source and a pulse generator (STG2004, Multichannel Systems, Reutlingen, Germany). Electrodes were implanted bilaterally in electrophysiology-only experiments.

#### (i) Electrophysiology-only recordings

Electrodes were silicon electrode arrays (single shank, 100  $\mu$ m spacing, 32 channels; Neuronexus Technologies) implanted bilaterally placed at 3.5 mm caudal and 2.5 mm lateral from bregma to record across different CA1 and DG levels in the dorsal hippocampus of both hemispheres.

#### (ii) Combined fMRI–electrophysiology recordings

Glass-micropipette electrodes were guided to the hilus of the DG using the typical profile of evoked potentials [96]. Stimulating and recording electrodes were secured to the skull with dental cement and plastic screws and the animal was transferred to the scanner and fixed in a custom-made MRI-compatible stereotaxic device.

#### (iii) Stimulation protocols

LTP was induced in all experiments as previously described [49]. In short, LTP was induced by high-frequency stimulation of the PP with episodes of six trains of pulses (each train delivered at 200 Hz and lasting 40 ms, with four pulses per train and trains delivered every 10 s) repeated three times with pauses of 2 min between episodes. Test stimulation for electrophysiological recording consisted of single pulses at different current intensities (input–output curves) delivered bilaterally, before, immediately after and 3 h after LTP induction. For fMRI recordings, a block design was used that consisted of 10 periods of 4 s stimulation epochs at 5–10 Hz and current intensities evoking half-maximal population spikes in the DG, each followed by a resting epoch of 26 s (10 min in total), which was repeated five times per animal. Functional maps were acquired before and 3 h after LTP induction.

After filtering (0.1 Hz–3 kHz) and amplification, the electrophysiological signals were digitized (20 kHz acquisition rate) and stored in a personal computer for offline processing with MatLab and Spike2. The population spike in the hilus of the DG was measured as the amplitude from the precedent positive crest and the negative peak, and the EPSPs were measured as the maximal slope of the falling potentials recorded in the molecular layer.

#### (b) MR imaging

For MRI experiments, urethane-anaesthetized animals were placed in a custom-made animal holder with adjustable bite and ear bars and positioned on the magnet bed. Their temperature, heart rate, oxygen saturation (SpO<sub>2</sub>) and breathing rate were monitored throughout the session, and the experiments were carried out in a horizontal 7 T scanner with a 30 cm diameter bore (Biospec 70/30v, Bruker Medical, Ettlingen, Germany). Data were acquired during stimulation of the PP with test stimuli (see above) before and after LTP induction. Acquisition was performed in 15 coronal slices using a GE-EPI sequence applying the following parameters: FOV, 25  $\times$  25 mm; slice thickness, 1 mm; matrix, 96  $\times$  96; segments, 1; FA, 60°; TE, 15 ms; TR, 2000 ms. T2 weighted anatomical images were collected using a rapid acquisition relaxation enhanced sequence (RARE): FOV, 25  $\times$  25 mm; 15 slices; slice thickness, 1 mm; matrix, 192  $\times$  192; TE<sub>eff</sub>, 56 ms; TR, 2 s; RARE factor, 8. A <sup>1</sup>H rat brain receive-only phase array coil with integrated combiner and preamplifier, and no tune/no match, was employed in combination with the actively detuned transmit-only resonator (Bruker BioSpin MRI GmbH, Germany).

Functional MRI data were analysed offline using our own software developed in Matlab, which included Statistical Parametric

Mapping package (SPM8, [www.fil.ion.ucl.ac.uk/spm](http://www.fil.ion.ucl.ac.uk/spm)), Analysis of Functional NeuroImages (AFNI, <http://afni.nimh.nih.gov/afni>) and FSL Software (FMRIB <http://fsl.fmrib.ox.ac.uk/fsl/>). For electric-stimulation fMRI, after linear detrending, temporal (0.015–0.2 Hz) and spatial filtering ( $3 \times 3$  Gaussian kernel of 1.5 sigma) of voxel time series, a general linear model or cross-correlation analysis was applied with a simple boxcar model shifted forward in time, typically by 2 s, or a boxcar convolved with a gamma probability density function (Matlab). Functional maps were generated from voxels that had a significant component for the model and they were clustered together in space. Similar results were obtained with the different analytical methods. For functional connectivity between bilateral hippocampal structures, images are brain extracted, co-registered and intensity normalized. Afterwards, temporal data were corrected by applying detrending, global regression and time filtering (0.002–0.1 Hz). BOLD time courses of hippocampal voxels, extracted using a rat atlas registered to the functional images [97], were used to compute the bilateral cross-correlation coefficients.

### 3. Results and discussion

In combined electrophysiology–fMRI experiments, we performed high-resolution echo-planar imaging (EPI) acquisitions in coronal orientation to facilitate the identification of hippocampal subfields in functional images. Electric stimulation of the PP with 4 s trains at 5 Hz and current intensities producing half-maximal population spike amplitude produced the expected activation of all ipsilateral hippocampal subfields. No contralateral propagation of activity was found in the group analysis with this mild stimulation protocol (figure 2*b*). Three hours after LTP induction the BOLD signal amplitude was increased (figure 2*a*) and the polysynaptic recruitment of contralateral hippocampal territories largely enhanced (figure 2*b*), in agreement with previous findings. Activation maps in coronal orientation showed activity propagation mainly concentrated in the septal portion of the contralateral hippocampus. To further investigate the spatial distribution of the enhanced bilateral coupling, we analysed interhemispheric communication by computing the voxel-wise cross-correlation of BOLD time series between all voxels in homotopic hippocampal regions, before and after LTP induction. As clearly illustrated for group analysis (figure 2*e*) and individual examples (figure 2*f–g*), ipsilateral LTP selectively enhanced the correlation between regions of the DG activated by a test stimulus applied to the ipsilateral PP. This result suggests that the LTP-triggered increase in bilateral coupling is in fact supported by the MC associational/commissural pathway with no (or limited) contribution of the CA3 network. Previous electrophysiological investigations demonstrated that the crossed entorhinal monosynaptic input to the contralateral DG is not potentiated by LTP protocols inducing a robust facilitation in the ipsilateral GC, while the convergent monosynaptic input from the contralateral entorhinal cortex is depressed [87]. To investigate the synaptic underpinnings of the above fMRI finding, we therefore focused on the polysynaptically evoked field potentials recorded across the ipsilateral (R1) and contralateral (R2) DG in response to the activation of the conditioned (tetanized, S1) or unconditioned (contralateral, S2) PPs (see Methods).

Electric stimulation of the medial PP produced the well-known profile of evoked potentials across the ipsilateral DG [55,98], with a negative-going monosynaptic EPSP (approx. 2 ms delay) recorded in the middle third of the molecular layer corresponding to the current sink and a positive potential

in the soma and polymorphic layers interrupted at suprathreshold intensities by a fast population spike with maximal amplitude in the centre of the hilus (figure 3*a*). Stimulation of the contralateral PP generates a polysynaptic EPSP (approx. 9–10 ms delay) with a current sink in the inner third of the molecular layer (figure 3*b*), in good agreement with previous reports [99,100] and the known anatomy of the commissural projection of the MCs [54,101,102]. Using this preparation, we followed the electrophysiological consequences of unilateral LTP induction as a measure of commissural communication. As shown in figure 3*c*, LTP induction produced in the ipsilateral side (S1 → R1) the expected long-lasting potentiation of the monosynaptic EPSP without affecting the unconditioned pathway (S2 → R2) (figure 3*d*). Interestingly, it also induced a long-lasting potentiation of the polysynaptic EPSP in the contralateral inner molecular layer of the dentate (S1 → R2) (figure 3*e*). This result demonstrates, in good agreement with the fMRI findings (figure 2), that LTP enhances the MC commissural output. Concomitantly, with this potentiation we found a long-term depression of the ipsilateral EPSP evoked by activation of the convergent contralateral (unconditioned) PP (S2 → R1), which we interpret as heterosynaptic depression in a pathway inactive during tetanization (figure 3*f*). These results together with those reported by Levi & Steward [87] on monosynaptic bilateral entorhino–hippocampal connections are summarized in figure 3*g*. Although initial studies did not find changes in polysynaptic associational responses after PP LTP [103], more recent electrophysiological studies in mice clearly show LTP of the ipsilateral trisynaptic associative pathway (PP → GC → MC → GC) in response to PP tetanization [104]. Furthermore, the authors also demonstrate plastic associations between ipsilateral entorhinal and MC inputs into GCs [104].

Overall the results illustrate a hilar commissural system with synapses able to potentiate and depress in response to PP activity, and therefore well suited to associate or eliminate (update) items in a hippocampal memory trace, respectively. The highly divergent connectivity pattern of MCs spreading longitudinally in the ipsilateral DG and contralaterally to not only homotopic but also heterotopic territories [105] indicates a main role in the redistribution and integration of information among GCs at different septo-temporal levels. The reported enhancement of activity propagation in the MC-commissural system, but not in the CA3 network, triggered by LTP most probably reflects the bilateral coordination of both MC associational loops. The relevance of this finding for memory processing is not yet clear, but we suggest, in line with existing theories on MC function [106,107], an increased specificity in the recollection of bilaterally stored activity patterns by increasing sparsification and integration in a bilaterally coordinated MC associational network. The mechanism supporting the commissural selectivity (MC versus CA3) is not known but may suggest, as for the specificity in the extrahippocampal recruited regions, that LTP opens specific information channels within the hippocampus.

#### (a) Concluding remarks

Functional MRI investigations of classical LTP experiments [16] have unveiled a number of additional and, to a certain extent, unexpected effects of local strengthening of synaptic currents in the PP input to the hippocampus. This LTP-induced network reorganization was demonstrated to enhance the functional coupling between the hippocampus and neocortical

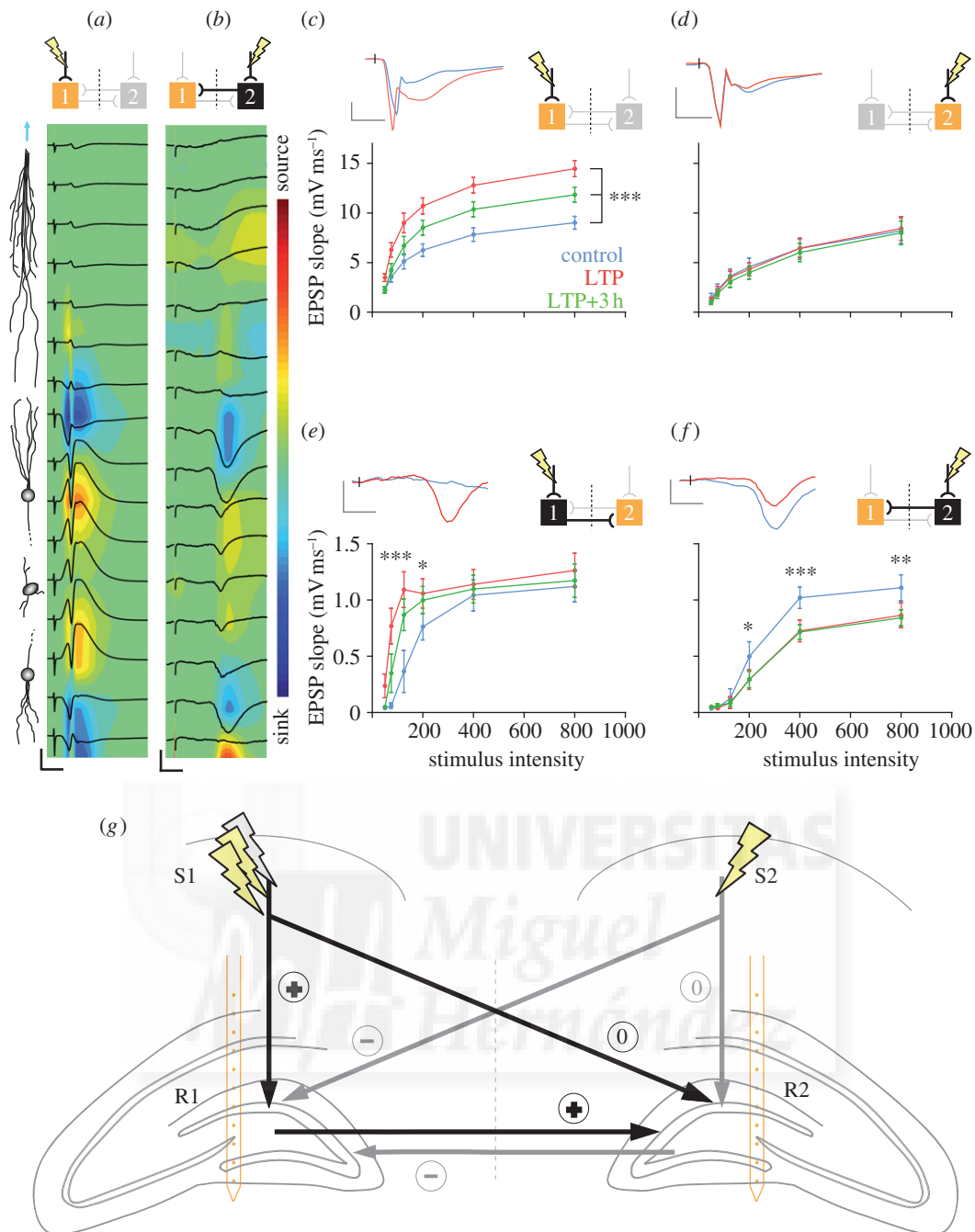


**Figure 3.** Electrophysiological commissural changes induced by LTP of the perforant pathway. (a) Current source density (CSD) analysis with evoked potentials overlaid in black. A representative example of the activity pattern recorded in the ipsilateral hippocampus across stratum radiatum (most dorsal recordings) and dentate gyrus (ventral) under stimulation of the ipsilateral perforant path (S1 → R1) is shown. The location of the different strata is illustrated by cell drawings on the left. The cartoons displayed in the top of all panels indicate the relevant positions of stimulating and recording electrodes for each particular case. (b) CSD and evoked potentials recorded in the same electrode as in (a) under contralateral perforant path stimulation (S2 → R1). Note the shift of the EPSP and associated current sink to more inner territories of the granule cell dendrite. (c–f) EPSP slopes as a function of stimulus intensity recorded before (blue), immediately after (red) and 3 h after (green) LTP induction, for all stimulation-recording pairs; S1 → R1 (c), S2 → R2 (d), S1 → R2 (e) and S2 → R1 (f). Insets show representative evoked potentials. (g) Scheme summarizing the effects of perforant LTP on the polysynaptic commissural activity propagation found in this study, together with the monosynaptic effects in the ipsilateral and crossed entorhinal projection described by Levy & Steward [87]. The pathways originating from the conditioned ipsilateral pathway are in black, the ones from the convergent (unconditioned) contralateral pathway are in grey. LTP is induced in S1. Symbols represent the direction of the recorded change on each pathway after LTP induction: '+' potentiation, '-' depression and '0' unaltered. Statistical analysis was performed by a two-way ANOVA followed by Bonferroni post-hoc test (\* $p < 0.05$ , \*\* $p < 0.01$ , \*\*\* $p < 0.001$ ). Horizontal calibration bars represent 5 ms for all panels; vertical bars represent (a) 10 mV, (b) 2 mV, (c,d) 5 mV, (e) 1 mV, (f) 0.5 mV.

structures, such as the PFC or the PRh, and subcortical nucleus, for example the accumbens [49]. We have interpreted these findings in the context of memory processing and have suggested that the reported NMDA receptor-dependent and fast increase in hippocampal–PFC communication may

represent a mechanism to coordinate two memory buffers operating in parallel, even during memory encoding, as suggested by the fast consolidation of new information in pre-existing cortical schemas [64]. We have also shown that functional activation in the contralateral hippocampus is

largely increased by ipsilateral LTP induction [49]. In the present experiments using high-resolution fMRI, we demonstrate that the increased bilateral coupling in the hippocampus is specifically supported by the MC commissural pathway. This enhanced MC commissural output may represent bilateral coordination of associational networks with a role in pattern separation and sequence learning [94].

**Acknowledgements.** The authors acknowledge Begoña Fernández for excellent technical assistance.

**Funding statement.** E.A.S. is supported by a JAE-pre fellowship from CSIC cofounded by the 'European Social Fund' of the EU. Research in S.C. laboratory is supported by grants of the Spanish Ministry of Science and Innovation MICINN BFU2009-09938 and PIM2010ERN-00679 (part of the coordinated ERA-Net NEURON project TRANSALC).

## References

- Rumelhart DE, McClelland JL, Group PR. 1986 *Parallel distributed processing*, vols 1 and 2. Cambridge, MA: MIT Press.
- Goldman-Rakic PS. 1988 Topography of cognition: parallel distributed networks in primate association cortex. *Annu. Rev. Neurosci.* **11**, 137–156. (doi:10.1146/annurev.ne.11.030188.001033)
- Dehaene S, Naccache L. 2001 Towards a cognitive neuroscience of consciousness: basic evidence and a workspace framework. *Cognition* **79**, 1–37. (doi:10.1016/S0010-0277(00)00123-2)
- Bassett DS, Greenfield DL, Meyer-Lindenberg A, Weinberger DR, Moore SW, Bullmore ET. 2010 Efficient physical embedding of topologically complex information processing networks in brains and computer circuits. *PLoS Comput. Biol.* **6**, e1000748. (doi:10.1371/journal.pcbi.1000748)
- Felleman DJ, Van Essen DC. 1991 Distributed hierarchical processing in the primate cerebral cortex. *Cereb. Cortex* **1**, 1–47. (doi:10.1093/cercor/1.1.1)
- Treisman A. 1996 The binding problem. *Curr. Opin. Neurobiol.* **6**, 171–178. (doi:10.1016/S0959-4388(96)80070-5)
- Lavenex P, Amaral DG. 2000 Hippocampal–neocortical interaction: a hierarchy of associativity. *Hippocampus* **10**, 420–430. (doi:10.1002/1098-1063(2000)10:4<420::AID-HIPO8>3.0.CO;2-5)
- Tanabe HC, Honda M, Sadato N. 2005 Functionally segregated neural substrates for arbitrary audiovisual paired-association learning. *J. Neurosci.* **25**, 6409–6418. (doi:10.1523/JNEUROSCI.0636-05.2005)
- Shams L, Seitz AR. 2008 Benefits of multisensory learning. *Trends Cogn. Sci.* **12**, 411–417. (doi:10.1016/j.tics.2008.07.006)
- Driver J, Noesselt T. 2008 Multisensory interplay reveals crossmodal influences on 'sensory-specific' brain regions, neural responses, and judgments. *Neuron* **57**, 11–23. (doi:10.1016/j.neuron.2007.12.013)
- Scoville WB, Milner B. 1957 Loss of recent memory after bilateral hippocampal lesions. *J. Neurol. Neurosurg. Psychiatry* **20**, 11–21. (doi:10.1136/jnnp.20.1.11)
- Squire LR. 1992 Memory and the hippocampus: a synthesis from findings with rats, monkeys, and humans. *Psychol. Rev.* **99**, 195–231. (doi:10.1037/0033-295X.99.2.195)
- Amaral D, Lavenex P. 2007 Hippocampal neuroanatomy. *Hippocampus Book* **1**, 37–114.
- Moser MB, Moser EI. 1998 Functional differentiation in the hippocampus. *Hippocampus* **8**, 608–619. (doi:10.1002/(SICI)1098-1063(1998)8:6<608::AID-HIPO3>3.0.CO;2-7)
- Fanselow MS, Dong HW. 2010 Are the dorsal and ventral hippocampus functionally distinct structures? *Neuron* **65**, 7–19. (doi:10.1016/j.neuron.2009.11.031)
- Bliss TV, Lomo T. 1973 Long-lasting potentiation of synaptic transmission in the dentate area of the anaesthetized rabbit following stimulation of the perforant path. *J. Physiol.* **232**, 331–356.
- Hebb DO. 1949 *The organisation of behaviour: a neuropsychological theory*. New York, NY: Wiley.
- Bliss TV, Collingridge GL. 1993 A synaptic model of memory: long-term potentiation in the hippocampus. *Nature* **361**, 31–39. (doi:10.1038/361031a0)
- Bliss TV, Collingridge GL. 2013 Expression of NMDA receptor-dependent LTP in the hippocampus: bridging the divide. *Mol. Brain* **6**, 5. (doi:10.1186/1756-6606-6-5)
- Wang S-H, Morris RG. 2010 Hippocampal–neocortical interactions in memory formation, consolidation, and reconsolidation. *Annu. Rev. Psychol.* **61**, 49–79. (doi:10.1146/annurev.psych.093008.100523)
- Weisz DJ, Clark GA, Thompson RF. 1984 Increased responsivity of dentate granule cells during nictitating membrane response conditioning in rabbit. *Behav. Brain Res.* **12**, 145–154. (doi:10.1016/0166-4328(84)90037-8)
- Moser E, Moser M-B, Andersen P. 1993 Synaptic potentiation in the rat dentate gyrus during exploratory learning. *Neuroreport* **5**, 317–320. (doi:10.1097/00001756-199312000-00035)
- Whitlock JR, Heynen AJ, Shuler MG, Bear MF. 2006 Learning induces long-term potentiation in the hippocampus. *Sci. Signal.* **313**, 1093–1097. (doi:10.1126/science.1128134)
- Gruart A, Muñoz MD, Delgado-García JM. 2006 Involvement of the CA3–CA1 synapse in the acquisition of associative learning in behaving mice. *J. Neurosci.* **26**, 1077–1087. (doi:10.1523/JNEUROSCI.2834-05.2006)
- Rogan MT, Stäubli UV, LeDoux JE. 1997 Fear conditioning induces associative long-term potentiation in the amygdala. *Nature* **390**, 604–607. (doi:10.1038/37601)
- Tang J, Wotjak CT, Wagner S, Williams G, Schachner M, Dityatev A. 2001 Potentiated amygdaloid auditory-evoked potentials and freezing behavior after fear conditioning in mice. *Brain Res.* **919**, 232–241. (doi:10.1016/S0006-8993(01)03020-7)
- Monfils M, Teskey G. 2004 Skilled-learning-induced potentiation in rat sensorimotor cortex: a transient form of behavioural long-term potentiation. *Neuroscience* **125**, 329–336. (doi:10.1016/j.neuroscience.2004.01.048)
- Roman FS, Truchet B, Chaillan FA, Marchetti E, Soumireu-Mourat B. 2004 Olfactory associative discrimination: a model for studying modifications of synaptic efficacy in neuronal networks supporting long-term memory. *Rev. Neurosci.* **15**, 1–18. (doi:10.1515/REVNEURO.2004.15.1.1)
- Sevelinges Y, Gervais R, Messaoudi B, Granjon L, Mouly A-M. 2004 Olfactory fear conditioning induces field potential potentiation in rat olfactory cortex and amygdala. *Learn. Mem.* **11**, 761–769. (doi:10.1101/lm.83604)
- Sacchetti B, Scelfo B, Tempia F, Strata P. 2004 Long-term synaptic changes induced in the cerebellar cortex by fear conditioning. *Neuron* **42**, 973–982. (doi:10.1016/j.neuron.2004.05.012)
- Rumpel S, LeDoux J, Zador A, Malinow R. 2005 Postsynaptic receptor trafficking underlying a form of associative learning. *Science* **308**, 83–88. (doi:10.1126/science.1103944)
- Morris R, Anderson E, Lynch G, Baudry M. 1986 Selective impairment of learning and blockade of long-term potentiation by an N-methyl-D-aspartate receptor antagonist, AP5. *Nature* **319**, 774–776. (doi:10.1038/319774a0)
- Kentros C, Hargreaves E, Hawkins RD, Kandel ER, Shapiro M, Muller RV. 1998 Abolition of long-term stability of new hippocampal place cell maps by NMDA receptor blockade. *Science* **280**, 2121–2126. (doi:10.1126/science.280.5372.2121)
- Moser EI, Krobret KA, Moser M-B, Morris RG. 1998 Impaired spatial learning after saturation of long-term potentiation. *Science* **281**, 2038–2042. (doi:10.1126/science.281.5385.2038)
- Gloor P. 1990 Experiential phenomena of temporal lobe epilepsy. Facts and hypotheses. *Brain* **113**, 1673–1694. (doi:10.1093/brain/113.6.1673)
- Manchanda R, Freeland A, Schaefer B, McLachlan RS, Blume WT. 2000 Auras, seizure focus, and psychiatric disorders. *Cogn. Behav. Neurol.* **13**, 13–19.
- Rempel-Clower NL, Zola SM, Squire LR, Amaral DG. 1996 Three cases of enduring memory impairment after bilateral damage limited to the hippocampal formation. *J. Neurosci.* **16**, 5233–5255.

38. Zola-Morgan SM, Squire LR. 1990 The primate hippocampal formation: evidence for a time-limited role in memory storage. *Science* **250**, 288–290. (doi:10.1126/science.2218534)
39. Kim JJ, Fanselow MS. 1992 Modality-specific retrograde amnesia of fear. *Science* **256**, 675–677. (doi:10.1126/science.1585183)
40. Olton DS, Papas BC. 1979 Spatial memory and hippocampal function. *Neuropsychologia* **17**, 669–682. (doi:10.1016/0028-3932(79)90042-3)
41. Brewer JB, Zhao Z, Desmond JE, Glover GH, Gabrieli JD. 1998 Making memories: brain activity that predicts how well visual experience will be remembered. *Science* **281**, 1185–1187. (doi:10.1126/science.281.5380.1185)
42. Takashima A, Petersson K, Rutters F, Tendolkar I, Jensen O, Zwarts M, McNaughton BL, Fernandez G. 2006 Declarative memory consolidation in humans: a prospective functional magnetic resonance imaging study. *Proc. Natl Acad. Sci. USA* **103**, 756–761. (doi:10.1073/pnas.0507774103)
43. Siapas AG, Lubenov EV, Wilson MA. 2005 Prefrontal phase locking to hippocampal theta oscillations. *Neuron* **46**, 141–151. (doi:10.1016/j.neuron.2005.02.028)
44. Teyler TJ, Rudy JW. 2007 The hippocampal indexing theory and episodic memory: updating the index. *Hippocampus* **17**, 1158–1169. (doi:10.1002/hipo.20350)
45. Marr D. 1970 A theory for cerebral neocortex. *Proc. R. Soc. Lond. B* **176**, 161–234. (doi:10.1098/rspb.1970.0040)
46. Alvarez P, Squire LR. 1994 Memory consolidation and the medial temporal lobe: a simple network model. *Proc. Natl Acad. Sci. USA* **91**, 7041–7045. (doi:10.1073/pnas.91.15.7041)
47. Frankland PW, Bontempi B. 2005 The organization of recent and remote memories. *Nat. Rev. Neurosci.* **6**, 119–130. (doi:10.1038/nrn1607)
48. Canals S, Beyerlein M, Murayama Y, Logothetis NK. 2008 Electric stimulation fMRI of the perforant pathway to the rat hippocampus. *Magn. Reson. Imaging* **26**, 978–986. (doi:10.1016/j.mri.2008.02.018)
49. Canals S, Beyerlein M, Merkle H, Logothetis NK. 2009 Functional MRI evidence for LTP-induced neural network reorganization. *Curr. Biol.* **19**, 398–403. (doi:10.1016/j.cub.2009.01.037)
50. Tolias AS, Sultan F, Augath M, Oeltermann A, Tehovnik EJ, Schiller PH, Logothetis NK. 2005 Mapping cortical activity elicited with electrical microstimulation using fMRI in the macaque. *Neuron* **48**, 901–911. (doi:10.1016/j.neuron.2005.11.034)
51. Logothetis NK, Pauls J, Augath M, Trinath T, Oeltermann A. 2001 Neurophysiological investigation of the basis of the fMRI signal. *Nature* **412**, 150–157. (doi:10.1038/35084005)
52. Fox MD, Snyder AZ, Vincent JL, Corbetta M, Van Essen DC, Raichle ME. 2005 The human brain is intrinsically organized into dynamic, anticorrelated functional networks. *Proc. Natl Acad. Sci. USA* **102**, 9673–9678. (doi:10.1073/pnas.0504136102)
53. Ramón y Cajal S. 1904 *Textura del Sistema Nervioso del Hombre y de los Vertebrados*. Madrid, Spain: Moya.
54. Lorente de Nó R. 1934 Studies on the structure of the cerebral cortex. II. Continuation of the study of the ammonic system. *J. Psychol. Neurol.* **46**, 113–177.
55. Andersen P, Bliss T, Skrede KK. 1971 Lamellar organization of hippocampal excitatory pathways. *Exp. Brain Res.* **13**, 222–238. (doi:10.1007/BF00234087)
56. Amaral D, Witter M. 1989 The three-dimensional organization of the hippocampal formation: a review of anatomical data. *Neuroscience* **31**, 571–591. (doi:10.1016/0306-4522(89)90424-7)
57. Yeckel MA, Berger TW. 1990 Feedforward excitation of the hippocampus by afferents from the entorhinal cortex: redefinition of the role of the trisynaptic pathway. *Proc. Natl Acad. Sci. USA* **87**, 5832–5836. (doi:10.1073/pnas.87.15.5832)
58. Moreno A, Jago P, de la Cruz F, Canals S. 2013 Neurophysiological, metabolic and cellular compartments that drive neurovascular coupling and neuroimaging signals. *Front. Neuroenergetics* **5**, 3. (doi:10.3389/fnene.2013.00003)
59. van Strien NM, Cappaert NL, Witter MP. 2009 The anatomy of memory: an interactive overview of the parahippocampal-hippocampal network. *Nat. Rev. Neurosci.* **10**, 272–282. (doi:10.1038/nrn2614)
60. Squire LR, Stark CE, Clark RE. 2004 The medial temporal lobe. *Annu. Rev. Neurosci.* **27**, 279–306. (doi:10.1146/annurev.neuro.27.070203.144130)
61. Eichenbaum H, Cohen NJ. 2004 *From conditioning to conscious recollection: memory systems of the brain*. New York, NY: Oxford University Press.
62. Fuster JM. 2001 The prefrontal cortex—an update: time is of the essence. *Neuron* **30**, 319–333. (doi:10.1016/S0896-6273(01)00285-9)
63. Morris RG, Moser E, Riedel G, Martin S, Sandin J, Day M, Carroll CO. 2003 Elements of a neurobiological theory of the hippocampus: the role of activity-dependent synaptic plasticity in memory. *Phil. Trans. R. Soc. Lond. B* **358**, 773–786. (doi:10.1098/rstb.2002.1264)
64. Tse D, Takeuchi T, Kakeyama M, Kajii Y, Okuno H, Tohyama C, Bito H, Morris RGM. 2011 Schema-dependent gene activation and memory encoding in neocortex. *Science* **333**, 891–895. (doi:10.1126/science.1205274)
65. Logothetis NK, Wandell BA. 2004 Interpreting the BOLD signal. *Annu. Rev. Physiol.* **66**, 735–769. (doi:10.1146/annurev.physiol.66.082602.092845)
66. Mathiesen C, Caesar K, Akgören N, Lauritzen M. 1998 Modification of activity-dependent increases of cerebral blood flow by excitatory synaptic activity and spikes in rat cerebellar cortex. *J. Physiol.* **512**, 555–566. (doi:10.1111/j.1469-7793.1998.555be.x)
67. Mathiesen C, Caesar K, Lauritzen M. 2000 Temporal coupling between neuronal activity and blood flow in rat cerebellar cortex as indicated by field potential analysis. *J. Physiol.* **523**, 235–246. (doi:10.1111/j.1469-7793.2000.101-1-00235.x)
68. Thomsen K, Offenhauser N, Lauritzen M. 2004 Principal neuron spiking: neither necessary nor sufficient for cerebral blood flow in rat cerebellum. *J. Physiol.* **560**, 181–189. (doi:10.1113/jphysiol.2004.068072)
69. Hamadate N *et al.* 2011 Regulation of cerebral blood flow in the hippocampus by neuronal activation through the perforant path: relationship between hippocampal blood flow and neuronal plasticity. *Brain Res.* **1415**, 1–7. (doi:10.1016/j.brainres.2011.08.008)
70. Lewis CM, Baldassarre A, Comitteri G, Romani GL, Corbetta M. 2009 Learning sculpts the spontaneous activity of the resting human brain. *Proc. Natl Acad. Sci. USA* **106**, 17 558–17 563. (doi:10.1073/pnas.0902455106)
71. Sigman M, Pan H, Yang Y, Stern E, Silbersweig D, Gilbert CD. 2005 Top-down reorganization of activity in the visual pathway after learning a shape identification task. *Neuron* **46**, 823–835. (doi:10.1016/j.neuron.2005.05.014)
72. Bontempi B, Laurent-Demir C, Destrade C, Jaffard R. 1999 Time-dependent reorganization of brain circuitry underlying long-term memory storage. *Nature* **400**, 671–675. (doi:10.1038/23270)
73. Takehara K, Kawahara S, Kirino Y. 2003 Time-dependent reorganization of the brain components underlying memory retention in trace eyeblink conditioning. *J. Neurosci.* **23**, 9897–9905.
74. McGaugh JL. 2000 Memory—a century of consolidation. *Science* **287**, 248–251. (doi:10.1126/science.287.5451.248)
75. Frankland PW, Bontempi B. 2006 Fast track to the medial prefrontal cortex. *Proc. Natl Acad. Sci. USA* **103**, 509–510. (doi:10.1073/pnas.0510133103)
76. Wilson MA, McNaughton BL. 1994 Reactivation of hippocampal ensemble memories during sleep. *Science* **265**, 676–679. (doi:10.1126/science.8036517)
77. Wilson MA. 2002 Hippocampal memory formation, plasticity, and the role of sleep. *Neurobiol. Learn. Mem.* **78**, 565–569. (doi:10.1006/nlme.2002.4098)
78. Diba K, Buzsáki G. 2007 Forward and reverse hippocampal place-cell sequences during ripples. *Nat. Neurosci.* **10**, 1241–1242. (doi:10.1038/nn1961)
79. Peyrache A, Khamassi M, Benchenane K, Wiener SI, Battaglia FP. 2009 Replay of rule-learning related neural patterns in the prefrontal cortex during sleep. *Nat. Neurosci.* **12**, 919–926. (doi:10.1038/nn.2337)
80. Siapas AG, Wilson MA. 1998 Coordinated interactions between hippocampal ripples and cortical spindles during slow-wave sleep. *Neuron* **21**, 1123–1128. (doi:10.1016/S0896-6273(00)80629-7)
81. Girardeau G, Benchenane K, Wiener SI, Buzsáki G, Zugaro MB. 2009 Selective suppression of hippocampal ripples impairs spatial memory. *Nat. Neurosci.* **12**, 1222–1223. (doi:10.1038/nn.2384)
82. King C, Henze DA, Leinekugel X, Buzsáki G. 1999 Hebbian modification of a hippocampal population pattern in the rat. *J. Physiol.* **521**, 159–167. (doi:10.1111/j.1469-7793.1999.00159.x)

83. Tse D, Langston RF, Kakeyama M, Bethus I, Spooner PA, Wood ER, Witter MP, Morris RGM. 2007 Schemas and memory consolidation. *Science* **316**, 76–82. (doi:10.1126/science.1135935)
84. Osada T, Adachi Y, Kimura HM, Miyashita Y. 2008 Towards understanding of the cortical network underlying associative memory. *Phil. Trans. R. Soc. B* **363**, 2187–2199. (doi:10.1098/rstb.2008.2271)
85. Morris RG. 2006 Elements of a neurobiological theory of hippocampal function: the role of synaptic plasticity, synaptic tagging and schemas. *Eur. J. Neurosci.* **23**, 2829–2846. (doi:10.1111/j.1460-9568.2006.04888.x)
86. Bramham CR, Southard T, Sarvey JM, Herkenham M, Brady LS. 1996 Unilateral LTP triggers bilateral increases in hippocampal neurotrophin and trk receptor mRNA expression in behaving rats: evidence for interhemispheric communication. *J. Comp. Neurol.* **368**, 371–382. (doi:10.1002/(SICI)1096-9861(19960506)368:3<371::AID-CNE4>3.0.CO;2-2)
87. Levy WB, Steward O. 1979 Synapses as associative memory elements in the hippocampal formation. *Brain Res.* **175**, 233–245. (doi:10.1016/0006-8993(79)91003-5)
88. Kohl MM, Shipton OA, Deacon RM, Rawlins JNP, Deisseroth K, Paulsen O. 2011 Hemisphere-specific optogenetic stimulation reveals left-right asymmetry of hippocampal plasticity. *Nat. Neurosci.* **14**, 1413–1415. (doi:10.1038/nn.2915)
89. Wu Y, Kawakami R, Shinohara Y, Fukaya M, Sakimura K, Mishina M, Watanabe M, Ito I, Shigemoto R. 2005 Target-cell-specific left-right asymmetry of NMDA receptor content in Schaffer collateral synapses in  $\epsilon$ 1/NR2A knock-out mice. *J. Neurosci.* **25**, 9213–9226. (doi:10.1523/JNEUROSCI.2134-05.2005)
90. Shinohara Y, Hirase H, Watanabe M, Itakura M, Takahashi M, Shigemoto R. 2008 Left-right asymmetry of the hippocampal synapses with differential subunit allocation of glutamate receptors. *Proc. Natl Acad. Sci. USA* **105**, 19 498–19 503. (doi:10.1073/pnas.0807461105)
91. Kawakami R, Shinohara Y, Kato Y, Sugiyama H, Shigemoto R, Ito I. 2003 Asymmetrical allocation of NMDA receptor  $\epsilon$ 2 subunits in hippocampal circuitry. *Sci. Signal.* **300**, 990–994. (doi:10.1126/science.1082609)
92. Treves A, Rolls ET. 1992 Computational constraints suggest the need for two distinct input systems to the hippocampal CA3 network. *Hippocampus* **2**, 189–199. (doi:10.1002/hipo.450020209)
93. McNaughton BL, Morris RGM. 1987 Hippocampal synaptic enhancement and information-storage within a distributed memory system. *Trends Neurosci.* **10**, 408–415. (doi:10.1016/0166-2236(87)90011-7)
94. Scharfman HE, Myers CE. 2012 Hilar mossy cells of the dentate gyrus: a historical perspective. *Front. Neural Circuits* **6**, 106. (doi:10.3389/fncir.2012.00106)
95. Paxinos G, Watson C. 2007 *The rat brain in stereotaxic coordinates*. New York, NY: Academic Press.
96. Andersen P, Holmqvist B, Voorhoeve P. 1966 Entorhinal activation of dentate granule cells. *Acta Physiol. Scand.* **66**, 448–460. (doi:10.1111/j.1748-1716.1966.tb03223.x)
97. Schwarz AJ, Danckaert A, Reese T, Gozzi A, Paxinos G, Watson C, Merlo-Pich EV, Bifone A. 2006 A stereotaxic MRI template set for the rat brain with tissue class distribution maps and co-registered anatomical atlas: application to pharmacological MRI. *Neuroimage* **32**, 538–550. (doi:10.1016/j.neuroimage.2006.04.214)
98. Lomo T. 1971 Patterns of activation in a monosynaptic cortical pathway: the perforant path input to the dentate area of the hippocampal formation. *Exp. Brain Res.* **12**, 18–45. (doi:10.1007/BF00234414)
99. Deadwyler S, West JR, Cotman C, Lynch GS. 1975 A neurophysiological analysis of commissural projections to dentate gyrus of the rat. *J. Neurophysiol.* **38**, 167–184.
100. Golarai G, Sutula TP. 1996 Bilateral organization of parallel and serial pathways in the dentate gyrus demonstrated by current-source density analysis in the rat. *J. Neurophysiol.* **75**, 329–342.
101. Amaral DG. 1978 A Golgi study of cell types in the hilar region of the hippocampus in the rat. *J. Comp. Neurol.* **182**, 851–914. (doi:10.1002/cne.901820508)
102. Laurberg S, Sørensen K. 1981 Associational and commissural collaterals of neurons in the hippocampal formation (hilus fasciae dentatae and subfield CA3). *Brain Res.* **212**, 287–300. (doi:10.1016/0006-8993(81)90463-7)
103. Golarai G, Sutula TP. 1996 Functional alterations in the dentate gyrus after induction of long-term potentiation, kindling, and mossy fiber sprouting. *J. Neurophysiol.* **75**, 343–353.
104. Kleschevnikov AM, Routtenberg A. 2003 Long-term potentiation recruits a trisynaptic excitatory associative network within the mouse dentate gyrus. *Eur. J. Neurosci.* **17**, 2690–2702. (doi:10.1046/j.1460-9568.2003.02709.x)
105. Ribak CE, Seress L, Amaral DG. 1985 The development, ultrastructure and synaptic connections of the mossy cells of the dentate gyrus. *J. Neurocytol.* **14**, 835–857. (doi:10.1007/BF01170832)
106. Lisman JE, Talamini LM, Raffone A. 2005 Recall of memory sequences by interaction of the dentate and CA3: a revised model of the phase precession. *Neural Netw.* **18**, 1191–1201. (doi:10.1016/j.neunet.2005.08.008)
107. Myers CE, Scharfman HE. 2009 A role for hilar cells in pattern separation in the dentate gyrus: a computational approach. *Hippocampus* **19**, 321–337. (doi:10.1002/hipo.20516)